Optical solitary waves in two- and three-dimensional nonlinear photonic band-gap structures

Neşet Aközbek and Sajeev John
Department of Physics, University of Toronto, 60 St. George Street, Toronto, Ontario, Canada M5S 1A7
(Received 9 September 1997)

We present a detailed analysis of finite energy solitary waves in two- and three-dimensional nonlinear periodic structures exhibiting a complete photonic band gap. Solitary waves in photonic crystals with a two-dimensional (2D) square and triangular symmetry group as well as a 3D fcc symmetry group are described in terms of an effective nonlinear Dirac equation derived using the slowly varying envelope approximation for the electromagnetic field. Unlike one-dimensional Bragg solitons, the multiple symmetry points of the 2D and 3D Brillouin zones give rise to two distinct classes of solitary wave solutions. Solutions associated with a higher order symmetry point of the crystal exist for both positive and negative Kerr nonlinearities, whereas solutions associated with a twofold symmetry point occur only for positive Kerr coefficient. Using a variational method we derive the important physical features such as the size, shape, peak intensity, and total energy of the solitary waves. This is then confirmed numerically using the finite element Ritz-Galerkin method. It is shown that the initial variational method and the finite element numerical method are in good agreement. We discuss the stability of these solitary waves with respect to small perturbations. It is suggested that an analytical stability criterion for spinor fields satisfying the nonlinear Dirac type of equation may exist, similar to the well known stability criterion for solitary waves in the nonlinear Schrödinger equation. Our stability criterion correctly reproduces the stability conditions of other nonlinear Dirac type of equations which have been studied numerically. Our study suggests that for an ideal Kerr medium, two-dimensional solitary waves in a band gap are stable, whereas three-dimensional ones are stable only in certain regions of the gap. [S1063-651X(98)05401-4]

PACS number(s): 42.65.Tg, 42.70.Qs

I. INTRODUCTION

Electromagnetic wave propagation and localization in nonlinear periodic structures has been the subject of considerable activity over the last decade. The stationary properties of one-dimensional (1D) Bragg gratings were first analyzed by Winful, Marburger, and Garmire [1], who showed that these structures exhibit bistable optical transmission behavior. The term ''gap soliton'' was introduced by Chen and Mills [2] in subsequent numerical work. This terminology was based on the fact that the electric field envelope function inside the medium resembles a hyperbolic secant, reminiscent of solitary wave solutions of other well known nonlinear wave equations, such as the nonlinear Schrödinger equation obtained in the propagation of optical solitons in fibers [3]. An analytical solution was obtained for stationary gap solitary waves by Mills and Trullinger [4]. These authors derived the existence of one-dimensional self-localized solutions of the optical field throughout the band gap of a 1D Bragg grating for both positive and negative nonlinear Kerr coefficients. They showed that the phase modulation of the gap solitons satisfies the double sine-Gordon equation, which has kink type solutions. The electric field amplitude of their solution is a localized function with a more complex structure than a simple hyperbolic secant function. A general analytical solution to the time-dependent 1D nonlinear optical gap soliton problem was obtained by Aceves and Wabnitz [5], using an analogy with the massive Thirring model [6]. Unlike the integrable Thirring model, the optical coupled mode equations for a Bragg grating are not integrable, and the gap solutions are not truly solitons but rather solitary waves. A useful review of one-dimensional gap solitons was given by de Sterke and Sipe [7]. In the continuous wave (CW) limit, optical switching [8] and bistability [9] have been experimentally demonstrated. Most recently the generation and propagation of gap solutions were observed by Eggleton *et al.* [10].

Gap solitons are in some ways similar to optical fiber solitons [11]. They are both formed by the balance between the group velocity dispersion (GVD) and the nonlinearity of the medium. When an optical pulse propagates through a nonlinear medium, it gains an additional intensity-dependent phase due to the nonlinear index of refraction, referred to as self-phase modulation. In a medium with positive nonlinearity, the phase modulation causes the leading edge of the pulse to be redshifted, while the trailing edge is blueshifted. In general, a pulse propagating in a linear dispersive medium will spread. A material in which the GVD parameter $\beta_2 \equiv (d/d\omega)(1/v_g)$ is negative is said to exhibit anomalous dispersion. Here v_g is the group velocity at frequency ω. In the anomalous dispersion regime, the leading edge of the pulse is blueshifted, while the trailing edge is redshifted. When both GVD and nonlinearity are present in the medium, then, under certain conditions, these two effects can cancel each other, resulting in a pulse which propagates without changing its shape. In the appropriate limit, both fiber solitons and solitary waves in a Bragg grating can be described by a nonlinear Schrödinger equation. The difference is that the GVD in fibers is mainly due to the material dispersion (frequency-dependent refractive index), whereas in the latter, GVD is due to the periodic variation in the linear (frequency independent) dielectric constant. The latter variation is many orders of magnitude larger than the dispersive variation in fibers. Unlike the fiber soliton which experiences only self-

 © 1998 The American Physical Society

phase modulation, the gap soliton experiences additional cross-phase modulation with light that is Bragg scattered by the grating. Another difference is that gap solitons may attain any velocity between zero and the average speed of light in the medium, whereas fiber solitons travel only with the average speed of light in the medium. Despite these differences, the optical coupled mode equations in a photonic band-gap (PBG) material can be reduced to an effective nonlinear Schrödinger equation for the electric field envelope function when the optical frequency is near one of the photonic band edges. The soliton arising in pulse propagation in fibers is usually referred to as a temporal soliton, whereas in the PBG material it is a spatial soliton. Optical solitons have received tremendous interest for their technological applications in the area of optical fiber communications and photonic switching [12].

Qualitatively similar considerations arise in the problem of steady (CW) beam propagation in a medium with a self-focusing Kerr nonlinearity. When a CW beam propagates through a nonlinear medium, the nonlinear effect can balance the diffraction of the beam, such that the beam can travel without changing its transverse profile [13]. In a 3D geometry this soliton is unstable to perturbations. However, in a 2D system, where diffraction is allowed in only one transverse dimension due to linear confinement in the other transverse direction, the beam can propagate through the medium without changing its shape. The nonlinear Schrödinger equation that governs this solitary wave follows from interpreting the time variable as the spatial propagation direction.

The linear electromagnetic band structures of periodic dielectric structures have been extensively studied recently [14]. Frequency gaps have been demonstrated in 2D and 3D systems in which there are no propagating solutions of the Maxwell's equations for a medium with a real positive refractive index. This picture changes significantly if the medium also exhibits a Kerr nonlinearity in which the dielectric constant is intensity dependent. As the intensity of the incoming radiation with frequency inside the gap is increased, it is possible for the underlying dispersion relation to change locally, and for the incoming light pulse to tune itself outside the band-gap region by locally deforming the band structure, and to propagate through the medium. Nearly all work so far has been done on one-dimensional structures. Recently, we have shown that localized finite energy solitary waves exist inside the photonic band gap of a two-dimensional periodic structure [15]. In one-dimensional photonic band gaps, the propagation of light is only forbidden over a very small fraction of k space. Three-dimensional periodic structures with nonoverlapping gaps in different directions were studied by Ohtaka [16]. A complete band gap of a three-dimensional periodic medium with the point group symmetry of a fcc lattice was independently suggested by John [17] and Yablonovitch [18]. Potential applications of these structures for optical filters, pulse compression [19], zero-threshold microlasers [20], and all-optical transistors [21] have been proposed. Although three-dimensional PBG materials have been fabricated in the microwave regime [20], the ultimate goal is to obtain complete gaps in the visible spectrum and near infrared (1.5 μm) for applications such as optical interconnects, all-optical amplifiers, and wavelength demultiplexers [22,23] in the telecommunication industry. Using a PBG interconnect containing an active region, optical fiber solitons may be reshaped, amplified, or otherwise processed. The efficiency of these processes is greatly enhanced by virtue of the inhibition of spontaneous emission by the PBG structure. Recently, Özbay *et al.* [24] constructed a three-dimensional structure with a PBG at around 100 GHz. The existence of photonic band gaps in two dimensions has been demonstrated both theoretically [25–27] and experimentally in the microwave regime [28,29]. In the optical regime, fabrication of two-dimensional periodic structures has proved to be much more straightforward. Such structures have been fabricated on a small scale in the optical regime for square [30] and triangular lattices (2.5–1.1 μm) [31]. Very large array, 2D square and triangular lattice PBG's, in the 6 μm range, have been demonstrated in macroporous silicon by Grüning *et al.* [32]. These latter structures are easily fabricated using the self-organizing property of columnar voids in Si under suitable electrochemical etching conditions. Most recently, large scale 3D PBG structures on the optical scale have been demonstrated using infiltrated opals [33]. In these systems a close-packed fcc lattice of SiO_2 spheres with diameter on the micron scale is infiltrated with a high refractive index material such as diamond or silicon [34]. The higher index material fills the interstitial regions between the SiO_2 spheres, forming a connected solid network. The SiO_2 spheres are then removed by chemical etching, leaving behind a PBG crystal with a complete 3D gap [35].

Unlike their 1D counterparts, 2D solitary waves are localized in two spatial dimensions. Another difference is the existence of multiple symmetry points in the 2D Brillouin zone (BZ). This gives rise to new types of solitary waves that have no analog in one dimension. In general, there are two specific symmetry points in BZ's which determine the upper and lower band edges of the full photonic band gap. We define the order of the symmetry point by the total number of such points that are connected to each other by reciprocal lattice vectors of the photonic crystal. One of them (usually a twofold symmetry point) gives rise to a solitary wave with low symmetry, whereas the higher order point gives a solitary wave with higher symmetry. We find that the low symmetry solution exists only for positive Kerr coefficient, whereas higher symmetry solutions may exist for both negative and positive Kerr coefficient. The underlying nonlinear electromagnetic wave equation can be reduced, using the slowly varying envelope approximation to a nonlinear Dirac type of equation where the number of components of the slowly varying spinor field depends on the order of the symmetry point about which the electric field is expanded. In general the solitary wave can be described as a localized amplitude function accompanied by a self-phase modulation kink in the direction of the Bragg scattering.

In this paper, we derive solitary wave solutions for 2D square and triangular lattices, and the 3D fcc lattice. As in the 1D case, near the photonic band edges it is possible to establish an analogy between the effective nonlinear electromagnetic wave equation and the equation for a particle moving in a classical potential well. This analogy furnishes an existence proof for the higher-dimensional solitary waves. Unlike the one-dimensional case, where an exact analytical solution exists throughout the PBG, in higher dimensions,

simple solutions can be obtained only near the photonic band edges where the ''effective mass approximation'' for the photon dispersion is valid. For a general frequency within the gap one must use numerical or approximate methods. We have introduced a variational method which recaptures most of the important physics of these 2D and 3D solitary waves. First we test the accuracy of our variational method by applying it to the 1D case. This yields excellent qualitative agreement with the exact solution of Mills and Trullinger [4]. In order to generalize the variational ansatz for $d>1$, we use the Ritz-Galerkin numerical method based on the expansion of the solitary wave in terms of a suitable set of eigenfunctions. In one dimension we show that by retaining sufficient terms in this finite element expansion the solution converges to the exact solution for the entire band-gap region. In $d>1$, we include more terms in the expansion until there is no significant difference in the solution between two successive iterations.

Given the existence of 2D solitary waves, we then discuss their stability with respect to small perturbations. In an ideal Kerr medium with no periodic modulation, it is well known that solitary waves satisfying the nonlinear Schrödinger equation (NLSE) are unstable for $d>1$. On the other hand, saturation effects of the nonlinear susceptibility tend to stabilize solitary waves in all dimensions, as do the inclusion of higher order derivative terms [36]. Materials exhibiting quadratic nonlinearities are also known to exhibit stable solitary waves for $d>1$ [37]. Using a linear stability analysis, we derive a criterion for the stability of solitary wave solutions of the nonlinear Dirac equation analogous to the criterion for the NLSE. For spinor fields with an unbounded negative spectrum, we show that the minimum property of the energy functional is neither a necessary nor sufficient condition for stability. We test our criterion on a number of models with known stability properties. In each of these cases our criterion reproduces the known result. Our stability criteria suggests that two-dimensional solitary waves in a PBG with a purely Kerr nonlinearity are stable throughout the gap region, whereas three-dimensional ones are stable only for $\omega>\omega_{\rm cr}$, where $\omega_{\rm cr}$ is the frequency at which there is a local minimum of the total energy as a function of ω. A similar minimum point exists in the 3D nonlinear Schrödinger equation with a saturable nonlinear index of refraction.

II. SLOWLY VARYING ENVELOPE APPROXIMATION

Consider a two-dimensional periodic nonlinear dielectric where the electric field $\vec{E}$ and medium polarization $\vec{P}$ are linearly polarized in the $\hat{z}$ direction perpendicular to the plane of the 2D lattice. Denoting the z component of the electric field by E, Maxwell's equations take the form of a scalar wave equation,

$$\nabla^2 E(\vec{r},t)-\frac{\epsilon(\vec{r})}{c^2}\frac{\partial^2 E(\vec{r},t)}{\partial t^2}-\frac{4\pi}{c^2}\frac{\partial^2 P_{\rm NL}(\vec{r},t)}{\partial t^2}=0, \tag{2.1}$$

where the nonlinear polarization $P_{\rm NL}=\chi^{(3)}|E|^2E$. Here we assume that the nonlinear susceptibility $\chi^{(3)}$ is independent of $\vec{r}$, and that medium responds instantaneously to the applied field. For the square lattice we choose the linear part of the dielectric constant to have the simple form

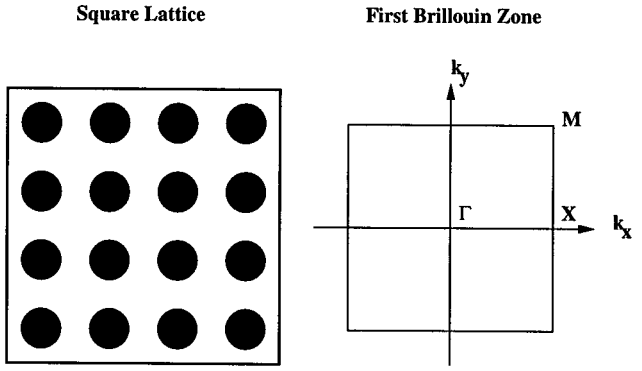

FIG. 1. Top view of a 2D square lattice PBG structure (left) in the (x,y) plane. The medium is assumed to be homogenous in the z direction. The dark circular spots represent a long circular rod with dielectric constant ϵ_A embedded in a background medium with a dielectric constant ϵ_B. The first Brillouin zone (right) is labeled with the corresponding symmetry points X $(\pi/a_o,0)$ and M $(\pi/a_o,\pi/a_o)$, where a_o is the lattice constant.

$$\epsilon(\vec{r})=\tilde{\epsilon}+\Delta\epsilon[\cos(\vec{G}_1\cdot\vec{r})+\cos(\vec{G}_2\cdot\vec{r})] \tag{2.2}$$

where $\vec{G}_1=(2\pi/a_o)\hat{x}$ and $\vec{G}_2=(2\pi/a_o)\hat{y}$ are the reciprocal lattice vectors, $\tilde{\epsilon}$ is average dielectric constant of the medium, and a_o is the lattice constant. This model exhibits an indirect photonic band gap with the upper band edge occurring at the face center (X point) of the 2D BZ and the lower band edge occurring at the corner (M point) of the BZ. In Fig. 1 we show a possible 2D square lattice structure with its corresponding Brillouin zone.

The slowly varying envelope approximation (SVEA) to Eq. (2.1) is obtained by expanding the electric field amplitude about the band edges. The field amplitude at the X point $[\vec{k}_o=(G/2)\hat{x}]$ is connected to $-\vec{k}_o$ by the reciprocal lattice vector $\vec{G}_1$, leading to the expansion

$$E(\vec{r},t)=(E_1(\vec{r},t)e^{i\vec{k}_o\cdot\vec{r}}+E_2(\vec{r},t)e^{-i\vec{k}_o\cdot\vec{r}})e^{-i\omega t}+\text{c.c.} \tag{2.3}$$

Here, we assume that E_1 and E_2 vary slowly in time and space on the scales ω^{-1} and k_o^{-1}, respectively. Substituting Eq. (2.3) into Eq. (2.1) with Eq. (2.2), we obtain two coupled equations for E_1 and E_2 in the SVEA:

$$i\frac{\partial E_1}{\partial t}+i\frac{\partial E_1}{\partial x}+\frac{\partial^2 E_1}{\partial y^2}+\delta E_1+\beta E_2+\tfrac{2}{3}\alpha[|E_1|^2+2|E_2|^2]E_1=0, \tag{2.4a}$$

$$i\frac{\partial E_2}{\partial t}-i\frac{\partial E_2}{\partial x}+\frac{\partial^2 E_2}{\partial y^2}+\delta E_2+\beta E_1+\tfrac{2}{3}\alpha[|E_2|^2+2|E_1|^2]E_2=0. \tag{2.4b}$$

Here we have introduced the change variables $Gx\to x$, $Gy\to y$, $\omega/\omega_o\to\omega$ and $\sqrt{\lambda}E_{1,2}\to E_{1,2}$, $2\omega_o t\to t$, so that Eq.

(2.4) is dimensionless. The other parameters are defined as $\omega_o \equiv cG/2\sqrt{\tilde{\epsilon}}$, $\beta \equiv \Delta\epsilon/8\tilde{\epsilon}$, and $\lambda \equiv 9\pi|\chi^{(3)}|/2\tilde{\epsilon}$. $\delta \equiv (\omega^2 - 1)/4$ describes the detuning of the average soliton frequency from the photonic midgap, and $\alpha = \pm 1$ for positive-negative nonlinearity. Strictly speaking, expansion (2.3) corresponds to a ''nearly free photon approximation'' which is valid when the periodic dielectric modulation is a weak perturbation to the vacuum wave equation ($\Delta\epsilon \ll \tilde{\epsilon}$). In a real PBG material, $\Delta\epsilon$ is comparable to $\tilde{\epsilon}$, and the carrier waves, $e^{-i\omega t \pm i\vec{k}\cdot\vec{r}}$ must be replaced by Bloch functions [38] obtained from a realistic band structure calculation. Nevertheless, the overall structure of the solitary wave equation for the envelope functions E_1 and E_2 is quite similar to that obtained from Eq. (2.3). Consequently, even for strong scattering materials, we expect that Eq. (2.3) yields the important underlying physics and qualitative properties of the solitary wave solutions. In the standard SVEA, we retain only first order derivatives in space and time for E_1 and E_2. Higher derivative terms tend to become significant only for frequencies deep within the PBG when the envelope function is localized on the scale of the lattice constant a_o. However, when $\Delta\epsilon \ll \tilde{\epsilon}$, Eq. (2.4) is valid throughout the gap region.

Equation (2.4) can be succinctly rewritten in terms of a two-component spinor field $\Psi^\dagger \equiv (E_1^*, E_2^*)$:

$$\{i\partial_t + \partial_{yy} + i\sigma_z\partial_x + \delta + \beta\sigma_x + \alpha[(\Psi^\dagger\Psi) - (\Psi^\dagger\sigma_z\Psi)\sigma_z/3]\}\Psi = 0 \tag{2.5}$$

Here, $\sigma_{x,y,z}$ are the usual 2×2 Pauli matrices. Multiplying Eq. (2.5) by $\Psi^\dagger$, adding the complex conjugate, and then integrating over the transverse space variable y, the following continuity equation can be obtained:

$$\frac{\partial\rho}{\partial t} + \frac{\partial j}{\partial x} = 0. \tag{2.6}$$

Here the energy density $\rho = \int dy(\Psi^\dagger\Psi) = \int dy(|E_1|^2 + |E_2|^2)$, and the current density $j = \int dy(\Psi^\dagger\sigma_z\Psi) = \int dy(|E_1|^2 - |E_2|^2)$ describes the net power flow of the solitary wave. Integrating Eq. (2.6) over x reveals that the conserved quantity $Q \equiv \int dxdy(\Psi^\dagger\Psi)$ describes the total energy of the solitary wave within the PBG.

We first consider static solutions of Eqs. (2.5) for which $\partial_t\Psi = 0$ and $E_1 = E_2^*$. In this case $j = 0$. Writing $\Psi^\dagger = (E^*, E)$, Eq. (2.5) reduces to

$$[\partial_{yy} + i\sigma_z\partial_x + \delta + \beta\sigma_x + \alpha(\Psi^\dagger\Psi)]\Psi = 0. \tag{2.7}$$

The SVEA simplifies the true single photon band structure of Eq. (2.1) to an approximate one. This approximate band structure follows from Eq. (2.7) by setting $\alpha = 0$ and considering solutions of the form $\Psi = \Phi e^{i\vec{q}\cdot\vec{r}}$, with Φ independent of $\vec{r}$. The approximate one-photon dispersion relation is obtained by setting the resulting 2×2 determinant equal to zero:

$$[\delta - q_x - q_y^2][\delta + q_x - q_y^2] - \beta^2 = 0. \tag{2.8}$$

Solving Eq. (2.8) for the detuning frequency δ, keeping only terms of order q^2, the dispersion relations for the upper and lower photonic band gaps become $\omega_\pm^2(q_x, q_y) = 1 - 4q_y^2 \pm 4\sqrt{q_x^2 + \beta^2}$. The Bragg condition is satisfied at the band edge defined by $|\vec{q}| = 0$. The frequency gap at the X point is determined by

$$\omega_\pm^{(X)} = \sqrt{1 \pm 4\beta}, \tag{2.9}$$

where $\omega_\pm^X$ are the upper and lower band edge frequencies at X. For a frequency within the gap region, $|\vec{q}|$ becomes imaginary, and linear wave propagation is exponentially damped.

Alternatively, we may consider a wave vector close to the M symmetry point at $\vec{k}_o = (G/2)(\hat{x} + \hat{y})$. In this case there are four components in the Fourier expansion of the electric field which are resonantly coupled by reciprocal lattice vectors of the photonic crystal. Accordingly, we expand the electric field about the four symmetry-related M points:

$$E(\vec{r}, t) = (E_1 e^{ik_o(x+y)} + E_2 e^{-ik_o(x+y)} + E_3 e^{ik_o(x-y)} + E_4 e^{-ik_o(x-y)})e^{-i\omega t} + \text{c.c.} \tag{2.10}$$

Substituting Eq. (2.10) into Eq. (2.1) we obtain a set of four coupled nonlinear equations for the slowly varying envelope functions E_1, E_2, E_3, and E_4:

$$i\frac{\partial E_1}{\partial t} + i\left(\frac{\partial}{\partial x} + \frac{\partial}{\partial y}\right)E_1 + (\omega^2 - 2)E_1/4 + \beta(E_3 + E_4) + \frac{2\lambda}{3}[|E_1|^2E_1 + 2(|E_2|^2 + |E_3|^2 + |E_4|^2)E_1 + 2E_2^*E_3E_4] = 0, \tag{2.11a}$$

$$i\frac{\partial E_2}{\partial t} - i\left(\frac{\partial}{\partial x} + \frac{\partial}{\partial y}\right)E_2 + (\omega^2 - 2)E_2/4 + \beta(E_3 + E_4) + \frac{2\lambda}{3}[|E_2|^2E_2 + 2(|E_1|^2 + |E_3|^2 + |E_4|^2)E_2 + 2E_1^*E_3E_4] = 0, \tag{2.11b}$$

$$i\frac{\partial E_3}{\partial t} + i\left(\frac{\partial}{\partial x} - \frac{\partial}{\partial y}\right)E_3 + (\omega^2 - 2)E_3/4 + \beta(E_1 + E_2) + \frac{2\lambda}{3}[|E_3|^2E_3 + 2(|E_1|^2 + |E_2|^2 + |E_4|^2)E_3 + 2E_4^*E_1E_2] = 0, \tag{2.11c}$$

$$i\frac{\partial E_4}{\partial t} - i\left(\frac{\partial}{\partial x} - \frac{\partial}{\partial y}\right)E_4 + (\omega^2 - 2)E_4/4 + \beta(E_1 + E_2) + \frac{2\lambda}{3}[|E_4|^2E_4 + 2(|E_1|^2 + |E_2|^2 + |E_3|^2)E_4 + 2E_3^*E_1E_2] = 0. \tag{2.11d}$$

Equation (2.11) yield a similar continuity relation,

$$\frac{\partial\rho}{\partial t} + \vec{\nabla}\cdot\vec{j} = 0, \tag{2.12}$$

where the energy density $\rho=|E_1|^2+|E_2|^2+|E_3|^2+|E_4|^2$ and the net power flux $j=j_x\hat{x}+j_y\hat{y}$, with $j_x=|E_1|^2-|E_2|^2+|E_3|^2-|E_4|^2$ and $j_y=|E_1|^2-|E_2|^2-|E_3|^2+|E_4|^2$. Integration of Eq. (2.12) over x and y gives the conservation of the total energy $Q=\int dx\ dy\ \rho$ of the solitary wave.

A particular solution of Eq. (2.11) follows from setting $E_2=E_1^*$ and $E_4=E_3^*$. In this case we may write the static equations for the stationary M solitary wave in spinor field notation by defining the four-component $\Psi=(E_1^*,E_2^*,E_3^*,E_4^*)$:

$$\{i(\gamma_1\partial_x+\gamma_2\partial_y)+\delta_M+\beta\gamma_3+\alpha[3(\Psi^\dagger\Psi)-(\Psi^\dagger\gamma_4\Psi)\gamma_4]\}\Psi=0. \quad (2.13)$$

Here, we have performed the rescaling $\sqrt{\lambda/2}\Psi\rightarrow\Psi$ and $\delta_M=(\omega^2-2)/4$. γ_1, γ_2, and γ_3 are 4×4 matrices defined as

$$\gamma_1=\begin{pmatrix}\sigma_z & 0\\ 0 & \sigma_z\end{pmatrix},\quad \gamma_2=\begin{pmatrix}\sigma_z & 0\\ 0 & -\sigma_z\end{pmatrix}, \quad (2.14a)$$

$$\gamma_3=\begin{pmatrix}0 & \sigma_x+I\\ \sigma_x+I & 0\end{pmatrix},\quad \gamma_4=\begin{pmatrix}I & 0\\ 0 & -I\end{pmatrix}, \quad (2.14b)$$

We make the important observation here that although Eq. (2.13) formally resembles a Dirac equation there is at least one important distinction. In a truly relativistic Dirac formalism, the structure matrices $\gamma_1\cdots\gamma_3$ exhibit a completely anticommuting algebra. This is clearly not the case for the matrices defined by Eq. (2.14). Unlike the 1D solitary wave equation, in the 2D case the analogy with the relativistic Dirac equation is not complete. The above matrices, which are determined by the anisotropy properties of the photonic crystal, lead to a more complicated wave equation than one would obtain in a truly relativistic (2+1)-dimensional field theory.

For the M symmetry point we obtain the effective one-photon dispersion relation in the SVEA by setting the appropriate 4×4 determinant equal to zero. The resulting roots yield the dispersion relations $\omega_{1,2}^2(q_x,q_y)=2\pm4(\sqrt{q_x^2+\beta^2}+\sqrt{q_y^2+\beta^2})$ and $\omega_{3,4}^2(q_x,q_y)=2\pm4(\sqrt{q_x^2+\beta^2}-\sqrt{q_y^2+\beta^2})$. For $|\vec{q}|=0$, there are two nondegenerate solutions at frequencies $\sqrt{2\pm8\beta}$ and a doubly degenerate solution at frequency $\sqrt{2}$. Therefore, the SVEA predicts approximate gaps at the M point for $\sqrt{2-8\beta}<\omega<\sqrt{2}$ and $\sqrt{2}<\omega<\sqrt{2+8\beta}$. In order to have a *complete* band gap, the gaps at X and M must overlap. This leads to the requirement that $\Delta\epsilon/\tilde{\epsilon}\geq0.6$. The upper ω_+ and lower ω_- band edges of the resulting *indirect* photonic band gap are given by $\omega_+^{(X)}$ and $\omega_-^{(M)}$, respectively. Equations (2.7) and (2.13) describe two distinct types of solitary waves. The X solitary wave is a generalization of the one-dimensional soliton state, whereas the M soliton is a new type of state corresponding to a higher symmetry group of the Brillouin zone.

In addition to the two fundamental solitons described above, a symmetric X solitary wave solution is possible. This arises from the interaction of two X solitary waves, one being Bragg scattered in the $\hat{x}$ direction and the other in the $\hat{y}$ direction. In this case the electric field can be expanded as

$$E(\vec{r},t)=(E_1e^{ik_ox}+E_2e^{-ik_ox}+E_3e^{ik_oy}+E_4e^{-ik_oy})e^{-i\omega t}+\text{c.c.} \quad (2.15)$$

Inserting this expansion into Eq. (2.1) and using the SVEA, we obtain the following coupled mode equations for the static, composite X soliton:

$$i\frac{\partial E_1}{\partial x}+\frac{\partial^2E_1}{\partial y^2}+\delta E_1+\beta E_2+2\alpha[|E_1|^2+2|E_3|^2]E_1=0, \quad (2.16a)$$

$$-i\frac{\partial E_2}{\partial x}+\frac{\partial^2E_2}{\partial y^2}+\delta E_2+\beta E_1+2\alpha[|E_2|^2+2|E_3|^2]E_2=0, \quad (2.16b)$$

$$i\frac{\partial E_3}{\partial y}+\frac{\partial^2E_3}{\partial x^2}+\delta E_3+\beta E_4+2\alpha[|E_3|^2+2|E_1|^2]E_3=0, \quad (2.16c)$$

$$-i\frac{\partial E_4}{\partial y}+\frac{\partial^2E_4}{\partial x^2}+\delta E_4+\beta E_3+2\alpha[|E_4|^2+2|E_1|^2]E_4=0. \quad (2.16d)$$

It is easy to see when $E_3=E_4=0$ we recover the simple X solitary wave equations.

A. Mechanical analogy for the 1D gap soliton

The existence of a soliton solution in one dimension can be easily demonstrated by considering a solution of the form $E(x)=A(x)e^{-i\phi(x)}$. Putting $E(x)$ into Eq. (2.7) with $\partial_{yy}\Psi=0$, we obtain a set of coupled equations for the phase angle $\phi(x)$ and amplitude $A(x)$ [4]:

$$-\frac{d\phi}{dx}+\delta+\beta\cos[2\phi(x)]+2\alpha A(x)^2=0, \quad (2.17a)$$

$$\frac{dA(x)}{dx}=\beta A(x)\sin[2\phi(x)]. \quad (2.17b)$$

By differentiating Eq. (2.17a) with respect to x and using Eq. (2.17b) it follows that the phase $\phi(x)$ satisfies the double sine-Gordon equation

$$\frac{d^2\phi}{dx^2}+2\beta\delta\sin(2\phi)+\beta^2\sin(4\phi)=0. \quad (2.18)$$

It is well known that Eq. (2.18) has kink type solutions [39]. Nevertheless, it is instructive to demonstrate the existence of the solution to Eq. (2.17) by means of a simple mechanical analogy. For illustrative purposes we consider $\alpha=1$. Equation (2.17a) can be rewritten as

$$\dot{\phi}=-\frac{dU}{d\phi}+F_{\text{ext}}(x), \quad (2.19)$$

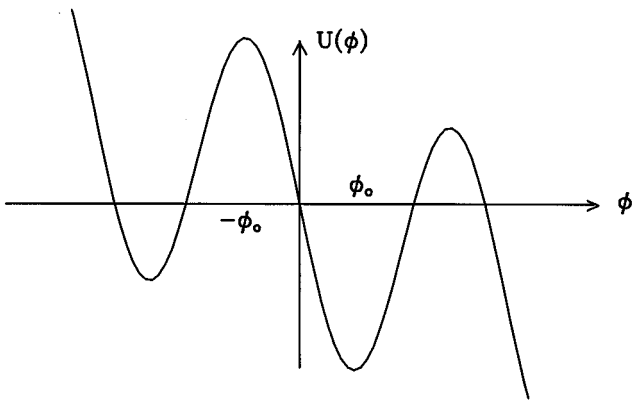

FIG. 2. The existence of 1D solitary waves in a PBG is apparent using an analogy with a mechanical potential $U(\phi)=-\delta\phi-\beta\sin(2\phi)/2$, in which a particle is pushed up by the external force $F_{\rm ext}=A^2(x)$ from the equilibrium position at ϕ_o $(x\to-\infty)$ to the unstable equilibrium point at $-\phi_o$ $(x\to+\infty)$. This results in a kink type solution for the phase angle ϕ of the optical solitary wave.

where ϕ may be regarded as the coordinate of a classical particle, $U(\phi)=-\delta\phi-(\beta/2)\sin(2\phi)$ is the potential in which it moves, and $F_{\rm ext}=A^2(x)$ is an external force which acts on the particle and x plays the role of a time variable. If we add an inertia term $m\ddot{\phi}$ to the left hand side of Eq. (2.19), it is formally equivalent to a Newtonian equation of motion for a particle experiencing a viscous drag force $-\dot{\phi}$. As it stands, Eq. (2.19) is the overdamped limit of this Newtonian problem in which the particle mass m is negligible, and the viscosity is large. The potential $U(\phi)$ is sketched in Fig. 2. From Eq. (2.17b), we easily see that for a localized amplitude solution, we require that $\sin(2\phi)=\pm c_o$ when $x\to\pm\infty$. In other words when $x\to\infty$ the particle is at rest at $\phi=\phi_o=\arccos(-\delta/\beta)/2$, which corresponds to the extremum points of the potential U. The external force acts on the particle, and moves it to the unstable equilibrium position at $\phi=-\phi_o$ for $x\to+\infty$. This results in a kink type solution for the phase function, ϕ, and a localized amplitude function A. For $\alpha=+1$, the exact solution is given by

$$A(x)=A\frac{\operatorname{sech}(ax)}{\sqrt{1+b^2\tanh(ax)}} \tag{2.20a}$$

and

$$\phi(x)=\pi/2+\arctan[b\tanh(ax)], \tag{2.20b}$$

where $A=\sqrt{\beta-\delta}$, $a=\sqrt{\beta^2-\delta^2}$, and $b=\sqrt{(\beta-\delta)/(\beta+\delta)}$.

B. Moving solitary waves in a PBG material

The general time-dependent solitary wave solutions to the one-dimensional version of Eq. (2.5) have been studied by Aceves and Wabnitz [5]. Moving solitary waves can be obtained from stationary ones by applying the appropriate Lorentz transformation to Eq. (2.5). We seek a solution of the form

$$\Psi(x,y,t)=\Psi(\zeta,y)e^{i\Delta kx} \tag{2.21}$$

using the new variables $\zeta=(x-vt)$ and $\tau=t$. Then Eq. (2.5) can be written as

$$i\frac{\partial E_1}{\partial\tau}+i(1-v)\frac{\partial E_1}{\partial\zeta}+\frac{\partial^2E_1}{\partial y^2}+(\delta-\Delta k)E_1+\beta E_2+\frac{2\alpha}{3}[|E_1|^2+2|E_2|^2]E_1=0, \tag{2.22a}$$

$$i\frac{\partial E_2}{\partial\tau}-i(1+v)\frac{\partial E_2}{\partial\zeta}+\frac{\partial^2E_2}{\partial y^2}+(\delta+\Delta k)E_2+\beta E_1+\frac{2\alpha}{3}[|E_2|^2+2|E_1|^2]E_2=0. \tag{2.22b}$$

These equations can be mapped onto a static equation by means of the change of variables

$$E_1=\lambda^{1/4}\tilde{E}_1,\quad E_2=\lambda^{-1/4}\tilde{E}_2 \tag{2.23a}$$

$$\delta=\gamma\tilde{\delta},\quad \Delta k=v\gamma\tilde{\delta},\quad \gamma\zeta\to\zeta, \tag{2.23b}$$

where $\lambda=[(1+v)/(1-v)]$ and $\gamma=1/\sqrt{1-v^2}$. Inserting Eq. (2.23) into Eqs. (2.22) yields

$$i\frac{\partial\tilde{E}_1}{\partial\zeta}+\lambda^{1/2}\frac{\partial^2\tilde{E}_1}{\partial y^2}+\tilde{\delta}\tilde{E}_1+\beta\tilde{E}_2+\frac{2\alpha}{3}[\lambda|\tilde{E}_1|^2+2|\tilde{E}_2|^2]\tilde{E}_1=0, \tag{2.24a}$$

$$-i\frac{\partial\tilde{E}_2}{\partial\zeta}+\lambda^{-1/2}\frac{\partial^2\tilde{E}_2}{\partial y^2}+\tilde{\delta}\tilde{E}_2+\beta\tilde{E}_1+\frac{2\alpha}{3}[\lambda^{-1}|\tilde{E}_2|^2+2|\tilde{E}_1|^2]\tilde{E}_2=0. \tag{2.24b}$$

In addition to the conserved energy, Eqs. (2.24) exhibits the property that $(\partial/\partial\zeta)\int dy[|\tilde{E}_1|^2-|\tilde{E}_2|^2]=0$. We first consider the 1D case by setting $\partial/\partial y=0$ in Eqs. (2.24), and seeking solutions of the form $\tilde{E}_{1,2}=\varepsilon(\zeta)e^{i\phi_{1,2}(\zeta)}$. Introducing the new phase angles $\phi\equiv(\phi_1-\phi_2)/2$ and $\psi=(\phi_1+\phi_2)/2$, and the rescaled variable $\varepsilon=\eta A$, where $3/\eta^2=[2+(1+v^2)/(1-v^2)]$, it follows from Eq. (2.24) that

$$\left(-\frac{\partial\phi}{\partial\zeta}+\beta\cos(2\phi)+\tilde{\delta}+2\alpha A^2\right)A=0, \tag{2.25a}$$

$$\frac{\partial A}{\partial\zeta}-\beta A\sin(2\phi)=0. \tag{2.25b}$$

It can easily be seen that Eqs. (2.25a) and (2.25b) are identical to the static equations given in Eq. (2.17) for which the solutions are given by Eqs. (2.20). The only difference is that δ is replaced by $\tilde{\delta}$. In this new notation, the solitary wave is described by two independent parameters $\tilde{\delta}$ and v. Equations (2.25a) and (2.25b) have solitary wave solutions for $-1<\tilde{\delta}/\beta<1$, for which the average soliton frequency is given by Eq. (2.23b) as $\omega^2=1+4\gamma\tilde{\delta}$. Clearly the average frequency of the moving soliton is shifted from the corresponding average frequency of the stationary soliton. At pre-

cisely midgap ($\delta=0$), there is no frequency shift. For $\delta \neq 0$, the average soliton frequency is pulled away from the midgap in a strongly velocity-dependent manner. In fact for high velocity solitons, the average frequency may be completely outside the gap. Nevertheless, the existence of these out-of-gap solitons is contingent on the presence of the PBG.

For the sum ψ of the phase angles,

$$\frac{\partial \psi}{\partial \zeta}=\frac{4}{3}\alpha \eta^2 v \gamma^2 A^2. \tag{2.26}$$

Using solution (2.20a), this can be integrated to give

$$\psi=\frac{4}{3}\frac{\alpha v \eta^2}{(1-v^2)}\arctan[b\ \tanh(a\zeta)] \tag{2.27}$$

Combining these results, we obtain (for $\alpha=1$)

$$\Psi(x,t)=\eta A(\zeta)e^{iv\gamma\tilde{\delta}x}\begin{pmatrix}\lambda^{1/4}e^{i[\psi(\zeta)+\phi(\zeta)]}\\ \lambda^{-1/4}e^{i[\psi(\zeta)-\phi(\zeta)]}\end{pmatrix}. \tag{2.28}$$

Clearly, if $v=0$, then $\eta=1$ and $\psi=0$. Solution (2.28) then reduces to the static solution as required. In other words, once the static 1D solitary wave solution is known, it is easy to generalize it to a moving solitary wave using the preceding steps.

For $d>1$, the generalization to moving solitons is nontrivial since the Lorentz transformation does not completely reduce the time-dependent nonlinear wave equations to the corresponding static equations. In Sec. IV, we use a variational method to obtain an approximate time-dependent solution for the 2D X solitary wave.

III. EXISTENCE OF SOLITARY WAVE SOLUTIONS FOR $D>1$: NEAR BAND EDGE APPROXIMATION

Unlike the 1D case, for $d>1$ an analytic solution to the solitary wave equation is not always possible. Our approach to the higher-dimensional solitary waves is to obtain an approximate solution using a variational method. This variational method recaptures all the important features of the soliton solution in one dimension. For $d>1$, we begin by considering the condition for the existence of a solitary wave solution. We also consider the limiting case of near band edge solitary waves in which the full nonlinear wave equation reduces to a simple NLSE. In this case the existence of a solitary wave can be reduced by means of analogy to the existence of a finite action trajectory of a classical particle in a potential well.

First we derive a *necessary* condition for the existence of the solitary wave solutions to Eq. (2.7). Consider the function

$$\Psi=\frac{1}{\sqrt{ab}}\tilde{\Psi}\left(\frac{x}{a},\frac{y}{b}\right), \tag{3.1}$$

where $\tilde{\Psi}$ is a solution to Eq. (2.7). Clearly, $Q=\int d^2\vec{r}\ \Psi^\dagger\Psi$ is invariant under the scale transformations defined by the parameters a and b. It is useful to construct an ''action'' functional for the static solitary wave defined by

$$S_X(a,b)\equiv\int d^2\vec{r}\Big(b^{-2}|\partial_y\Psi|^2-a^{-1}\Psi^\dagger\sigma_z\partial_x\Psi - \Psi^\dagger(\delta+\beta\sigma_x)\Psi-\frac{\alpha}{2}a^{-1}b^{-1}(\Psi^\dagger\Psi)^2\Big). \tag{3.2}$$

Using this definition, it is straightforward to verify that Eq. (2.7) is the stationary point of Eq. (3.2) with respect to variation of $\Psi^\dagger(r)$, i.e., $\delta S_X/\delta\Psi^\dagger=0$. Since Ψ is a solution to Eq. (2.7), it follows (as a special case of the extremum principle) that

$$\frac{\partial S_X}{\partial a}=\left.\frac{\partial S_X}{\partial b}\right|_{a=b=1}=0. \tag{3.3}$$

This leads to the following two conditions:

$$\int d^2\vec{r}(\Psi^\dagger i\sigma_z\partial_x\Psi)=-\frac{\alpha}{2}\int d^2\vec{r}(\Psi^\dagger\Psi), \tag{3.4a}$$

$$2\int d^2\vec{r}|\nabla_y\Psi|^2=\frac{\alpha}{2}\int d^2\vec{r}(\Psi^\dagger\Psi)^2. \tag{3.4b}$$

Clearly condition (3.4b) can only be satisfied when $\alpha>0$, since both integrals are positive. This means that a localized X solitary wave does not exist for a negative nonlinear Kerr coefficient. This simple scaling argument can also be applied to the M solitary wave solution by constructing an appropriate ''action'' functional S_M. This leads in an analogous manner to the following necessary conditions for the existence of an M solitary wave:

$$\int d^2\vec{r}(\Psi^\dagger i\gamma_1\partial_x\Psi)=-\frac{\alpha}{2}\int d^2\vec{r}U_{\rm NL}(\Psi^\dagger,\Psi) \tag{3.5a}$$

and

$$\int d^2\vec{r}(\Psi^\dagger i\gamma_2\partial_y\Psi)=-\frac{\alpha}{2}\int d^2\vec{r}U_{\rm NL}(\Psi^\dagger,\Psi). \tag{3.5b}$$

Here, $U_{\rm NL}$ is defined as

$$U_{\rm NL}(\Psi^\dagger\Psi)=3(\Psi^\dagger\Psi)^2-(\Psi^\dagger\gamma_4\Psi)^2.$$

Clearly Eqs. (3.5) can be satisfied for both signs of α. In other words, the symmetrical M solitary wave exists for either sign of the Kerr coefficient. Although the present argument only provides a necessary condition of soliton existence, in practice this often provides a sufficient condition as well. In order to proceed further, we consider a frequency close to the band edge. In this case it is possible to derive an effective nonlinear Schrödinger equation, from which a complete existence proof of solitary wave solutions can be obtained by means of a mechanical analogy. First we consider the X solitary wave Eq. (2.7). Introducing the Fourier transformation $\Psi(\vec{q})=\int_{\vec{r}}e^{-i\vec{q}\cdot\vec{r}}\Psi(\vec{r})$ and using the notation $\int_{\vec{r}}\equiv\int d^2\vec{r}$, $\int_{\vec{q}}\equiv\int d^2\vec{q}/(2\pi)^2$, Eq. (2.7) becomes

$$[-q_x\sigma_z-q_y^2+\delta]\Psi(\vec{q})+F_{\rm NL}\{\Psi\}=0, \tag{3.6}$$

where the nonlinear functional $F_{\mathrm{NL}}\{\Psi\} \equiv \alpha \int_{\vec{q}_1}\int_{\vec{q}_2}(\Psi^{\dagger}(\vec{q}_1)\Psi(\vec{q}_2))\Psi(\vec{q}+\vec{q}_1-\vec{q}_2)$.

The linear part of Eq. (3.6) can be diagonalized using the $\vec{q}$-dependent unitary operator

$$S(\vec{q})=\begin{pmatrix} \sin\left(\frac{\theta}{2}\right) & \cos\left(\frac{\theta}{2}\right) \\ \cos\left(\frac{\theta}{2}\right) & -\sin\left(\frac{\theta}{2}\right) \end{pmatrix}, \tag{3.7}$$

where $\tan(\theta)=\beta/q_x$. Introducing the new spinor field $\Phi(\vec{q})\equiv S^{\dagger}(\vec{q})\Psi(\vec{q})$, Eq. (3.6) becomes

$$[\sqrt{q_x^2+\beta^2}\sigma_z - q_y^2+\delta]\Phi(\vec{q})+F_{\mathrm{NL}}\{\Phi(\vec{q})\}=0 \tag{3.8}$$

The photonic band edge occurs at $|\vec{q}|=0$. Near band edge behavior may be described by expanding the dispersion relation for small $|\vec{q}|$,

$$\sqrt{1+\left(\frac{q_x}{\beta}\right)^2}=\left[1+\frac{1}{2}\left(\frac{q_x}{\beta}\right)^2-\frac{1}{8}\left(\frac{q_x}{\beta}\right)^4+\cdots\right]. \tag{3.9}$$

Within this approximation, we replace $S(\vec{q})$ by $S(0)$, so that $\Phi(\vec{q})\simeq S^{\dagger}(0)\Psi(\vec{q})$. Retaining only quadratic terms in the dispersion and transforming the equation back to coordinate space, we obtain,

$$\{-\sigma_z\partial_{xx}/2\beta+\partial_{yy}+\delta+\beta\sigma_z+\alpha[\Phi^{\dagger}(\vec{r})\Phi(\vec{r})]\}\Phi(\vec{r})=0. \tag{3.10}$$

Solutions may be found for $\alpha=-1$ by choosing $\Phi^{\dagger}=(\tilde{E}_1,0)$, and for $\alpha=1$ by choosing $\Phi^{\dagger}=(0,\tilde{E}_2)$. In this case we obtain two uncoupled nonlinear equations for $\tilde{E}_1$ and $\tilde{E}_2$. Near the upper band edge ω_+,

$$\left[-\frac{1}{2\beta}\partial_{xx}-\partial_{yy}+\frac{(\omega_+^2-\omega^2)}{4}-\alpha|\tilde{E}_2|^2\right]\tilde{E}_2=0. \tag{3.11a}$$

Near the lower band edge ω_-,

$$\left[-\frac{1}{2\beta}\partial_{xx}+\partial_{yy}+\frac{(\omega^2-\omega_-^2)}{4}+\alpha|\tilde{E}_1|^2\right]\tilde{E}_1=0. \tag{3.11b}$$

In Eq. (3.11a), the term $-\alpha|\tilde{E}_2|^2$ acts as an attractive scattering potential (for $\alpha>0$) in both x and y directions, and a repulsive potential for ($\alpha<0$). This leads to a self-trapped state of light (solitary wave) only when $\alpha>0$. On the other hand, the term $\alpha|\tilde{E}_1|^2$ in Eq. (3.11b) acts as attractive potential in the x direction, but a repulsive potential in the y direction (for $\alpha<0$), or vice versa for ($\alpha>0$). Consequently, there exist no localized solitary wave solutions when $\alpha<0$ as predicted by the scaling argument in Eq. (3.4b). Equation (3.11b) has solutions which are extended in the y direction. These solutions have a total energy which increases linearly with the size of the sample, and we do not consider them here.

Following the same procedure, we can obtain near band edge equations for the M solitary wave. After the transformation to $\vec{q}$ space, and applying the ''effective mass approximation,'' Eq. (2.13) becomes

$$\left[\gamma_1\left(\beta+\frac{1}{2\beta}q_x^2\right)+\gamma_4\left(\beta+\frac{1}{2\beta}q_y^2\right)+\delta_M\right]\Phi(q) + \tilde{F}_{\mathrm{NL}}\{\Phi\}=0, \tag{3.12}$$

where $\delta_M=(\omega^2-1)/4$, $\Phi(\vec{q})=S^{\dagger}(0)\Psi(\vec{q})$,

$$S(0)=\begin{pmatrix} \frac{1}{2} & 0 & -1/\sqrt{2} & -\frac{1}{2} \\ \frac{1}{2} & 0 & 1/\sqrt{2} & -\frac{1}{2} \\ \frac{1}{2} & -1/\sqrt{2} & 0 & \frac{1}{2} \\ \frac{1}{2} & 1/\sqrt{2} & 0 & \frac{1}{2} \end{pmatrix}, \tag{3.13}$$

and $\tilde{F}_{\mathrm{NL}}\{\Phi\}$ is the appropriate nonlinear functional of $\Phi(\vec{q})$. Equation (3.12) in coordinate space yields

$$\left[-\frac{\gamma_1}{2\beta}\frac{\partial^2}{\partial x^2}-\frac{\gamma_4}{2\beta}\frac{\partial^2}{\partial y^2}+\beta(\gamma_1+\gamma_4)+\delta_M+\alpha[3(\Phi^{\dagger}\Phi) - (\Phi^{\dagger}\gamma_4'\Phi)\gamma_4']\right]\Phi(x,y)=0, \tag{3.14}$$

where $\gamma_4'=S^{\dagger}\gamma_4 S$. In this case, localized solitary wave solutions of the nonlinear Schrödinger equation are possible for both $\alpha=\pm 1$. Since the matrix (3.13) rotates the original spinor field Ψ, the symmetric M solitary wave amplitude takes the form $\Phi^{\dagger}=(\tilde{E}_1,0,0,0)$ near the lower band edge. Using this ansatz, Eq. (3.14) reduces to

$$\left[-\frac{1}{2\beta}\frac{\partial^2}{\partial x^2}-\frac{1}{2\beta}\frac{\partial^2}{\partial y^2}+\frac{(\omega^2-\omega_-^2)}{4}+3\alpha|\tilde{E}_1|^2\right]\tilde{E}_1(x,y)=0. \tag{3.15a}$$

Near the upper band edge, the ansatz $\Phi^{\dagger}=\Phi(0,0,0,\tilde{E}_4)$ yields

$$\left[-\frac{1}{2\beta}\frac{\partial^2}{\partial x^2}-\frac{1}{2\beta}\frac{\partial^2}{\partial y^2}+\frac{(\omega_+^2-\omega^2)}{4}-3\alpha|\tilde{E}_4|^2\right]\tilde{E}_4(x,y)=0. \tag{3.15b}$$

Using the quantum-mechanical potential well analogy, it can be seen that Eq. (3.15a) has a localized solution for $\alpha=-1$. Similarly Eq. (3.15b) leads to a finite energy solitary wave for $\alpha=+1$. In Sec. IV, we use a variational method to extend both of these solutions throughout the entire photonic band-gap region.

A. Mechanical analogy for the NLSE

To demonstrate the existence of a finite energy solitary wave solution near a band edge, we make use of a mechanical analogy. From the earlier discussion, it is apparent that within the near band edge ''effective mass'' approximation, the electric field envelope function, satisfies an isotropic,

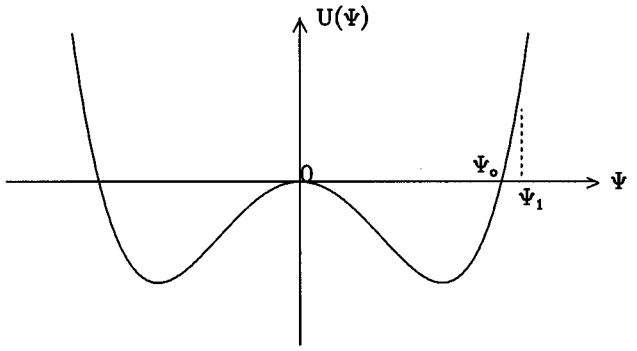

FIG. 3. The mechanical analogy for the NLSE consists of a potential, $U(\Psi)=-\alpha_1\Psi^2/2+\Psi^4/4$, in which a fictitious particle moves. For $d=1$, the particle is released from rest at $\Psi=\Psi_o$, and comes to rest at the top of the hill $\Psi=0$. This results in a nodeless localized solution in x. For $d>1$, the particle experiences a time-dependent, viscous damping force. Here the particle is released from a point $\Psi=\Psi_1>\Psi_o$ in order to compensate for the losses. The initial position Ψ_1 is chosen such that the particle comes to rest at the hill $\Psi=0$. This results in a nodeless localized solution. Unlike the 1D case, the particle may be released from a higher initial point such that it crosses the zero point and returns to $\Psi=0$. This solution results in one node. In general, there are an infinite number of solutions with more and more nodes.

nonlinear Schrödinger equation. If we consider an isotropic solution for each component of the spinor field, the effective NLSE in d dimensions near the upper band edge takes the form

$$\Psi_{rr}+\frac{(d-1)}{r}\Psi_r-\alpha_1\Psi+\Psi^3=0. \tag{3.16}$$

Here $\alpha_1=(\omega_+^2-\omega^2)/4$, and the x coordinate has been rescaled as $x'=x\sqrt{2\beta}$. It is useful to interpret Ψ as the coordinate of a classical particle at ''time'' r:

$$\Psi_{rr}=-\frac{\partial U}{\partial\Psi}-\frac{(d-1)}{r}\Psi_r, \tag{3.17}$$

where the potential U is given by

$$U=-\frac{\alpha_1\Psi^2}{2}+\frac{\Psi^4}{4}. \tag{3.18}$$

In addition to moving in the potential U, the particle experiences a ''time-dependent'' viscous damping force for $d>1$. For frequencies inside the gap ($\alpha_1>0$), in $d=1$, the soliton solution corresponds to a particle released from rest at position $\Psi=\Psi_o$ at ''time'' $r=0$. As $r\to\infty$, this particle comes to rest at $\Psi=0$ (see Fig. 3). Clearly, this is the only finite action solution. For $d>1$, it is necessary for the particle to be released at a position $\Psi_1>\Psi_o$ in order for it to overcome the viscous damping effect and come to rest at $\Psi=0$ as $r\to\infty$. This solution corresponds to a nodeless solitary wave solution. For $d>1$, if the particle is released from an even higher point, then it can cross $\Psi=0$, move to the second well, and then return to $\Psi=0$ as $r\to\infty$. This solution will have a node, and is a higher energy solitary wave solution. In this manner it is possible to create solutions of higher and higher energy with more and more nodes. For $d>1$, the solitary wave solution, for a given frequency ω, is not unique as it is for $d=1$. In this paper we consider only the nodeless solution which corresponds to the fundamental solution. The near band edge solutions that we derived using this mechanical analogy provide a plausibility argument for the existence of solitary wave solutions throughout the PBG for $d>1$. It also suggests that nonlinear wave solutions of finite energy in a PBG are not unique at a given frequency for $d>1$.

B. Solitary wave propagation in a lossy-gain medium

Real PBG materials will invariably have small absorption losses. If the solid backbone is of ''fiber-optic quality'' these losses may be small. However, nonresonant impurities and vibrations of constituent atoms of the solid, will tend to slowly dissipate energy from the solitary wave. In addition, the sculpting processes required to construct a PBG from a bulk semiconductor creates a large amount of surface area for the solid PBG backbone. Surfaces of electronic semiconductors can lead to unoccupied surface electronic states which may be excited by light within the PBG. Finally, the PBG material can be doped with resonant impurities which can either absorb light or provide gain. A realistic treatment of nonlinear wave propagation in a PBG material must account for these effects. We discuss, below, a special case for which a simple analytic solution is possible.

The NLSE may be generalized to include linear loss (gain) and/or nonlinear loss (gain). In the case of only linear loss (gain) or nonlinear loss (gain), stable stationary solutions may not exist. However, when both linear and nonlinear losses or gain are included, the two processes may balance each other, resulting in a stable solution. We illustrate this effect for $d=1$ using the nonlinear Schrödinger equation, obtained from the ''effective mass approximation,'' near the upper band edge with a complex refractive index

$$i\frac{\partial E}{\partial t}+\frac{1}{2\beta}\frac{d^2E}{dx^2}-\alpha_1E+i\Gamma_LE+(n_{\rm NL}+i\Gamma_{\rm NL})|E|^2E=0. \tag{3.19}$$

Here the imaginary part of the linear susceptibility Γ_L is positive for a lossy medium, and negative in a gain medium. The imaginary part $\Gamma_{\rm NL}$ of the nonlinear susceptibility is positive when there is two-photon absorption loss, and negative when there is two-photon gain. We seek solutions to Eq. (3.19) in which the electric field amplitude can be written as $E(x,t)=\varepsilon(\zeta)e^{i[kx+\phi(\zeta)]}$, where $\zeta=t-x/V$, and V is velocity of the soliton. Inserting this into Eq. (3.19), and separating the real and imaginary parts, yields

$$-\tau\dot{\varepsilon}+(\dot{\varepsilon}\dot{\phi})/\beta+\varepsilon\ddot{\phi}+\Gamma_L\varepsilon+\Gamma_{\rm NL}\varepsilon^3=0, \tag{3.20a}$$

$$\tau\varepsilon\dot{\phi}+\ddot{\varepsilon}/2\beta-\varepsilon(\dot{\phi})^2/2\beta-\alpha\varepsilon+n_{\rm NL}\varepsilon^3=0, \tag{3.20b}$$

where $\alpha=(\alpha_1+k^2/2\beta)$, $\tau=(k/\beta-V)$, and the dot represents the derivative with respect to the independent variable ζ. Equtaions (3.20) allow a solution of the forms

$$\varepsilon(\zeta)=A\ \mathrm{sech}(a\zeta), \tag{3.21}$$

$$\phi(\zeta)=b\ \ln[\mathrm{sech}(a\zeta)], \tag{3.22}$$

where $A^2=-3\Gamma_L/2\Gamma_{\rm NL}$, $a^2=-\Gamma_L\beta/b$, $b=\alpha_1/\Gamma_L \pm\sqrt{(\alpha/\Gamma_L)^2+1}$, and $V=k/\beta$. For a physically admissible stationary solution, we require that Γ_L and $\Gamma_{\rm NL}$ have opposite signs. Also Γ_L and b must have opposite signs.

IV. VARIATIONAL METHOD

For many one-dimensional nonlinear wave equations, an exact analytical solution can be found. In higher dimensions this is no longer possible. Since numerical methods are generally quite cumbersome, it is useful to develop an approximate analytical approach. We do this by reformulating the problem variationally. A variational approach for nonlinear pulse propagation in optical fibers was used by Anderson [40] for the nonlinear Schrödinger equation. By using a simple Gaussian trial function, the pulse width, amplitude, and frequency chirp were recaptured, in good agreement with the numerical analysis. Our variational method is based on minimizing a functional of the system using a suitable trial solitary wave function. We show that with only a few variational parameters, most of the important physics can be recaptured. The effectiveness of the method is confirmed by comparing the variational solution to the exact solution in one dimension. For $d>1$, our variational solution provides a good approximation to the numerical solution obtained in Sec. V.

We first illustrate the variational method for one-dimensional gap solitons, and then generalize the method to higher dimensions. Consider the Lagrangian density for the 1D spinor field in the SVEA:

$$\mathcal{L}=\frac{i}{2}(\Psi_t^\dagger\Psi-\Psi^\dagger\Psi_t+\Psi_x^\dagger\sigma_z\Psi-\Psi^\dagger\sigma_z\Psi_x) -\Psi^\dagger(\delta+\beta\sigma_x)\Psi-\frac{\alpha}{2}[(\Psi^\dagger\Psi)^2-(\Psi^\dagger\sigma_z\Psi)^2]. \tag{4.1}$$

The nonlinear wave equation follows from the least action principle

$$\delta\widetilde{S}=0 \tag{4.2}$$

where the action $\widetilde{S}=\int dx\,dt\,\mathcal{L}$. In particular, the Euler-Lagrange equation

$$\frac{\delta\mathcal{L}}{\delta\Psi^\dagger}=\frac{\partial}{\partial t}\left(\frac{\partial\mathcal{L}}{\partial\Psi_t^\dagger}\right)+\frac{\partial}{\partial x}\left(\frac{\partial\mathcal{L}}{\partial\Psi_x^\dagger}\right)-\frac{\partial\mathcal{L}}{\partial\Psi^\dagger}=0 \tag{4.3}$$

is equivalent to the one-dimensional version of Eq. (2.5). We consider a special class of solutions moving with velocity v of the form

$$\Psi(x,t)=\Psi(\zeta,\tau)e^{i\Delta kx}, \tag{4.4}$$

where $\zeta=x-vt$ and $\tau=t$. In this case the Lagrangian density (4.1) takes the form

$$\mathcal{L}=\frac{i}{2}[\Psi_\tau^\dagger\Psi-\Psi^\dagger\Psi_\tau+(1-v)(\Psi_\zeta^\dagger\sigma_z\Psi-\Psi^\dagger\sigma_z\Psi_\zeta)] -\Psi^\dagger(\delta-\Delta k\sigma_z)\Psi-\beta\Psi^\dagger\sigma_x\Psi-\frac{\alpha}{2}[(\Psi^\dagger\Psi)^2 -(\Psi^\dagger\sigma_z\Psi)^2]. \tag{4.5}$$

The Euler-Lagrange equation is now equivalent to the one-dimensional version of Eq. (2.22), where the action is given as $\widetilde{S}=\int d\tau\,d\zeta\,\mathcal{L}$. Rather than solving the wave Eq. (2.22) directly, we consider extrema of the action parametrized by the variational trial function

$$E_{1,2}(\zeta)=\varepsilon_{1,2}(\zeta)e^{i\phi_{1,2}(\zeta)}. \tag{4.6}$$

Here $\varepsilon_{1,2}(\zeta)$ is the amplitude of the solitary wave, and $\phi_{1,2}(\zeta)$ is the corresponding phase angle function. The integration over the independent variable τ from 0 to T becomes trivial in this case. Accordingly, we define $S=\widetilde{S}/T$. Substituting the trial function into the functional (4.5), we obtain

$$S=\int d\zeta\Bigg[(1-v)\varepsilon_1^2\frac{\partial\phi_1}{\partial\zeta}-(1+v)\varepsilon_2^2\frac{\partial\phi_2}{\partial\zeta}-(\delta-\Delta k)\varepsilon_1^2 -(\delta+\Delta k)\varepsilon_2^2-2\beta\cos(\phi_1-\phi_2)-\frac{\alpha}{3}(\varepsilon_1^4+\varepsilon_2^4 +4\varepsilon_1^2\varepsilon_2^2)\Bigg]. \tag{4.7}$$

When $v=0$, then ζ and τ reduce to the laboratory coordinates x and t, respectively. A particularly simple trial function consists of choosing a Gaussian amplitude $\varepsilon_{1,2}=A_{1,2}e^{-a^2\zeta^2}$ and a linear phase modulation $\phi_{1,2}=c+k_{1,2}\zeta$. Inserting this trial function into the functional S, we obtain

$$(S\sqrt{2})/\sqrt{\pi}=\Bigg[(1-v)A_1^2k_1-(1+v)A_2^2k_2-(\delta-\Delta k)A_1^2 -(\delta+\Delta k)A_2^2-2\beta\cos(2c)e^{-(k_1-k_2)/8a^2} -\frac{\sqrt{2}\alpha}{6}(A_1^4+A_2^4+4A_1^2A_2^2)\Bigg]\Big/\,a. \tag{4.8}$$

Solving the equations $\partial S/\partial\tau_i=0$ with $\tau_i=A_{1,2},a,k_{1,2},c$, we obtain a set of algebraic equations. It is convenient to define the following new variables: $k=(k_1-k_2)/2$, $k'=(k_1+k_2)/2$, $A_{1,2}=\lambda_{1,2}\eta A^2$, $(\lambda_1=\lambda^{1/4},\ \lambda_2=\lambda^{-1/4})$, $\widetilde{\delta}=\delta/\gamma$, and $\Delta k=v\delta$. Here, λ, η, and γ are the same as given in Sec. II B. In terms of these new variables, the variational equations take the forms

$$\beta\cos(2c)e^{-\xi/2}(1-\xi)+\widetilde{\delta}=0, \tag{4.9a}$$

$$k/\gamma=-\beta\cos(2c)\xi e^{-\xi/2}, \tag{4.9b}$$

$$\alpha A^2=-2\beta\cos(2c)\xi e^{-\xi/2}/\sqrt{2}, \tag{4.9c}$$

$$k'/\gamma=\frac{2\sqrt{2}}{3}v\gamma^2\alpha\eta^2A^2, \tag{4.9d}$$

where $\xi = k^2/a^2$, and $\cos(2c) = \pm 1$. For a given detuning $\tilde{\delta}$, we solve for ξ in Eq. (4.9a). All other parameters are then evaluated easily. However, for this simple trial function, a soliton solution cannot be found for the entire band-gap region. There is a critical value of $\tilde{\delta}_c = 0.445\beta \cos(2c)$, such that for positive nonlinearity [$\alpha > 0$, $\cos(2c) = -1$] a solution can be obtained for $\delta_+ < \tilde{\delta} < \tilde{\delta}_c$ and for negative nonlinearity [$\alpha < 0$, $\cos(2c) = 1$] a solution can be obtained for $\tilde{\delta}_c < \tilde{\delta} < \delta_-$. The reason for this is that the phase modulation and the exponential localization of the exact solution differ significantly from the above trial function at either band edge. We discuss this effect in more detail below, for the case when $v = 0$. Consider the midgap case $\delta = 0$ and $\alpha = 1$. Then $a = 0.6\beta/\sqrt{1-v^2}$, describes Lorentz contraction of the soliton along the direction of propagation. The peak intensity is given by $A^2 = 0.86\eta^2\beta$. Thus, using a simple trial function, the qualitative physical features of the time-dependent solution can be recaptured.

When $v = 0$, Eqs. (4.9) reduce to the static solution, where $\delta = \tilde{\delta}$, $\gamma = 1$, $\eta = 1$, and $k' = 0$. For $\alpha = +1$, and a frequency close to the upper band edge ($\delta \simeq \beta$), $\xi \ll 1$. In this limit, $A^2 = (\omega_+^2 - \omega^2)/3\sqrt{2}$, $a = \sqrt{(\omega_+^2 - \omega^2)\beta/6}$, $k = (\omega_+^2 - \omega^2)/6$, and $\cos(2c) = -1$. Near the band edge the total energy scales as $Q = \sqrt{2\pi(\omega_+^2 - \omega^2)/3\beta}$. As $\omega \to \omega_+$, the soliton energy vanishes.

For $\alpha = +1$, when the frequency is close to the upper band edge ($\delta \simeq \beta$), then $A, a, b \ll 1$. In this limit, the exact solution in Eq. (2.20) can be approximated as $A^2(x) = A\ \mathrm{sech}(ax)$ and $\phi = \pi/2 + b \tanh(ax)$. Here the phase angle increases linearly with x in the core of the amplitude function $A(x)$, but saturates in the wings when $A^2(x) \to 0$. On the other hand, when the frequency is close to the lower band edge $\delta \simeq -\beta$, the scale parameter a in Eq. (2.20) goes to zero, but the parameter b becomes very large and determines the size of solitary wave. In the core region ($ax \ll 1$), the amplitude takes the approximate form $A^2(x) = a/[1 + (abx)^2]$ and the phase angle is approximately $\phi = \pi/2 + \arctan(bax)$. Here the phase angle saturates well before the exponential decay of the amplitude sets in. Our simple trial function fails to capture the required phase modulation near the lower band edge. A variational result for the *entire* band-gap region can be obtained by choosing a trial phase angle of the form $\phi(x) = c + \arctan(kx)$. However, with this trial function all the integrals cannot be evaluated analytically. As an alternative, we may separate the real and imaginary parts of $E = u + iv$, and use the trial functions ($\alpha = +1$), $u = Bxe^{-a^2x^2}$ and $v = Ae^{-a^2x^2}$, where A, a, and b are variational parameters. This trial function yields an analytical solution for the entire band-gap region. In Fig. 4 we compare the exact solution to this variational Gaussian trial function at midgap $\omega^2 = 1$.

Having obtained a variational solution for the one-dimensional gap soliton, we proceed to apply this method to the two-dimensional PBG. The simplest gap solitary wave for the 2D PBG is the X solitary wave. The corresponding action functional is similar to Eq. (4.7), except for the addition of the y coordinate. Using the trial function $E_{1,2}(\zeta, y) = \varepsilon_{1,2}(\zeta, y)e^{i\phi_{1,2}(\zeta)}$, the appropriate action functional takes the form

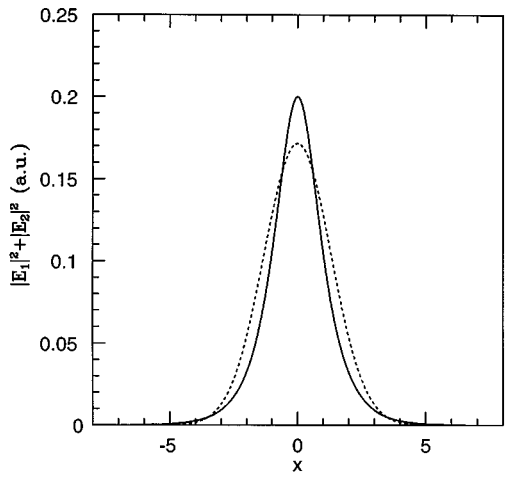

FIG. 4. Plotted is the quantity $|E_1|^2 + |E_2|^2$ (in arbitrary units) vs the spatial variable x (arbitrary units), for the exact analytical gap solitary wave solution (solid line) and the variational Gaussian trial function (dotted line) for the midgap frequency $\delta = 0$. The other parameters are chosen as $\beta = 0.1$ and $\alpha = +1$.

$$S_X = \int d\zeta\, dy \Bigg\{ (1-v)\varepsilon_1^2 \frac{\partial \phi_1}{\partial \zeta} - (1+v)\varepsilon_2^2 \frac{\partial \phi_2}{\partial \zeta} + \left(\frac{\partial \varepsilon_1}{\partial y}\right)^2 + \left(\frac{\partial \varepsilon_2}{\partial y}\right)^2 - (\delta - \Delta k)\varepsilon_1^2 - (\delta + \Delta k)\varepsilon_2^2 - 2\beta \cos(\phi_1 - \phi_2) - \frac{\alpha}{3}(\varepsilon_1^4 + \varepsilon_2^4 + 4\varepsilon_1^2\varepsilon_2^2) \Bigg\}. \quad (4.10)$$

In order to obtain a localized, finite energy solitary wave, we choose $\varepsilon_{1,2}(\zeta, y) = A_{1,2}e^{-a^2\zeta^2 - b^2y^2}$ and $\phi_{1,2} = c + k_{1,2}\zeta$. Inserting this into the functional and performing the integration, we obtain

$$2S_X/\pi = \Bigg[(1-v)A_1^2k_1 - (1+v)A_2^2k_2 + A_1^2b^2 + A_2^2b^2 - (\delta - \Delta k)A_1^2 - (\delta + \Delta k)A_2^2 - 2\beta \cos(2c)e^{-(k_1-k_2)/8a^2} - \frac{\sqrt{2}\alpha}{6}(A_1^4 + A_2^4 + 4A_1^2A_2^2) \Bigg] \Big/ ab. \quad (4.11)$$

Extremizing S_X with respect to the variational parameters $A_{1,2}, a, b, c$ and $k_{1,2}$ leads to a set of conditions analogous to Eq. (4.9):

$$\beta \cos(2c)e^{-\xi/2}(1 - \xi/2) + \tilde{\delta} = 0, \quad (4.12a)$$

$$k/\gamma = -\beta \cos(2c)\xi e^{-\xi/2}/2, \quad (4.12b)$$

$$\gamma b^2 = -\beta \cos(2c)\xi e^{-\xi/2}/2, \quad (4.12c)$$

$$\alpha A^2 = -2\beta \cos(2c)\xi e^{-\xi/2}, \quad (4.12d)$$

$$k'/\gamma = -v\gamma b^2 + \tfrac{2}{3}\alpha v \eta^2 A^2. \quad (4.12e)$$

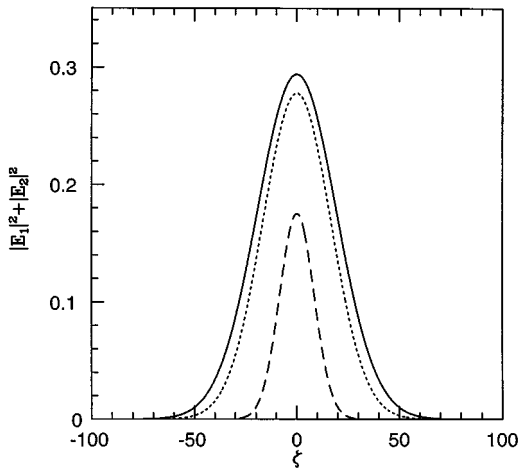

FIG. 5. Plotted is the energy density $|E_1|^2+|E_2|^2$ (a.u.) for the 2D X solitary wave as a function of the propagation direction $\zeta=x-vt$ ($y=0$), for the case when $v=0$ (solid line), $v=0.5$ (dotted line), and $v=0.9$ (long-dashed line). Here the velocity is in units of the average speed of the light in the medium. The Lorentz contraction becomes more apparent as the velocity approaches the speed of light in the medium ($v\rightarrow 1$). Here $\delta=0$ and $\beta=0.1$.

Here all the parameters are defined as in Eq. (4.9). The significant difference from the 1D case is the additional term $-v\gamma b^2$ in Eq. (4.12e). To illustrate how the moving solitary wave differs from the stationary one, we consider the midgap case $\delta=0$. In Fig. 5 we compare the energy density $|E_1|^2+|E_2|^2$ (as a function of $\zeta=x-vt$) for the the stationary solitary wave $v=0$, $\zeta=x$ (solid line) with moving ones of velocity $v=0.5$ (dotted line) and $v=0.9$ (long-dashed line). Similarly, in Fig. 6 the energy density is plotted in the transverse direction y for the same parameters. The solitary wave undergoes a Lorentz contraction in the moving direction, whereas it expands in the transverse direction when $v\neq 0$. These effects are most apparent when velocity approaches the average speed of light in the medium. The required incident intensity can be estimated by

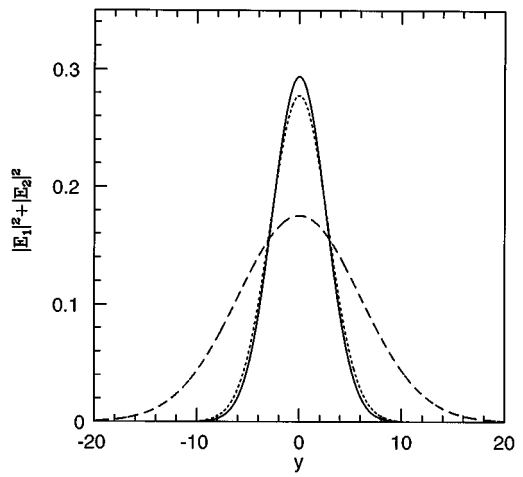

FIG. 6. Plotted is the energy density $|E_1|^2+|E_2|^2$ (a.u.) for the 2D X solitary wave as a function of the transverse direction y ($\zeta=0$), for the case when $v=0$ (solid line) $v=0.5$ (dotted line) and $v=0.9$ (long-dashed line), where the velocity is in units of the average speed of the light in the medium. This expansion of the solitary wave in the transverse direction becomes more apparent as the velocity approaches the speed of light in the medium ($v\rightarrow 1$). Here $\delta=0$ and $\beta=0.1$.

$$I_{in}\propto|E_1|^2=3(1+v)^{3/2}\sqrt{1-v}A^2/(3-v^2), \quad (4.13)$$

which vanishes as v approaches the speed of light in the medium. The backward flux is proportional to $|E_2|^2$, and can be found by replacing v with $-v$ in Eq. (4.13). Similarly, the total energy $Q=\int d^dr(|E_1|^2+|E_2|^2)$ of a solitary wave associated with a twofold symmetry point in a d-dimensional PBG material can be scaled as

$$Q(v)=(1-v^2)^{(5-d)/4}\frac{3}{3-v^2}Q(0). \quad (4.14)$$

This describes both the 2D X solitary wave and the 3D L solitary wave, which we introduce in Sec. VII.

As in the 1D case, the Gaussian trial function with linear phase modulation yields a solitary wave throughout most, but not all of the gap at the X point. The complete photonic band gap for the 2D square lattice consists of the intersection of the gap at the X point and the gap at the M point. For this complete gap region, the above ansatz nevertheless provides a simple but valuable approximation to the solitary wave solution.

Since the asymptotic behavior of the soliton wave function is actually of the form $e^{\pm x}$, a more accurate trial function is (for $v=0$)

$$A(x,y)=A\ \mathrm{sech}(ax)\mathrm{sech}(by) \quad (4.15a)$$

and

$$\phi(x,y)=c+\arctan[d\ \tanh(ax)]. \quad (4.15b)$$

Inserting the ansatz (4.15) for Ψ_{trial} into the functional S_X, we obtain,

$$\begin{aligned} S_X/8=&A^2[\arctan(d)-1/d+\arctan(d)/d^2]/b+A^2b/3a\\ &-A^2\delta/ab-4\alpha A^4/9ab\\ &-\cos(2c)\beta A^2[2\arctan(d)/d-1]/ab. \end{aligned} \quad (4.16)$$

The extremum conditions $\partial S_X/\partial\tau_i=0$ for the variational parameters $\tau_i=A,a,b,d$, and c leads to the algebraic equations

$$b^2=2\alpha A^2/3, \quad (4.17a)$$

$$a=\beta\cos(2c)[d^2/(1+d^2)-d\arctan(d)]/[d-\arctan(d)], \quad (4.17b)$$

$$\begin{aligned} &a[\arctan(d)-1/d+\arctan(d)/d^2]/2+\delta\\ &+\cos(2c)\beta[2\arctan(d)/d-1]=0, \end{aligned} \quad (4.17c)$$

$$\alpha A^2=9[\arctan(d)-1/d+\arctan(d)/d^2]a/4, \quad (4.17d)$$

$$\cos(2c)=\pm 1. \quad (4.17e)$$

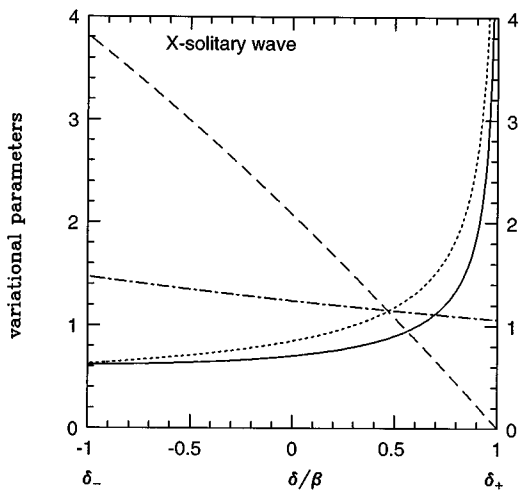

FIG. 7. Plotted are the variational parameters, for the X-solitary wave solution versus the detuning frequency δ/β, $(\beta=\Delta\epsilon/8\tilde{\epsilon})$ measured in units of ω_o^{-1}. The soliton size parameters are $\beta/(a)$ (solid line) and $\sqrt{\beta}/(b)$ (dotted line) in units of $a_o/2\pi$, where a_o is the lattice constant. The intensity is given by A^2/β (short-dashed line) in units of λ^{-1}, where $\lambda=2\tilde{\epsilon}/9\pi|\chi^{(3)}|$. The quantity $\sqrt{\beta}A^2/(ab)$ (dotted short-dashed line), is proportional to the total energy of the solitary wave.

Here a solution is possible for the entire band gap $\omega_-^X<\omega<\omega_+^X$, for $\alpha=+1$. From Eq. (4.17a) it is easy to see that a localized solution is not possible when $\alpha=-1$ (negative Kerr coefficient), as predicted in the scaling argument. In Fig. 7 the solution for the variational parameters is plotted as a function of the detuning frequency δ from the mid gap. Near the upper band edge, ω_+, $d\ll 1$, so that we may expand arctan(d) in a Taylor series. This leads to the analytical solution $a=\sqrt{3\beta(\omega_+^2-\omega^2)/4}$, $A^2=9(\omega_+^2-\omega^2)/16$, $b=\sqrt{3(\omega_+^2-\omega^2)/8}$ and $d=\sqrt{3(\omega_+^2-\omega^2)/16\beta}$. The total energy can be found for frequencies close to the the upper band edge as $Q=3\sqrt{8/\beta}$.

The M solitary wave is a new type of solution for which there is no analog in one dimension. It is purely a result of the 2D PBG structure. It resembles the structure of two interacting 1D solitary waves. The general time-dependent solution is more complicated, so we only discuss the static solution. The action for the M solitary wave is given by

$$S_M=\int d^2\vec{r}\{\Psi^\dagger[i(\gamma_1\partial_x+\gamma_2\partial_y)+\delta_M+\beta\gamma_3]\Psi - \tilde{U}_{\rm NL}(\Psi^\dagger,\Psi)\}, \tag{4.18}$$

where $\tilde{U}_{\rm NL}(\Psi^\dagger,\Psi)=\frac{1}{2}\alpha(3(\Psi^\dagger\Psi)^2-(\Psi^\dagger\gamma_4\Psi)^2)$. The M solitary wave is described by a four-component spinor field resulting from Bragg scattering in both the x and y directions. We use the trial function $\Psi_{\rm trial}^\dagger=(\Psi_1^\dagger,\Psi_2^\dagger)$, where

$$\Psi_j=A_j(x,y)\begin{pmatrix} e^{i\phi_j(x,y)} \\ e^{-i\phi_j(x,y)}\end{pmatrix}, \quad j=1,2. \tag{4.19}$$

In terms of these amplitudes and phases,

$$S_M/2=\int d^2\vec{r}\Big(-A_1^2\frac{\partial\phi_1}{\partial x}-A_1^2\frac{\partial\phi_1}{\partial y}-A_2^2\frac{\partial\phi_2}{\partial x}+A_2^2\frac{\partial\phi_2}{\partial y} + \delta_M(A_1^2+A_2^2)+4A_1A_2\beta\cos(\phi_1)\cos(\phi_2) + 2\alpha(A_1^4+A_2^4+4A_1^2A_2^2)\Big). \tag{4.20}$$

Using the trial function

$$A_1(x,y)=A_2(x,y)=A\ \mathrm{sech}(ax)\mathrm{sech}(ay)$$

and

$$\phi_j(x,y)=c_j+\arctan[b\ \tanh(ax)] -(-1)^j\ \arctan(b\ \tanh(ax)), \quad j=1,2$$

we obtain

$$S_M/8=\{-2[\arctan(b)-1/b+\arctan(b)/b^2]/a + 2\beta[2\ \arctan(b)/b-1]\cos(c_1)\cos(c_2)/a^2+\delta_M/a^2 + 8\alpha A^2/3a^2\}A^2. \tag{4.21}$$

The extremum point of S_M with respect to the variational parameters is defined by the conditions:

$$a=\beta\cos(c_1)\cos(c_2)[b^2/(1+b^2) -b\arctan(b)]/[b-\arctan(b)],$$

$$\delta+2\beta\cos(c_1)\cos(c_2)[2\ \arctan(b)/b-1]=0,$$

$$\alpha A^2=[\arctan(b)-1/b+\arctan(b)/b^2]3a/8$$

and

$$\cos(c_1)\cos(c_2)=\pm 1.$$

These equations admit a solution for both $\alpha=\pm 1$. For $\alpha=+1$, $\cos(c_1)\cos(c_2)=-1$, and for $\alpha=-1$, $\cos(c_1)\cos(c_2)=1$. In Fig. 8, the solution to the variational problem is plotted against the detuning parameter $\delta_M=(\omega^2-2)/4$. Similarly, a variational solution can be obtained for the composite X solitary wave solution to Eq. (2.16). From the symmetry of the equations it can be seen that $E_{3,4}(x,y)=E_{1,2}(y,x)$. The results are qualitatively similar to those of the simple X solitary wave solution. Unlike the M solitary wave, the composite X solitary wave exists only for a positive Kerr coefficient.

A. Numerical estimates for 2D solitary waves in a PBG

The variational results are useful in determining some important physical quantities such as the total energy, peak intensity, and localization length of these solitary waves. The standard time-averaged electromagnetic field energy density is given by $\tilde{\epsilon}|E|^2/8\pi$, where the physical electric field is given by $\mathrm{Re}(\frac{1}{2}Ee^{-i\omega t})$. In our convention, the physical electric field is $\mathrm{Re}(Ee^{-i\omega t})$. Accordingly the energy density becomes $u=\tilde{\epsilon}|E|^2/2\pi$. Thus the total electromagnetic energy in our case is defined as $U=\tilde{\epsilon}Q/2\pi$, where $Q=\int d^dr(\Psi^\dagger\Psi)$. Similarly, the total time-averaged power

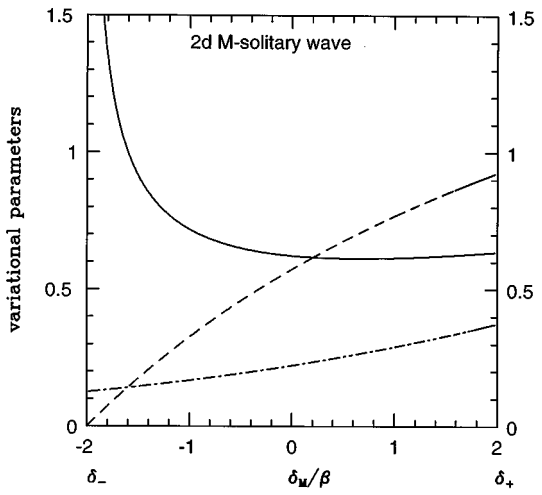

FIG. 8. Plotted are the variational parameters for the M solitary wave solution vs the detuning frequency δ_M/β, measured in terms of ω_o^{-1}. The soliton size parameter is $\beta/(a)$ (solid line), the intensity is A^2/β (short-dashed line), and the quantity $\sqrt{\beta}A^2/(2ab)$ (dotted short-dashed line) is proportional to the total energy of the M solitary wave.

flow (Poynting vector) is given by $S_p = c\,\bar{\epsilon}/2\pi\,(|E_1|^2 - |E_2|^2)$ for the X solitary wave solution. For a stationary soliton, $S_p = 0$, and there is no transfer of energy. Nevertheless, it is instructive to evaluate the forward flux, defined as $I_{\text{in}} = (c\,\bar{\epsilon}/2\pi)|E_1|^2$. This quantity provides a guide to the incident flux required to create a soliton using an external laser pulse. For the X solitary wave solution the total electromagnetic energy (per unit length transverse to the 2d Bragg grating) is given as

$$U\ \ (\text{J/cm}) = \frac{\bar{\epsilon}}{2\pi}\frac{8A^2}{\lambda abG^2} = 2.2\times 10^{-10}\frac{\bar{\epsilon}^2 a_o^2}{|\chi^{(3)}|}\left(\frac{A^2}{ab}\right). \tag{4.22}$$

Here, the lattice constant a_o and the Kerr coefficient $|\chi^{(3)}|$ are all given in (cgs) units. The total energy is measured in units of J/cm, since the medium is assumed to be translationally invariant along the z direction. The peak incident flux is given by

$$I_{\text{in}}\ \ (\text{W/cm}^2) = \frac{c\,\bar{\epsilon}}{2\pi}\frac{A^2}{\lambda} = 33.77\frac{\bar{\epsilon}^{3/2}}{|\chi^{(3)}|}A^2, \tag{4.23}$$

where the Kerr coefficient is given in (cgs) units. The parameters A^2, a, and b in Eqs. (4.22) and (4.23) are found from the variational results. Similar expressions exist for the M solitary wave solution. The total energy for the M solitary wave is given as

$$U\ \ (\text{J/cm}) = \frac{\bar{\epsilon}}{2\pi}\frac{16A^2}{\lambda abG^2} = 9.1\times 10^{-10}\frac{\bar{\epsilon}^2 a_o^2}{|\chi^{(3)}|}\left(\frac{A^2}{a^2}\right), \tag{4.24}$$

and the incident peak intensity is

$$I_{\text{in}}\ \ (\text{W/cm}^2) = \frac{c\,\bar{\epsilon}}{\pi}\frac{A^2}{\lambda} = 67.55\frac{\bar{\epsilon}^{3/2}}{|\chi^{(3)}|}A^2. \tag{4.25}$$

For the X solitary wave solution we consider two cases with $\chi^{(3)} > 0$, one with frequency close to the upper band edge and one at the middle of the X gap. For a frequency detuning from the midgap $\delta = 0.9975\beta$ (where the upper band edge $\delta_+ = \beta \equiv \Delta\epsilon/8\bar{\epsilon}$) the variational solution yields $A^2/\beta = 5.62\times 10^{-3}$, $a/\beta = 8.65\times 10^{-2}$, $b/\sqrt{\beta} = 6.12\times 10^{-2}$, and $A^2/ab = 1.061/\sqrt{\beta}$. At midgap, where $\delta_X = 0$, the parameters become $A^2/\beta = 2.1$, $a/\beta = 1.42$, $b/\sqrt{\beta} = 1.18$, and $A^2/ab = 1.24/\sqrt{\beta}$.

For the M solitary wave solution we consider two cases with $\chi^{(3)} > 0$, one with frequency close to the upper band edge and one at the middle of the M gap. Near the upper band edge, we choose $\delta_M = 1.9975\beta$, and the following results are obtained: $A^2/\beta = 9.4\times 10^{-4}$, $a/\beta = 8.65\times 10^{-2}$, and $A^2/a^2 = 0.125/\beta$. At midgap $\delta_M = 0$, we have $A^2/\beta = 0.6$, $a/\beta = 1.6$, and $A^2/a^2 = 0.22/\beta$. The results for $\chi^{(3)} < 0$, can easily be found by mirror reflection about the midgap.

In general, the required peak intensity and power for the excitation of these solitary waves decreases as the Kerr coefficient $|\chi^{(3)}|$ increases. The choice of the material is dictated by the specific application. For instance, a PBG interconnect between fibers would be designed to have a gap centered at 1.5 μm, with a large Kerr coefficient at this wavelength. For applications in the picosecond regime, a fast nonlinear response is required. In addition to these requirements, the linear and nonlinear losses of these materials should be as low as possible.

The magnitude of the Kerr coefficient and the response time depends on the physical mechanism of the nonlinear interaction. For purely electronic polarization, which involves the distortion of the electron cloud about an atom and virtual electron-hole pairs in the material, the response is almost instantaneous (10^{-15} s). These nonlinearities are achieved by operating far from any resonances. For example, optical fibers are typically used below one-fifth of the energy gap and semiconductors are used below their half-band-gap energy. In transparent dielectrics, such as optical fibers, a typical susceptibility is $\chi^{(3)} \sim 10^{-14}$ esu [41]. In semiconductor materials, more general physical mechanisms may contribute to the nonlinear coefficient. The most important one involves the absorption of some of the electromagnetic energy accompanied by the creation of real electron-hole pairs. In this case, the response time is determined by the recombination time of the electron and hole, typically in the nanosecond regime. Ultrafast semiconductor materials with low absorption losses include $Al_xGa_{1-x}As$, where the nonlinear susceptibility $\chi^{(3)} \sim 10^{-11} - 10^{-10}$ esu [42] for 800–850 nm, and $\chi^{(3)} \sim 10^{-11}$ esu [43] for 1.55 μm, with femtosecond pulses. Materials such as CdS, ZnSe, and ZnS exhibit nonlinear susceptibilities $\chi^{(3)} \sim 10^{-12}$ esu at approximately 1.27 μm using femtosecond pulses [44]. Recent measurements on polymeric materials have revealed both high nonlinear index and a very fast response time on the picosecond time scale. Polymers such as p-toluene sulfonate have a nonlinear coefficient $\chi^{(3)} \sim 10^{-10}$ esu for 1.3 μm and 1.6 μm [45]. The nonlinear susceptibility of polydiacetylene 9-BCMU thin films has been measured in the 0.64-μm spectral window to be $\chi^{(3)} \sim 10^{-8}$ esu [46]. These materials, however, have a low optical damage threshold in the GW/cm^2 regime.

For illustrative purposes, consider a 2D PBG, containing polydiacetylene 9-BCMU material, where $\chi^{(3)}=1.2\times10^{-8}$ esu and the linear refractive index $n_o=1.6$ for 0.64 μm. Assuming that a comparable nonlinear response can be obtained at 1.55 μm, a suitable nonlinear PBG structure may be fabricated starting from a square lattice of air columns etched into a high index material such as silicon ($\epsilon=12$). The air columns may then be infiltrated with the polymer ($\epsilon=2.6$), creating a highly nonlinear PBG material. Since the medium is periodic, the dielectric constant can be expanded in a Fourier series. Comparing this expansion with our model requires that we associate $\bar{\epsilon}$ with the zeroth order expansion coefficient, and $\Delta\epsilon$ with the first order expansion coefficient. Then we have [26]

$$\bar{\epsilon}=(1-f)\epsilon_B+f\epsilon_A \tag{4.26}$$

and

$$\Delta\epsilon=4f(\epsilon_A-\epsilon_B)\frac{J_1(Gr_a)}{Gr_a}. \tag{4.27}$$

Here, $f=\pi(r_a/a_o)^2$ is the volume fraction of the cylinders with a radius of r_a, a_o is the lattice constant of the 2D square lattice, ϵ_A is the dielectric constant of the cylinders, ϵ_B is the background dielectric constant, $J_1(x)$ is a Bessel function, and $G=2\pi/a_o$. For a 2D square lattice, a complete gap for both polarizations (TE and TM) of the electromagnetic field is not possible. Thus we consider the case when there is a complete gap for the TE polarization. Choosing $f=0.38$, there is a band gap centered around $a_o/\lambda=0.25$ [47]. Then, from Eq. (4.26), $\bar{\epsilon}=8.4$, and from Eq. (4.27), $\Delta\epsilon=3.6$, yielding $\beta\equiv\Delta\epsilon/8\bar{\epsilon}\simeq0.05$. For a PBG constructed to have a gap centered at $\lambda=1.55$ μm, we require a lattice constant $a_o=0.4$ μm. For a soliton of average frequency near the upper band edge of the X gap (say $\delta=0.0489$), the total energy $U=9.8$ nJ/cm, with $I_{\rm in}=19.3$ MW/cm^2. At midgap $\delta=0$, $U=11.5$ nJ/cm with $I_{\rm in}=7.2$ GW/cm^2. Similarly, for the M solitary wave near the upper band edge of the M gap ($\delta_M=0.0998$) the total energy is $U=21.4$ nJ/cm with an incident flux of $I_{\rm in}=6.5$ MW/cm^2. At midgap ($\delta_M=0$), the total energy $U=37.6$ nJ/cm with $I_{\rm in}=4.1$ GW/cm^2. For a 2D PBG material which is translationally invariant in the transverse direction, the total energy of the soliton will be determined by the transverse size of the incident laser beam. If the 2d PBG structure is confined inside a planar dielectric waveguide, the total energy is determined by the thickness of the waveguide.

V. NUMERICAL METHOD AND RESULTS

The variational method provides an excellent qualitative description of solitary waves. In order to obtain a more quantitative picture of gap solitary waves, we solve the nonlinear wave equation numerically. In general, numerical algorithms for 2D nonlinear partial differential equations (PDE's) are more complicated than for 1D PDE's. There are two major approaches. The first one is to discretize the equations by defining the electric field on a suitable mesh. The second approach is to project the solution on a finite dimensional subspace of the full function space, and then to solve the resulting nonlinear equations for a finite number of expansion coefficients. Here we utilize the second method. We write the solitary wave envelope functions in the form of a finite element expansion

$$\Psi(\vec{r})\simeq\tilde{\Psi}(\vec{r})=\sum_{i,j}^{n} C_{ij}\phi_i(ax)\phi_j(by), \tag{5.1}$$

where $\{\phi_i(x)\}$ is a set of orthonormal basis functions. One advantage of this method is that we can perform a number of steps analytically. Expansion (5.1) is substituted into the action functional, and the expansion coefficients are found by solving the nonlinear equations $\partial S/\partial\tau_i=0$, where $\tau_i=C_{ij},a,b$. The number of terms N in expansion (5.1) is increased until convergence is achieved. We first illustrate the method by applying it to the 1D soliton problem. In this case we can compare the exact result with the numerical solution. Separating the real and imaginary parts of $E=u+iv$, the 1D action functional becomes

$$S_{1d}/2=\int dx[vu_x-uv_x+\delta(u^2+v^2)+\beta(u^2-v^2)+\alpha(u^2+v^2)^2]. \tag{5.2}$$

We then expand u and v using the complete, orthonormal basis functions,

$$\phi_i(x)=\mathrm{sech}(x)P_i[\tanh(x)]. \tag{5.3}$$

Here P_i are the Legendre polynomials, and ϕ_i satisfy the boundary conditions $x\to\infty$ and $\Psi\to0$. The orthogonality and normalization relation is given by

$$\int_{-\infty}^{+\infty}\phi_i(x)\phi_j(x)dx=\frac{2}{(2i+1)}\delta_{ij}. \tag{5.4}$$

We write

$$u(x)=\sum_{i}^{N} C_i^u\phi_i(ax), \tag{5.5a}$$

$$v(x)=\sum_{i}^{N} C_i^v\phi_i(ax), \tag{5.5b}$$

where (C_i^u, C_i^v, a) are variational parameters. The solution possesses some symmetry properties which reduce the number of independent parameters. For $\alpha>0$, u is an odd function of x and v an even function of x. Using these symmetries, u and v can be expanded as follows:

$$u(x)=\mathrm{sech}(ax)\sum_{i=1}^{N} C_i^u P_{2i-1}[\tanh(ax)] \tag{5.6a}$$

$$v(x)=\mathrm{sech}(ax)\sum_{i=1}^{N} C_i^v P_{2i-2}[\tanh(ax)]. \tag{5.6b}$$

Inserting Eq. (5.6) into the one-dimensional functional (5.2), all integrals can be evaluated analytically. The nonlinear terms have the form $\Sigma_{i,j,k,l}C_iC_jC_kC_lI(i,j,k,l)$, where

$I(i,j,k,l)=\int dx[\phi_i(x)\phi_j(x)\phi_k(x)\phi_l(x)]$. This integral can be evaluated analytically by using the following forms of the Legendre polynomials $P_n(x)$:

$$P_n(x)=\frac{1}{2^n}\sum_{m=0}^{[n/2]}(-1)^m\binom{n}{m}\binom{2n-2m}{n}x^{n-2m}. \quad (5.7)$$

$$\frac{S_{1d}}{2}=\sum_{i=1}^{N}\left[-C_i^uC_{i+1}^v\frac{8i^2}{(16i^2-1)}+C_i^uC_i^v\frac{4(2i-2)^2}{(4i-1)(4i-3)}-C_{i-1}^uC_i^v\frac{2(2i-2)^2}{(4i-3)(4i-5)}+\frac{2\delta}{a}\left(\frac{(C_i^u)^2}{4i-1}+\frac{(C_i^v)^2}{4i-3}\right)+\frac{\alpha}{a}I_{\mathrm{NL}}\right], \quad (5.8)$$

where I_{NL} contains the integration of the nonlinear term:

$$I_{\mathrm{NL}}=\sum_{i,j,k,l}[C_i^uC_j^uC_k^uC_l^uI(2i-1,2j-1,2k-1,2l-1)+2C_i^uC_j^uC_k^vC_l^vI(2i-1,2j-1,2k-2,2l-2)+C_i^vC_j^vC_k^vC_l^vI(2i-2,2j-2,2k-2,2l-2)]. \quad (5.9)$$

Applying the extremum condition to Eq. (5.8) results in $(2N+1)$ coupled nonlinear algebraic equations. Solving nonlinear equations is complicated by the fact that the solution is not necessarily unique. The numerical algorithm is highly sensitive to the initial guess. Here, we use the MINPACK routine HYBRID, based on the Powell hybrid method [48]. For the numerical calculation, we choose the gap parameter $\beta=0.1$ and $\alpha=+1$, yielding a 1D photonic band gap in the frequency range $-0.1<\delta<0.1$. To test the convergence of our numerical method we consider two gap solitons: one close to the upper band edge and one close to the lower band edge. Near the upper band edge ($\delta=0.099\,75$) we obtain convergence to the exact solution for $N=3$. Near the lower band edge ($\delta=-0.0875$), convergence is achieved for $N=12$. In Fig. 9 we plot the intensity profile near the lower band edge for $N=5$ and 12, and compare these with the exact solution. Near the upper band edge $|u|\ll|v|$, resulting in rapid convergence. Near the lower band edge $|u|\simeq|v|$, and more terms are needed to recapture the exact solution of Mills and Trullinger [4].

A. 2D Solitary Waves

Having demonstrated the effectiveness of our numerical method in recapturing the exact 1D solution, we now apply this method to the 2D case. First, we consider the X solitary wave solution. The real and imaginary parts of $E=u+iv$ are expanded as

$$u(x,y)=\sum_{i,j}^{N}C_{ij}^u\phi(ax)\phi(by), \quad (5.10a)$$

$$v(x,y)=\sum_{i,j}^{N}C_{ij}^v\phi(ax)\phi(by). \quad (5.10b)$$

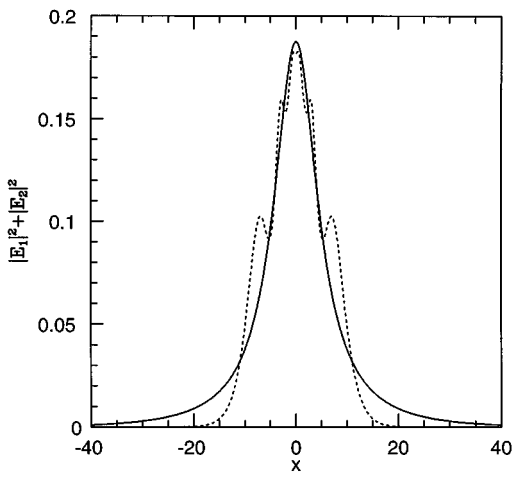

FIG. 9. The convergence of the numerical finite element method to the exact analytical solitary wave solution is demonstrated near the lower band edge for $\delta=-0.0875$ ($\delta_-=-0.1$). Plotted is the energy density $|E_1|^2+|E_2|^2$ (a.u) vs the spatial variable x (a.u). The dotted line is the finite element result by retaining only five eigenfunctions ($N=5$) in the expansion, and the solid line shows the exact solution. The converged numerical result for $N=12$ is indistinguishable from the exact solution. Here, $\beta=0.1$ and $\alpha=+1$.

The functional for the 2D X solitary wave in terms of $u(x,y)$ and $v(x,y)$ is given by

$$S_X/2=\int_{-\infty}^{+\infty}dx\,dy[(\partial_yu)^2+(\partial_yv)^2-(vu_x-uv_x)-\delta(u^2+v^2)-\beta(u^2-v^2)-\alpha(u^2+v^2)^2]. \quad (5.11)$$

In what follows, we choose the gap parameter $\beta=0.1$, and consider the case of the positive Kerr nonlinearity, $\alpha=+1$. Using the symmetry properties of u and v, we make the expansions

$$u(x,y)=\mathrm{sech}(ax)\mathrm{sech}(by)\sum_{i,j}^{N}C_{ij}^uP_{2i-1}\times[\tanh(ax)]P_{2j-2}[\tanh(by)] \quad (5.12a)$$

and

$$v(x,y)=\mathrm{sech}(ax)\mathrm{sech}(by)\sum_{i,j}^{N}C_{ij}^vP_{2i-2}[\tanh(ax)]\times P_{2j-2}[\tanh(by)]. \quad (5.12b)$$

Inserting Eq. (5.12) into Eq. (5.11), and applying extremum conditions, we obtain $(2N^2+2)$ coupled nonlinear algebraic equations for the variational parameters C_{ij}^u, C_{ij}^v, a, and b. For illustrative purposes we consider two solitary waves. Near the upper band edge, $\delta=0.099\,75$, a converged solitary wave solution is obtained for $N=6$. Near midgap, $\delta=0.0375$, $N=10$ is needed to obtain convergence. In Figs. 10 and 11 we plot the numerically converged total energy

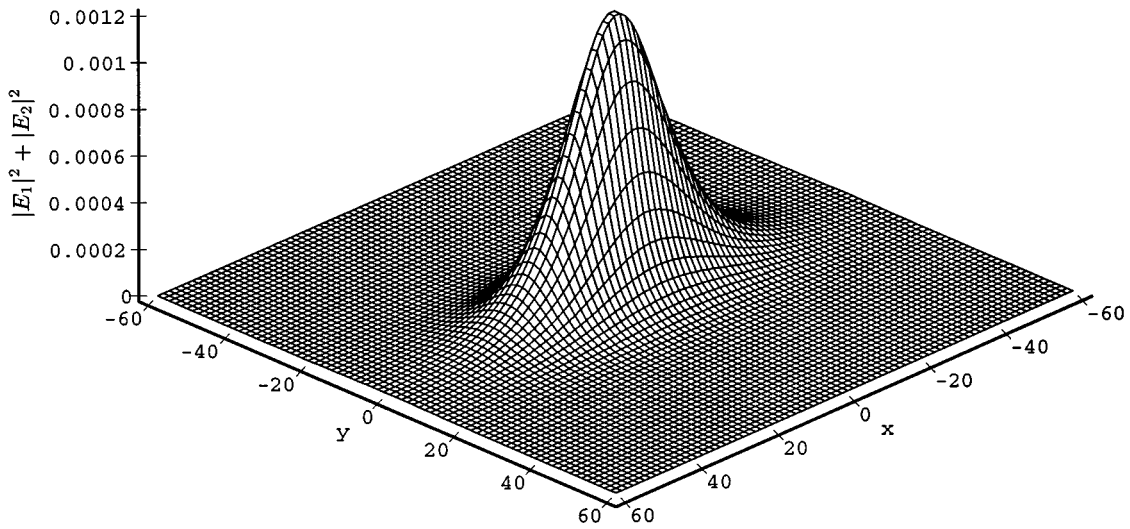

FIG. 10. Plotted is the energy density ($|E_1|^2+|E_2|^2$) (a.u.) of the X solitary wave using the numerical finite element method ($N=6$), for a frequency near the upper band edge of the X gap $\delta=0.09975$. The spatial coordinates x,y are scaled in units of the lattice constant a_o. Here, $\alpha=+1$ and $\beta=0.1$.

density $\rho=|E_1|^2+|E_2|^2$, within the structure, for the two solitary waves. As expected, for frequencies deeper in the band-gap region the solitary wave is more localized, and the intensity is greater than near the upper band edge.

In Table I we make a comparison of the conserved quantity Q and peak intensity of the X solitary wave with the variational and numerical results. Near the upper band edge the sech trial function gives a better result than the Gaussian trial function. Near the midgap the Gaussian trial function appears more accurate.

For the M solitary wave we again use the same basis functions (5.3). Separating the real and imaginary parts as $E_1=u_1+iv_1$, $E_2=E_1^*$, $E_3=u_3+iv_3$, and $E_4=E_3^*$, the action functional becomes L

$$
\begin{aligned}
S_M/2=\int dx\, dy\{&v_1(u_{1x}+u_{1y})-u_1(v_{1x}+v_{1y})\\
&+v_3(u_{3x}-u_{3y})-u_3(u_{3x}-u_{3y})\\
&+\delta_M(u_1^2+v_1^2+u_3^2+v_3^2)+4\beta u_1u_3\\
&+2\alpha[(u_1^2+v_1^2)^2+(u_3^2+v_3^2)^2\\
&+4(u_1^2+v_1^2)(u_3^2+v_3^2)]\}. \qquad (5.13)
\end{aligned}
$$

The finite element, numerical solution of the M solitary wave is facilitated by exploiting the underlying symmetries of the M solitary wave Eqs. (2.11). Equations (2.11a) and (2.11c) may be interchanged by the relabeling procedure

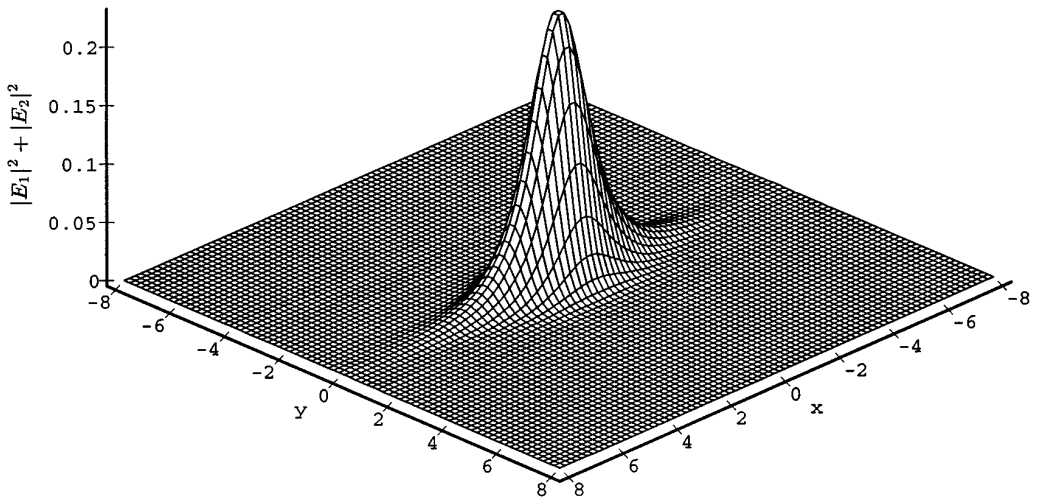

FIG. 11. Plotted is the energy density ($|E_1|^2+|E_2|^2$) (a.u.) of the X solitary wave using the numerical finite element method ($N=10$), for a frequency near the midgap of the X gap ($\delta=0.0375$). The spatial coordinates, x and y are measured in units of the lattice constant a_o. Close to midgap, the localization length is only several lattice constants and the intensity has increased when compared to the near upper band edge solution in Fig. 8. All other parameters are the same as in Fig. 8.

TABLE I. Comparison of the variational and numerical results for the X solitary wave solution for two frequency detunings, one close to the upper band edge, $\delta=(\omega^2-1)/4=0.099\,75$, and the other close to midgap, $\delta=0.0375$. We compare the peak intensity A^2 (a.u.) and total energy Q obtained the finite element numerical method, with that obtained by the Gaussian and sech variational trial functions. Both trial functions are in qualitatively good agreement with the numerical results. Here the material parameters are chosen as $\beta=0.1$ and $\alpha=+1$, and the midgap is defined by $\delta=0$.

	Gaussian	Sech	Numerical
$\delta=0.09975$			
Q	28.11	26.84	26.18
A^2	0.000 50	0.000 56	0.000 61
$\delta=0.0375$			
Q	34.77	29.56	37.15
A^2	0.111	0.134	0.117

$1\leftrightarrow 3$, $2\leftrightarrow 4$, and $y\leftrightarrow -y$. The same relabeling leads to the interchange of Eqs. (2.11b) and (2.11d). It follows that $E_3(x,y)=E_1(x,-y)$. Furthermore, some of the terms in the general finite element expansion are identically zero. We utilize the expansions

$$u_1(x,y)=\mathrm{sech}(ax)\mathrm{sech}(ay)\sum_{i,j}^{N}\{C_{ij}^{u}P_{2i-2}[\tanh(ax)]P_{2j-2}\times[\tanh(ay)]+B_{ij}^{u}P_{2i-1}[\tanh(ax)]P_{2j-1}\times[\tanh(ay)]\}, \tag{5.14a}$$

$$v_1(x,y)=\mathrm{sech}(ax)\mathrm{sech}(ay)\sum_{i,j}^{N}\{C_{ij}^{v}P_{2i-1}[\tanh(ax)]\times P_{2j-2}[\tanh(ay)]+B_{ij}^{v}P_{2i-2}[\tanh(ax)]P_{2j-1}[\tanh(ay)]\} \tag{5.14b}$$

along with the symmetry conditions $u_3(x,y)=u_1(x,-y)$ and $v_3(x,y)=v_1(x,-y)$. Inserting expansion (5.14) into functional (5.13), and applying the extremum condition, we obtain $(4N^2+1)$ nonlinear algebraic equations for the variational parameters C_{ij}^{u}, B_{ij}^{u}, C_{ij}^{v}, B_{ij}^{v}, and a. Here we consider two frequencies, one near the lower band edge $\delta_M=-0.199\,75$ and one deep inside the photonic band gap $\delta_M=-0.15$, for the case of the negative Kerr coefficient $\alpha=-1$. The numerically converged solutions are given in Figs. 12 and 13, where we plot the total energy density function $|E_1|^2+|E_2|^2+|E_3|^2+|E_4|^2$. The solitary wave is clearly more localized for frequencies deeper in the gap region. Also, the shape of the M solitary wave departs significantly from that of the X solitary wave for frequencies deeper in the gap.

VI. 2D TRIANGULAR SYMMETRY GROUP

In this section we apply the methods of Secs. IV and V to derive the existence of solitary waves in a photonic crystal with a 2D triangular symmetry group. This type of structure has already been fabricated [32] using silicon in the infrared regime (around 5 μm). For simplicity, we model the linear dielectric constant of the triangular lattice by

$$\epsilon(x,y)=\bar{\epsilon}+\Delta\epsilon\{\cos(\vec{G}_1\cdot\vec{r})+\cos(\vec{G}_2\cdot\vec{r})+\cos[(\vec{G}_1+\vec{G}_2)\vec{r}]\} \tag{6.1}$$

Here $\vec{G}_1=(2\pi/a_o)\,(1,-\sqrt{3}/3)$ and $\vec{G}_2=(2\pi/a_o)\,(0,2\sqrt{3}/3)$ are the reciprocal vectors of the triangular lattice with lattice constant a_o. As in the square lattice the photonic band edges are described by the two extremal symmetry points in the triangular BZ. These are the X symmetry point $\vec{k}_X=(2\pi/3a_o)(0,\sqrt{3})$ and the J symmetry point $\vec{k}_J=(2\pi/3a_o)(1,\sqrt{3})$. A possible lattice structure and the corresponding Brillouin zone is given the Fig. 14. Following the SVEA method, we expand the electric field around these symmetry points. The derivation of the nonlinear wave equa-

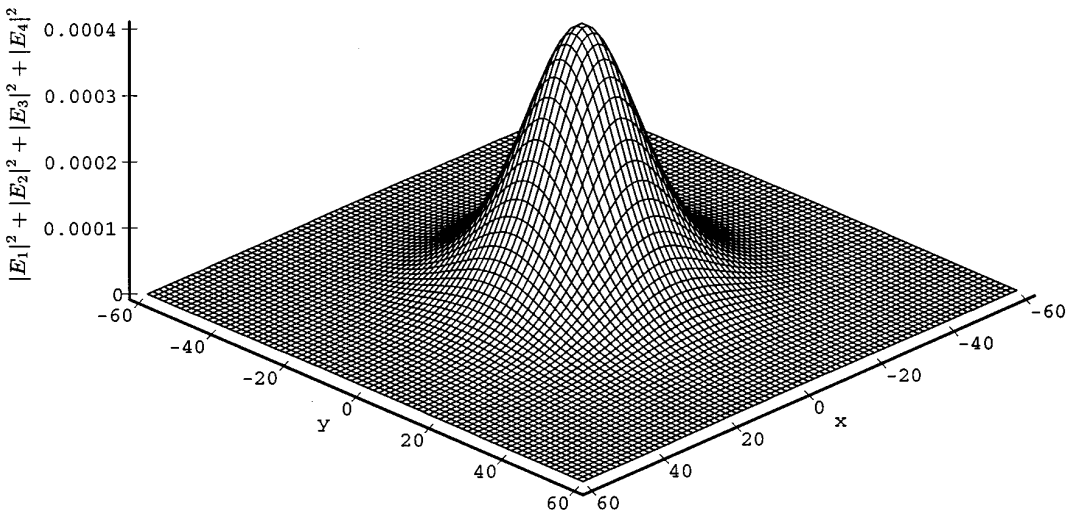

FIG. 12. Plotted is the energy density $\rho=(\Psi^{\dagger}\Psi)$ (a. u.) of the M solitary wave, for a frequency close to the lower band edge of the M gap ($\delta_M=-0.19975$). The spatial coordinates x and y are measured in units of the lattice constant a_o.

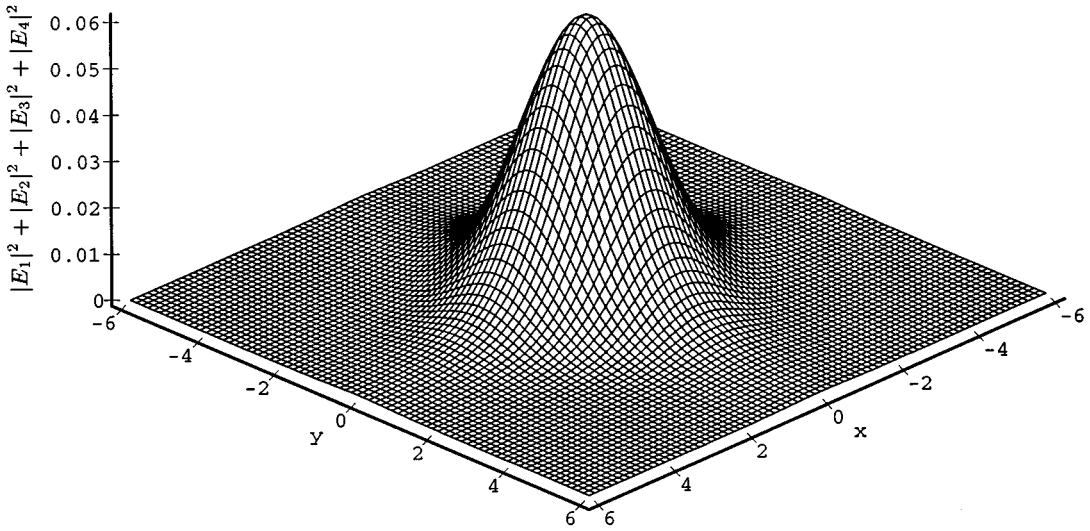

FIG. 13. Plotted is the energy density $\rho=(\Psi^{\dagger}\Psi)$ (a.u.), of the M solitary wave, for a frequency deeper in the band-gap region of the M gap ($\delta_M=-0.15$). The spatial coordinates x and y are measured in units of the lattice constant a_o.

tion is similar to that described earlier. We do not repeat these detailed steps here. Instead we simply state the resulting equations for the slowly varying envelope functions. For the twofold X symmetry point, the electric field is expanded in the usual manner:

$$E(x,y)=E_1(x,y)e^{i(G/2)y}+E_2(x,y)e^{-i(G/2)y} \tag{6.2}$$

For the J symmetry point, there are three points in k space connected by Bragg scattering:

$$E(x,y)=E_1(x,y)e^{i[(G/2\sqrt{3})x+(G/2)y]}+E_2(x,y)e^{-i(G/\sqrt{3})x}+E_3(x,y)e^{i[(G/2\sqrt{3})x-(G/2)y}. \tag{6.3}$$

Here $G=4\pi\sqrt{3}/3a_o$. For the X symmetry point the nonlinear wave equation is completely equivalent to Eq. (2.7), and the resulting gap solitary waves are identical to those described earlier for the square lattice. However, a new type of wave equation is required to describe the J symmetry point where three modes are resonantly coupled through the periodic dielectric function. In this case we obtain

$$i\left(\frac{1}{\sqrt{3}}\frac{\partial E_1}{\partial x}+\frac{\partial E_1}{\partial y}\right)+\delta_J E_1+\beta(E_2+E_3)+\frac{2\lambda}{3}[|E_1|^2+2(|E_2|^2+|E_3|^2)]E_1=0, \tag{6.4a}$$

$$-i\frac{2}{\sqrt{3}}\frac{\partial E_2}{\partial x}+\delta_J E_2+\beta(E_1+E_3)+\frac{2\lambda}{3}[|E_2|^2+2(|E_1|^2+|E_3|^2)]E_2=0, \tag{6.4b}$$

$$i\left(\frac{1}{\sqrt{3}}\frac{\partial E_3}{\partial x}-\frac{\partial E_3}{\partial y}\right)+\delta_J E_3+\beta(E_1+E_2)+\frac{2\lambda}{3}[|E_3|^2+2(|E_1|^2+|E_2|^2)]E_3=0. \tag{6.4c}$$

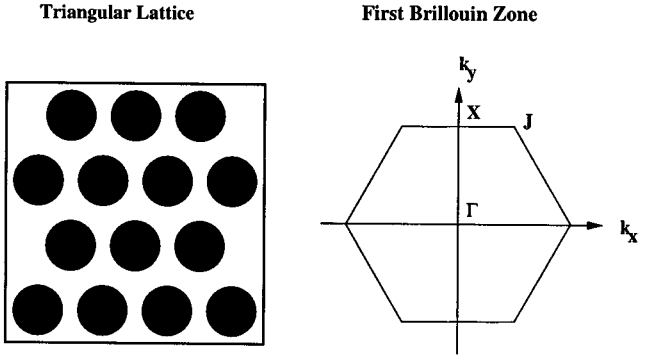

FIG. 14. Shown is a top view of a triangular lattice PBG structure (left) consisting of circular dielectric rods. The Brillouin zone (right) with the relevant $J(2\pi/3a_o,2\pi\sqrt{3}/3a_o)$ and $X(0,2\pi\sqrt{3}/3a_o)$ symmetry points are indicated.

Equations (6.4) can be written in a compact form by defining the three-component spinor field $\Psi^{\dagger}=(E_1^*,E_2^*,E_3^*)$:

$$[i(\gamma_1'\partial_x+\gamma_2'\partial_y)+\delta_J+\beta\gamma_3'+\alpha U_{\rm NL}(\Psi^{\dagger},\Psi)]\Psi=0. \tag{6.5}$$

Here $\delta_J=(\omega^2-4/3)/4$, and

$$U_{\rm NL}(\Psi^{\dagger},\Psi)=[\tfrac{5}{3}(\Psi^{\dagger}\Psi)-\tfrac{1}{6}(\Psi^{\dagger}\gamma_1'\Psi)\gamma_1'-\tfrac{1}{2}(\Psi\gamma_2'\Psi)\gamma_2']. \tag{6.6}$$

In arriving at the dimensionless wave equation (6.5), we performed the rescaling $\sqrt{2\lambda/3}\Psi\rightarrow\Psi$ where $\lambda\equiv 9\pi|\chi^{(3)}|/2\bar{\epsilon}$ is the nonlinear optical coefficient. x and y are dimensionless coordinate variables measured in units of G^{-1}, and γ_1', γ_2', and γ_3' are 3×3 matrices defined as

$$\gamma_1'=\begin{pmatrix}1&0&0\\0&-2&0\\0&0&1\end{pmatrix},\quad \gamma_2'=\begin{pmatrix}1&0&0\\0&0&0\\0&0&-1\end{pmatrix},$$

$$\gamma_3'=\begin{pmatrix}0&1&1\\1&0&1\\1&1&0\end{pmatrix} \tag{6.7}$$

The band gaps for the X and J symmetry points can be found for the SVEA by setting $\alpha=0$. Using the trial solution, $\Psi=\Phi e^{i\vec{q}\vec{r}}$, the band edges for the X symmetry point occur at $|\vec{q}|=0$, at the frequencies

$$\omega_{\pm}^{X}=\sqrt{1\pm 4\beta} \tag{6.8}$$

For the J symmetry point the upper and lower band edge frequencies are given by

$$\omega_{+}^{J}=\sqrt{4/3+4\beta},$$

$$\omega_{-}^{J}=\sqrt{4/3-8\beta}.$$

The complete photonic band gap is an indirect one determined by $\omega_{+}=\omega_{+}^{(X)}$ and $\omega_{-}=\omega_{-}^{(J)}$. In order to have a complete band gap we require that $(\Delta\epsilon/\bar{\epsilon})\geqslant 0.2$ in the context of the slowly varying envelope approximation.

Variational and numerical results

The variational method is implemented by introducing the action functional for the J symmetry point:

$$S_J=\int d^2\vec{r}\{\Psi^{\dagger}[i(\gamma_1'\partial_x+\gamma_2'\partial_y)+\delta_J+\beta\gamma_3']\Psi - \tilde{U}_{\mathrm{NL}}(\Psi^{\dagger},\Psi)\}, \tag{6.9a}$$

where

$$\tilde{U}_{\mathrm{NL}}=\frac{\alpha}{2}\{\tfrac{5}{3}(\Psi^{\dagger}\Psi)^2-\tfrac{1}{6}(\Psi^{\dagger}\gamma_1'\Psi)^2-\tfrac{1}{2}(\Psi^{\dagger}\gamma_2'\Psi)^2\} \tag{6.9b}$$

Using the variational trial solution

$$\Psi=\begin{pmatrix}A_1(x,y)e^{i\phi_1(x,y)}\\A_2(x,y)e^{i\phi_2(x,y)}\\A_3(x,y)e^{i\phi_3(x,y)}\end{pmatrix}, \tag{6.10}$$

the action functional functional takes the form

$$S_J=\int dx\,dy\Bigg[-A_1^2\left(\frac{\partial\phi_1}{\partial x}+\frac{\partial\phi_1}{\partial y}\right)-A_3^2\left(\frac{\partial\phi_3}{\partial x}-\frac{\partial\phi_3}{\partial y}\right)+2A_2^2\frac{\partial\phi_2}{\partial x}+\delta_J(A_1^2+A_2^2+A_3^2)+2\beta[A_1A_2\cos(\phi_1-\phi_2)+A_1A_3\cos(\phi_1-\phi_3)+A_3A_2\cos(\phi_2-\phi_3)]+\frac{\alpha}{2}[A_1^4+A_2^4+A_3^4+4(A_1^2A_2^2+A_1^2A_3^2+A_3^2A_2^2)]\Bigg] \tag{6.11}$$

The integrals in Eq. (6.11) may be evaluated explicitly using the following ansatz for the solitary wave amplitude and phase angles:

$$A_1(x,y)=A_3(x,y)=A\ \mathrm{sech}(ax)\mathrm{sech}(ay);$$

$$A_2(x,y)=bA_1(x,y), \tag{6,12a}$$

$$\phi_1(x,y)=c_1+\arctan[d\ \tanh(ax)]+\arctan[d\ \tanh(ay)], \tag{6.12b}$$

$$\phi_2(x,y)=c_2-\arctan[d\ \tanh(ax)], \tag{6.12c}$$

$$\phi_3(x,y)=c_3+\arctan[d\ \tanh(ax)]-\arctan[d\ \tanh(ay)]. \tag{6.12d}$$

In this case the action functional takes the form

$$S_J/4=\Bigg[\frac{2A^2}{a}\left(\arctan(d)-\frac{1}{d}+\frac{\arctan(d)}{d^2}\right)\left(1+\frac{(1+b^2)}{\sqrt{3}}\right)+\frac{2\beta A^2}{a^2}\left(\frac{2\arctan(d)}{d}-1\right)\times\left(b[\cos(c_1-c_2)+\cos(c_3-c_2)]\times\frac{\sinh^{-1}(d)}{d}+\cos(c_1-c_2)\right)+\frac{A^2\delta_J(2+b^2)}{a^2}+\frac{2\alpha A^4}{9a^2}(6+b^4+8b^2)\Bigg]. \tag{6.13}$$

The extremization of Eq. (6.13) with respect to the variational parameters A^2, a, b, and d leads to a cumbersome set of coupled nonlinear algebraic equations. From the conditions $\partial S_J/\partial A^2=0$ and $\partial S_J/\partial a=0$, we find

$$\delta_J(2+b^2)+2\beta[2\arctan(d)/d-1]\{b[\cos(c_1-c_2)+\cos(c_3-c_2)]\sinh^{-1}/d+\cos(c_1-c_2)\}=0, \tag{6.14}$$

$$\alpha A^4(6+b^4+8b^2)=9a\left(\arctan(d)-\frac{1}{d}+\frac{\arctan(d)}{d^2}\right)(2+b^2)/2, \tag{6.15}$$

and from the condition $\partial S_J/\partial d=0$ we may express the parameter a in terms of the others. The last condition $\partial S_J/\partial b=0$ together with Eq. (6.14) will be a function of b and d which then have to solved numerically.

We solve nonlinear algebraic equations numerically for the case $\alpha=-1$. The solution to the variational parameters

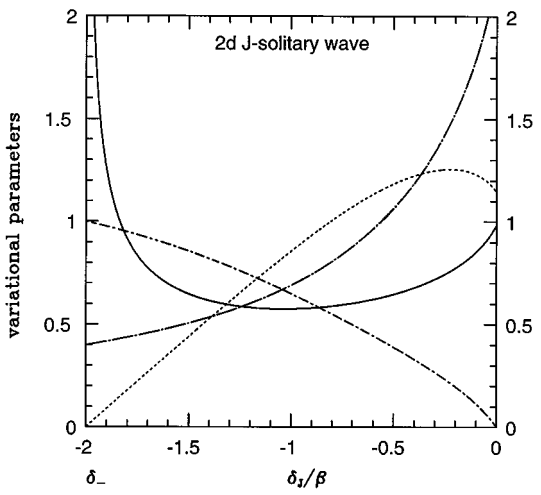

FIG. 15. The variational parameters for the J solitary wave shown are plotted as a function of the detuning frequency δ_J/β. Here the soliton size β/a (solid line) is measured in units of a_o, the intensity is A^2/β (dotted line), and the second amplitude parameter is b (dotted short-dashed line). The quantity $\beta A^2(2+b^2)/a^2$ (dotted long-dashed line) is proportional to the total energy of the J solitary wave.

are plotted versus the detuning frequency $\delta_J=(\omega^2-4/3)/4$ in Fig. 15. However, for $\delta_J>0$, these numerical results were not accurate thus we do not present them on the plot. When $\alpha=-1$, $\cos(c_1-c_3)=\cos(c_1-c_2)=\cos(c_3-c_2)=1$. Near the lower band edge, $b\simeq 1$. When $\alpha=1$, $\cos(c_1-c_3)=1$, and $\cos(c_1-c_2)=\cos(c_3-c_2)=-1$. Near the upper band edge $b\simeq 2$. Thus a solution is possible for either sign of the nonlinear optical coefficient λ. The variational method is useful in estimating important physical quantities of the solitary wave for various frequency detunings. The required incident intensity (flux) is given by

$$I_{\rm in}\ ({\rm W/cm^2})=50\frac{\tilde{\epsilon}^{3/2}}{|\chi^{(3)}|}A^2 \tag{6.16}$$

and the total energy of the J solitary wave yields

$$U\ ({\rm J/cm})=1.3\times 10^{-10}\left(\frac{\tilde{\epsilon}^2 a_o^2}{|\chi^{(3)}|}\right)\left(\frac{A^2(2+b^2)}{a^2}\right), \tag{6.17}$$

where the lattice constant is a_o (cm) and the Kerr coefficient $|\chi^{(3)}|$ esu. The magnitude of these quantities are qualitatively the same as in the 2D square lattice case.

In order to obtain a more detailed numerical solution, we separate the real and imaginary parts as $E_j=u_j+iv_j$, $j=1$, 2, and 3. The functional becomes

$$\begin{aligned}S_J=&\int dx\,dy(v_1(u_{1x}+u_{1y})-u_1(v_{1x}+v_{1y}))\\&+2(u_2v_{2x}-v_2u_{2x})+v_3(u_{3x}-u_{3y})-u_3(v_{3x}-v_{3y})\\&+\delta_J(u_1^2+v_1^2+u_2^2+v_2^2+u_3^2+v_3^2)\\&+2\beta(u_1u_2+u_1u_3+u_2u_3+v_1v_2+v_1v_3+v_2v_3)\\&+\frac{\alpha}{2}\left[\frac{5}{3}(u_1^2+v_1^2+u_2^2+v_2^2+u_3^2+v_3^2)^2\right.\\&-\frac{1}{6}(u_1^2+v_1^2-2(u_2^2+v_2^2)+u_3^2+v_3^2)^2\\&\left.-\frac{1}{2}(u_1^2+v_1^2-(u_3^2+v_3^2)^2\right].\end{aligned} \tag{6.18}$$

For $\alpha=-1$, we utilize the finite element expansion

$$\begin{aligned}u_1(x,y)=&\,{\rm sech}(ax){\rm sech}(by)\sum_{i,j}^{N} C_{ij}^u P_{2i-2}\\&\times[\tanh(ax)]P_{2j-2}[\tanh(by)]\\&+B_{ij}^u P_{2i-1}[\tanh(ax)]P_{2j-1}[\tanh(by)],\end{aligned} \tag{6.19a}$$

$$\begin{aligned}v_1(x,y)=&\,{\rm sech}(ax){\rm sech}(by)\sum_{i,j}^{N} C_{ij}^v P_{2i-1}\\&\times[\tanh(ax)]P_{2j-2}[\tanh(by)]\\&+B_{ij}^v P_{2i-2}[\tanh(ax)]P_{2j-1}[\tanh(by)],\end{aligned} \tag{6.19b}$$

$$\begin{aligned}u_2(x,y)=&\,{\rm sech}(ax){\rm sech}(by)\sum_{i,j}^{N} \tilde{C}_{ij}^u P_{2i-2}\\&\times[\tanh(ax)]P_{2j-2}[\tanh(by)],\end{aligned} \tag{6.19c}$$

$$\begin{aligned}v_2(x,y)=&\,{\rm sech}(ax){\rm sech}(by)\sum_{i,j}^{N} \tilde{B}_{ij}^v P_{2i-1}\\&\times[\tanh(ax)]P_{2j-2}[\tanh(by)].\end{aligned} \tag{6.19d}$$

From the symmetry of the Eq. (6.4) it can be seen that, $u_3(x,y)=u_1(x,-y)$ and $v_3(x,y)=v_1(x,-y)$. For illustrative purposes, a frequency close to the lower band edge $\delta_J=-0.1998$ (for $\alpha=-1$) is chosen. The result is plotted in Fig. 16. Deeper in the band-gap region more terms are needed for the convergence of the solitary wave solution, and also the solution to the coupled nonlinear algebraic equations is numerically more difficult.

VII. THREE-DIMENSIONAL SOLITARY WAVES (LIGHT BULLETS) IN A 3D PBG: FCC SYMMETRY GROUP

In order to have a complete photonic gap in all directions and polarizations, a three-dimensional periodic structure is needed. Structures with a face centered cubic symmetry have been fabricated in the microwave regime [20,24]. Very recently, 3D structures made of diamond or silicon on the optical scale have been fabricated [34] using infiltration techniques starting with a scaffolding of close-packed opal spheres which are later removed by chemical etching. The voids may then be filled with another nonlinear dielectric material. These structures facilitate complete localization of light [17] as well as the inhibition of spontaneous emission

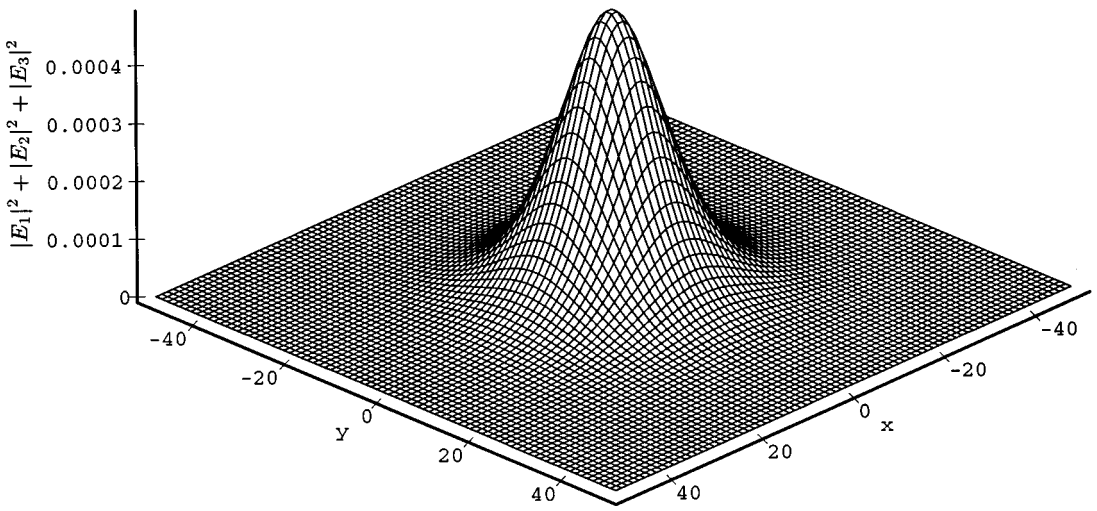

FIG. 16. Plotted is the numerically determined energy density ($|E_1|^2+|E_2|^2+|E_3|^2$), for the J solitary wave. The spatial coordinates x and y are measured in units of the lattice constant a_o. Here the frequency is chosen near to the lower band edge ($\delta_J=-0.0308$), $\alpha=-1$, and $\beta=0.1$.

from atoms [18]. Another possible self-organizing 3D structure arises in colloidal crystals [9]. Due to the relatively low index contrasts, these structures (even for TiO_2 spheres in water) do not exhibit a complete photonic band gap, but will have band gaps in specific directions. An advantage of these structures is that the lattice spacing can be adjusted by changing the particle concentration, particle size, and temperature [9]. In this section, we describe the nature of 3D localized solitary waves arising in such systems using the variational technique introduced in Sec. IV.

For a three-dimensional photonic crystal with point group of symmetry of a fcc lattice, we introduce a simple model dielectric function of the form:

$$\epsilon(r)=\bar{\epsilon}+\Delta\epsilon[\cos(\vec{G}_1\cdot\vec{r})+\cos(\vec{G}_2\cdot\vec{r})+\cos(\vec{G}_3\cdot\vec{r})+\cos(\vec{G}_4\cdot\vec{r})]. \tag{7.1}$$

Here, the reciprocal lattice vectors are given by $\vec{G}_1=(2\pi/a_o)(\hat{x}-\hat{y}+\hat{z})$, $\vec{G}_2=(2\pi/a_o)(\hat{x}+\hat{y}-\hat{z})$, $\vec{G}_3=(2\pi/a_o)(-\hat{x}+\hat{y}+\hat{z})$, and $\vec{G}_4=\vec{G}_1+\vec{G}_2+\vec{G}_3$; $G=2\pi\sqrt{3}/a_o$ is the magnitude of the reciprocal lattice vector; and a_o is the fcc lattice constant. In this simple model, the photonic band edges are again determined by the twofold L symmetry point and the fourfold W symmetry point of the Brillouin zone. The Brillouin zone to the fcc structure is shown in Fig. 17. As before, we expand the total electric field around these symmetry points, and derive the equations in the SVEA. Near the L symmetry point $[\vec{k}_o=\pi(1,1,1)/a_o]$ the electric field may be expanded as

$$E(x,y,z)=E_1(x,y,z)e^{i(\pi/a_o)(x+y+z)}+E_2(x,y,z)e^{-i(\pi/a_o)(x+y+z)}. \tag{7.2}$$

The wave equation for the two-component spinor field $\Psi^\dagger=(E_1^*,E_2^*)$ is given by

$$[i\sigma_z\partial_{x'}+\partial_{y'}y'+\partial_{z'}z'+\delta+\beta\sigma_x+\alpha(\Psi^\dagger\Psi)]\Psi=0. \tag{7.3}$$

Here we have introduced the new dimensionless variables $x'=(x+y+z)/\sqrt{3}$, $y'=(x-y)/\sqrt{2}$, and $z'=(x+y-2z)/\sqrt{6}$ (measured in units of G^{-1}) and we have performed the standard rescaling $\sqrt{\lambda}\Psi\to\Psi$. This is identical to Eq. (2.7) for the X solitary wave, except for the addition of the z' derivative term.

For the higher symmetry W point $[\vec{k}_o=2\pi(1,1/2,0)/a_o]$ there are four coupled envelope functions. In the SVEA, we write

$$E(x,y,z)=E_1e^{i(\pi/a)(2x+y)}+E_2e^{-i(\pi/a)(2x-y)}+E_3e^{-i(\pi/a)(y-2z)}+E_4e^{-i(\pi/a)(y+2z)}. \tag{7.4}$$

Defining the four-component spinor field $\Psi^\dagger=(E_1^*E_2^*E_3^*E_4^*)$, the resulting coupled equations can then be written compactly as:

$$[(i2\,\overline{\gamma}_1\partial_x+i\,\gamma_4\partial_y+i2\,\overline{\gamma}_2\partial_z)+\delta_W+\beta\gamma_3+\alpha U_{\rm NL}]\Psi=0, \tag{7.5a}$$

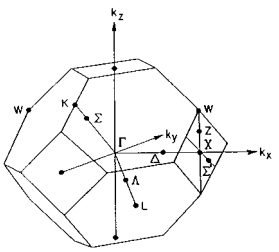

FIG. 17. Shown is the first Brillouin zone to the 3D fcc lattice structure labeled with the twofold L symmetry point and the fourfold W symmetry point.

where

$$U_{\rm NL}=[\tfrac{7}{4}(\Psi^\dagger\Psi)-\tfrac{1}{4}(\Psi^\dagger\gamma_4\Psi)\gamma_4-\tfrac{1}{2}(\Psi^\dagger\overline{\gamma}_1\Psi)\overline{\gamma}_1 -\tfrac{1}{4}(\Psi^\dagger\overline{\gamma}_2\Psi)\overline{\gamma}_2]. \quad (7.5b)$$

Here, $\delta_W=(\omega^2-5/3)/4$, and the matrices $\overline{\gamma}_1=(\gamma_1+\gamma_2)/2$ and $\overline{\gamma}_2=(\gamma_1-\gamma_2)/2$. The dimensionless coordinate variables are measured in units of $(\sqrt{3}G)^{-1}$, and the field is rescaled as $\sqrt{2\lambda/3}\Psi\rightarrow\Psi$.

The band gaps in the SVEA for the L and W symmetry points are found in the usual way from the linear dispersion relations. For the L symmetry point the band edges occur at the frequencies

$$\omega_{\pm}^{L}=\sqrt{1\pm 4\beta}, \quad (7.6a)$$

whereas, for the W symmetry point, the band edges occur at

$$\omega_{\pm}^{W}=\sqrt{5/3\pm 8\beta}, \quad (7.6b)$$

For a complete band gap in the SVEA, we require $\Delta\epsilon/\bar{\epsilon}\geqslant 0.66$.

Variational results

Equation (7.3) may be cast into a variational form by defining the action functional S_L: (for simplicity we drop the primes in x, y, z)

$$S_L=\int d^3\vec{r}\left(|\partial_y\Psi|^2+|\partial_z\Psi|^2-\Psi^\dagger(i\sigma_z\partial_x+\delta+\beta\sigma_x)\Psi -\frac{\alpha}{2}(\Psi^\dagger\Psi)^2\right). \quad (7.7)$$

Using the trial function $\Psi^\dagger=A(x,y,z)(e^{-i\phi(x)},e^{i\phi(x)})$, the action takes the form

$$S_L/2=\int d^3\vec{r}[(\partial_yA)^2+(\partial_zA)^2+A^2\partial_x\phi-\delta A^2 -\beta\cos(2\phi)A^2-\alpha A^4]. \quad (7.8)$$

This can be extremized using the variational ansatz $A(x,y,z)=A\ \mathrm{sech}(ax)\mathrm{sech}(by)\mathrm{sech}(bz)$ and $\phi(x)=c+\arctan[d\tanh(ax)]$. Using this trial function the integration in Eq. (7.8) can be performed analytically, yielding

$$S_L/16=2A^2/3a+A^2[d^2\arctan(d)+\arctan(d)-d]/d^2b^2 -\delta A^2/ab^2-A^2\beta\cos(2c)[2\arctan(d)/d-1]/ab^2 -8\alpha A^4/27ab^2. \quad (7.9)$$

The extremum condition $\partial S/\partial\tau_i=0$ for $\tau_i=A$, a, b yields

$$\alpha A^2=27[\arctan(d)+\arctan(d)/d^2-1/d]a/8, \quad (7.10a)$$

$$\delta+\beta\cos(2c)[2\arctan(d)/d-1]=0, \quad (7.10b)$$

$$b^2=4\alpha A^2/9, \quad (7.10c)$$

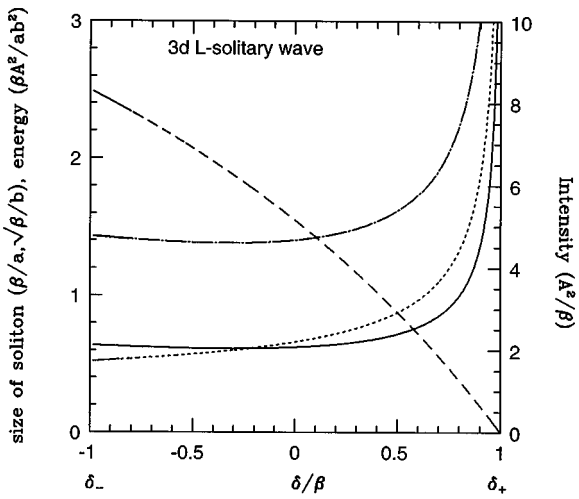

FIG. 18. Plotted are the variational parameters for the 3D L solitary wave. The soliton length β/a (solid line), and transverse size $\sqrt{\beta}/b$ (dotted line) are measured in units of a_o. The quantity $\beta A^2/ab^2$ (dotted long-dashed line) is proportional to the total energy of the L solitary wave, and the peak intensity (right scale) is given by A^2/β (short-dashed line).

$$a=\beta\cos(2c)[d^2/(1+d^2)-d\arctan(d)]/[d-\arctan(d)], \quad (7.10d)$$

$$\cos(2c)=\pm 1. \quad (7.10e)$$

From Eq. (7.10c) it is clear that a localized solution exists only for $\alpha=+1$ (positive Kerr coefficient). In Fig. 18, the intensity A^2, size scales a, and b, and the total energy are plotted as a function of detuning frequency δ. Clearly, the minimum energy solitary wave occurs near the midgap. Near the upper band edge the total energy diverges. The required incident intensity (flux) is given by

$$I_{\rm in}\ [\mathrm{W/cm^2}]=33.77\frac{\bar{\epsilon}^{3/2}}{|\chi^{(3)}|}A^2, \quad (7.11)$$

and the total energy of the ''light bullet'' of the L solitary wave is given by

$$U\ \ (\mathrm{J})=1.4\times 10^{-11}\left(\frac{\bar{\epsilon}^2a_o^3}{|\chi^{(3)}|}\right)\left(\frac{A^2}{ab^2}\right). \quad (7.12)$$

For the W symmetry point, the action functional corresponding to Eq. (7.5) is given by

$$S_W=\int d^3r\{\Psi^\dagger[i(2\overline{\gamma}_1\partial_x+\gamma_4\partial_y)+2\overline{\gamma}_2\partial_z+\delta_W+\beta\gamma_3]\Psi +\tilde{U}_{\rm NL}\}, \quad (7.13a)$$

where

$$\tilde{U}_{\rm NL}=\frac{\alpha}{2}[\tfrac{7}{4}(\Psi^\dagger\Psi)^2-\tfrac{1}{4}(\Psi^\dagger\gamma_4\Psi)^2-\tfrac{1}{2}(\Psi^\dagger\overline{\gamma}_1\Psi)^2 -\tfrac{1}{4}(\Psi^\dagger\overline{\gamma}_2\Psi)^2]. \quad (7.13b)$$

Using the trial function $\Psi^{\dagger}=A(x,y,z)(e^{-i\phi_1}, e^{-i\phi_2}, e^{-i\phi_3}, e^{-i\phi_4})$, the action becomes

$$S_W=\int d^3r\Bigg[-A^2\Bigg(2\frac{\partial}{\partial x}(\phi_1-\phi_2)+2\frac{\partial}{\partial z}(\phi_3-\phi_4)+\frac{\partial}{\partial y}(\phi_1+\phi_2-\phi_3-\phi_4)\Bigg)+4\delta_W A^2+2\beta A^2(\cos(\phi_1-\phi_3)+\cos(\phi_1-\phi_4)+\cos(\phi_2-\phi_3)+\cos(\phi_2-\phi_4))+14\alpha A^4\Bigg]. \tag{7.14}$$

Using phase angles $\phi_1=c_1+k(x+y)$, $\phi_2=c_2-k(x-y)$, $\phi_3=c_3-k(y-z)$, and $\phi_4=c_4-k(y+z)$, we obtain

$$\tilde{S}(A,a,k,c)=[-3k+\delta_W+2\beta\cos(2c)\times e^{-3k^2/4a^2}+\alpha' A^2]A^2/a^3. \tag{7.15}$$

Here $\cos(2c)=[\cos(c_1-c_3)+\cos(c_1-c_4)+\cos(c_2-c_3)+\cos(c_2-c_4)]/4$, $\alpha'=7\sqrt{2}\alpha/8$, and $\tilde{S}=S_W/\pi\sqrt{2\pi}$. The extremum condition gives

$$\delta_W+2\beta\cos(2c)e^{-3\xi/4}(2+\xi)=0, \tag{7.16a}$$

$$k=-\beta\cos(2c)\xi e^{-3\xi/4}, \tag{7.16b}$$

$$\alpha' A^2=-\beta\cos(2c)\xi e^{-3\xi/4}, \tag{7.16c}$$

where

$$\xi^2=k^2/a^2. \tag{7.16d}$$

Equations (7.16) yield a solution for both signs of the Kerr coefficient. As with the 2D X solitary wave, the Gaussian trial function does not give a physical solitary wave solution throughout the entire band-gap region. Moreover, the use of the sech trial function fails in this regard. This is probably because Bragg scattering occurs in several directions leading to a more complicated phase modulation behavior than considered above. Nevertheless, in Fig. 19 the variational parameters are plotted as a function of the detuning frequency δ_W, for the case of a negative Kerr coefficient ($\alpha=-1$), in the band-gap region where a solution is possible. As expected, the total energy of the solitary wave diverges as the frequency approaches the lower band edge. Unlike the L solitary wave, where the minimum energy is around midgap, the W solitary wave has a minimum energy much closer to the lower band edge. For the W solitary wave the required incident intensity (flux) is given by

$$I_{\rm in}\ ({\rm W/cm^2})=50\frac{\tilde{\epsilon}^{3/2}}{|\chi^{(3)}|}A^2, \tag{7.17a}$$

and the total energy

$$U\ ({\rm J})=8\times10^{-12}\left(\frac{\tilde{\epsilon}^2 a_o^3}{|\chi^{(3)}|}\right)\left(\frac{A^2}{a^3}\right). \tag{7.17b}$$

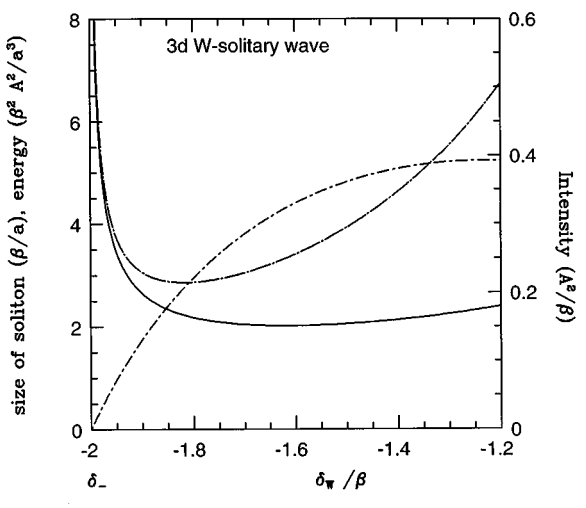

FIG. 19. The variational parameters for the 3D W solitary wave are plotted in terms of the detuning frequency δ_W/β. The soliton size β/a (solid line, left scale) is measured in units of G^{-1}, the quantity β^2A^2/a^3 (dotted long-dashed line) is proportional to the total energy of the W solitary wave, and the peak intensity (right scale) is A^2/β (dotted short-dashed line).

For concreteness, we consider a fcc lattice of air spheres in silicon. We consider the frequency where the total energy attains a local minimum. This is near the midgap $\delta=0$ for the L solitary wave. The variational parameters are given as ($\alpha=+1$): $A^2/\beta=5.15$, $a/\beta=1.6$, $b/\sqrt{\beta}=1.5$ and $A^2\beta/(ab^2)=1.4$. For the W solitary wave the minimum coupling energy is achieved for a detuning frequency $\delta_W/\beta=1.81$ ($\alpha=+1$), and the variational parameters are given as: $A^2/\beta=0.2$, $a/\beta=0.45$, and $A^2\beta^2/a^3=2.2$. The Kerr coefficient for silicon at 1.06 μm has been measured [49] to be $\chi^{(3)}=8\times10^{-8}$ esu. However, the nonlinear response time is in the nanosecond time scale. Considering a filling fraction $f=0.74$, there exists a complete photonic band gap region (of about 5 of the center frequency) centered at $a_o/\lambda=0.85$. In order to place the center of the PBG at $\lambda=1.55$ μm, we require a lattice constant $a_o=1.3$ μm. The expansion coefficients of the Fourier expansion are given by [26]:

$$\tilde{\epsilon}=(1-f)\epsilon_A+f\epsilon_B \tag{7.18a}$$

and

$$\Delta\epsilon=6f(\epsilon_A-\epsilon_B)\frac{[\sin(Gr_a)-Gr_a\cos(gr_a)]}{(Gr_a)^3}. \tag{7.18b}$$

Here, $\epsilon_A=12$ (silicon), $\epsilon_B=1$ (air) and $G=2\pi\sqrt{3}/a_o$. From these expressions $\tilde{\epsilon}=3.9$ and $\beta\equiv\Delta\epsilon/8\tilde{\epsilon}\simeq0.07$. For the L solitary wave with $\delta=0$, the total energy $U=0.1$ pJ with $I_{\rm in}=1.2$ GW/cm^2. For the W solitary wave with $\delta_W=0.127$, $U=1.5$ pJ, and $I_{\rm in}=67$ MW/cm^2.

VIII. STABILITY OF SOLITARY WAVES SATISFYING A NONLINEAR DIRAC TYPE EQUATION

Given the existence of gap solitary wave solutions in a nonlinear photonic crystal, the next important question to

consider is their stability with respect to small perturbations. Higher-dimensional solitary waves ($d \geq 2$) in a Kerr medium satisfying the nonlinear Schrödinger equation are known to be unstable to self-focusing wave collapse. Physically, the wave collapse will eventually be stopped by other physical mechanism not accounted for in the derivation of the nonlinear wave equation. These may include higher order nonlinearities, higher derivative terms of the power series expansion of the dispersion, or even optical damage of the material. In most materials the nonlinear index saturates at higher intensities, thereby stabilizing the solitary wave and preventing wave collapse. The inclusion of fourth and higher order derivatives in the nonlinear Schrödinger equation has been shown [36] to stabilize the solitary wave under suitable circumstances. It has also been shown that the addition of a ($\chi^{(5)}$) nonlinearity to the usual Kerr response ($\chi^{(3)}$) stabilizes the solitary wave solution [50]. The stability analysis of solitary waves falls into two main categories. The first consists of direct numerical stability analysis of the nonlinear wave equation. The second approach consists of linearizing the nonlinear wave equation with respect to small perturbations about the solitary wave, and considering the temporal growth or decay of the perturbation. In certain special cases one may use the minimum property of a suitable action functional to determine the stability of solitary waves. For scalar fields with a linear spectrum which is bounded from below, the existence of a local minimum of the action functional with respect to small perturbations of the solitary wave is equivalent to the condition of stability obtained from time-dependent perturbation theory. This was used by Derrick [51] to establish stability of the solutions to the nonlinear Klein-Gordon equation. However, for wave equations (such as the Dirac equation) with a sign indefinite linear spectrum, the action functional may not possess a local minimum in the vicinity of a stable solitary wave.

In order to determine the stability of the gap solitary waves derived in the previous sections, a small time-dependent perturbation is added to the solitary wave solution and the condition for exponential growth of the perturbation with time is found. Following this procedure, we conjecture an analytical stability criterion for optical gap solitary waves, analogous to the one found for the NLSE. Our conjectured stability criterion correctly recaptures the known stability characteristics of other widely studied nonlinear spinor field equations. It makes some distinctive predictions for optical solitary waves in PBG materials.

A. Linear stability method

We begin with a brief review of the linear stability properties for a scalar field Ψ satisfying the generalized nonlinear Schrödinger equation (GNLSE)

$$i\Psi_t + \nabla^{2p}\Psi + |\Psi|^{2s}\Psi = 0. \tag{8.1}$$

When $p=s=1$, Eq. (8.1) reduces to the well known NLSE. The hermiticity of the operator $\nabla^{2p}+|\Psi|^{2s}$ guarantees that the total ''field energy'' $Q=\int d^d\vec{r}|\Psi|^2$ is a conserved quantity.

Consider a stationary solution of Eq. (8.1) of the form $\Psi(r,t)=\Psi_o(r)e^{i\omega t}$ with $\omega>0$. It follows that Ψ_o satisfies the static GNLSE,

$$\nabla^{2p}\Psi_o - \omega\Psi_o + \Psi_o^{2s+1} = 0. \tag{8.2}$$

As described in Sec. III, for $d>1$, in addition to the nodeless ''ground state'' solution, there are also ''excited state'' solutions to Eq. (8.2) exhibiting one or more nodes. Here, we discuss the stability of the ground state solution only. Consider a small perturbation to the stationary solution $\Psi_o(r)$ of the form

$$\Psi(r,t)=\{\Psi_o(r)+[u(r,t)+iv(r,t)]\}e^{i\omega t} \tag{8.3}$$

for which the real valued functions $u,v \ll \Psi_o$. Inserting Eq. (8.3) into Eq. (8.1) and keeping only first order terms in u and v, we obtain two coupled equations for the real and imaginary parts:

$$u_t = L_o v, \tag{8.4a}$$

$$v_t = -L_1 u. \tag{8.4b}$$

Here $L_o=-\nabla^{2p}+\omega-\Psi_o^{2s}$ and $L_1=-\nabla^{2p}+\omega-(2s+1)\Psi_o^{2s}$. Using Eq. (8.2) it is easy to verify that $L_o\Psi_o=0$ and $L_1(\nabla\Psi_o)=0$, where $j=x,y,z$. Since the ground state solution, Ψ_o, has no nodes, the operator L_o is positive definite. On the other hand, the zero eigenvalue solution of the operator L_1 has one node. Therefore, L_1 has at least one negative eigenvalue. We consider solutions to Eqs. (8.4) of the form $u(r,t)=u(r)\sin(\Omega t)$ and $v(r,t)=v(r)\cos(\Omega t)$. The resulting time-independent equations

$$L_o v = \Omega u, \tag{8.5a}$$

$$L_1 u = \Omega v \tag{8.5b}$$

can be combined to give

$$L_o L_1 u = \Omega^2 u. \tag{8.6}$$

Our definition of marginal stability is that any small energy conserving perturbation added to the solitary wave should not grow in time. In other words, $\Omega^2>0$. Perturbations of the form $u(x)\propto\Psi_o(x)$ which simply increase the overall magnitude of the solitary wave without affecting its shape, require that energy be added to the system. We eliminate perturbations of this form in our stability considerations by requiring that $\langle u|\Psi_o\rangle=0$. Now the instability corresponds to the existence of a perturbation u, satisfying the constraint $\langle u|\Psi_o\rangle=0$, for which $\Omega^2<0$.

Within the subspace of perturbations for which $\langle u|\Psi_o\rangle=0$, the operator inverse L_o^{-1} exists. Accordingly we may act with L_o^{-1} on Eq. (8.6) to obtain:

$$\Omega^2=\frac{\langle u|L_1|u\rangle}{\langle u|L_o^{-1}|u\rangle}. \tag{8.7}$$

Since $\langle u|L_o^{-1}|u\rangle>0$ within this subspace, the sign of Ω^2 is determined entirely by the numerator. Therefore, it is useful to determine the minimum value of $\langle u|L_1|u\rangle$ subject to the constraints that $\langle u|\Psi_o\rangle=0$ and $\langle u|u\rangle=1$. This can be achieved by considering the functional $\langle u|L_1|u\rangle - \lambda\langle u|u\rangle - \alpha\langle u|\Psi_o\rangle$, where α and λ are undetermined

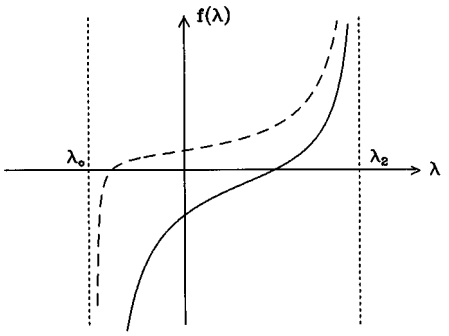

FIG. 20. Shown is the function $f(\lambda)$ which diverges at both $\lambda=-|\lambda_o|$ and $\lambda=\lambda_2$ and is continuous between these two values. The minimum value $\lambda_{\min}$ defines the point where $f(\lambda)$ intercepts the λ axis. If $f(0)>0$, then $\lambda_{\min}<0$, and if $f(0)<0$, then $\lambda_{\min}>0$.

Lagrange multipliers. The minimum of this functional is determined by solving the spectral problem

$$L_1 u=\lambda u+\alpha\Psi_o, \tag{8.8}$$

with α and λ chosen to satisfy the constraints. To solve this spectral problem, we expand u and Ψ_o in terms of the complete set of eigenfunctions of L_1, defined by the relation $L_1\varphi_n=\lambda_n\varphi_n$. Using the orthonormality of the function φ_n we obtain,

$$u=\alpha\sum_{n=0}^{\infty}\frac{\langle\Psi_o|\varphi_n\rangle}{\lambda_n-\lambda}\varphi_n. \tag{8.9}$$

The Lagrange multipliers α and λ may now be determined by imposing the constraints. The condition that $\langle u|\Psi_o\rangle=0$ yields

$$\alpha\sum_n\frac{|\langle\Psi_o|\varphi_n\rangle|^2}{\lambda_n-\lambda}\equiv\alpha f(\lambda)=0. \tag{8.10}$$

We note that the eigenfunction ϕ_1 corresponds to a ''Goldstone mode.'' In particular, $L_1(\nabla_j\Psi_o)=0$, $(j=x,y,z)$, and so $\lambda_1=0$ is a d-fold degenerate eigenvalue associated with the spatial translation of the solitary wave in each of the d, independent, Cartesian directions. Since $\langle\nabla\Psi_o|\Psi_o\rangle=0$, it follows that the $n=1$ term in Eq. (8.10) is absent. Clearly the lowest eigenvalue λ_o is negative and the first positive eigenvalue is λ_2. Consider a λ value between λ_o and λ_2. In this interval, $f(\lambda)$ changes monotonically from $-\infty$ to $+\infty$, passing through zero once. We define $\lambda_{\min}$ to be the value of λ at which $f(\lambda_{\min})=0$. Certainly, $\lambda_{\min}$ represents the minimum value of the numerator $\langle u|L_1|u\rangle$ of Eq. (8.7), subject to the constraints $\langle u|\Psi_o\rangle=0$ and $\langle u|u\rangle=1$. It follows that if $\lambda_{\min}>0$ the solitary wave $\Psi_o(r)$ is stable and if $\lambda_{\min}<0$, there exist a energy conserving perturbation which grows with time and Ψ_o is an unstable solution to the GNLSE. Since $f(\lambda)$ is a continuous and monotonic function, the sign of $\lambda_{\min}$ is determined by the following consideration: If $f(0)>0$, then $\lambda_{\min}<0$. If $f(0)<0$, then $\lambda_{\min}>0$. In Fig. 20 we illustrate this graphically. An alternative but equivalent expression for stability follows from the observation that

$$f(0)=\sum_n\frac{|\langle\Psi_o|\varphi_n\rangle|^2}{\lambda_n}=\langle\Psi_o|L_1^{-1}|\Psi_o\rangle. \tag{8.11}$$

The inverse of L_1 can be found by differentiating Eq. (8.2) with respect to ω:

$$\frac{\partial}{\partial\omega}(L_o\Psi_o)=L_1\left(\frac{\partial\Psi_o}{\partial\omega}\right)+\Psi_o=0. \tag{8.12}$$

It follows that in the subspace of perturbations orthogonal to $\nabla_j\Psi_o$,

$$L_1^{-1}\Psi_o=-\left(\frac{\partial\Psi_o}{\partial\omega}\right). \tag{8.13}$$

Using Eq. (8.13) in Eq. (8.11), we obtain

$$f(0)=-\left\langle\Psi_o\left|\frac{\partial\Psi_o}{\partial\omega}\right.\right\rangle=-\frac{1}{2}\frac{\partial Q}{\partial\omega}, \tag{8.14}$$

where $Q(\omega)=\int d^dr|\Psi(r)|^2$. Therefore, the soliton is stable if

$$\frac{\partial Q}{\partial\omega}>0. \tag{8.15}$$

For the particular case of the GNLSE, an analytical expression for the ω dependence of Q can be found by rescaling Eq. (8.2). Introducing the scaled coordinate variable $y=\omega^{1/2p}r$ and writing $\Psi_o(r)=\omega^{1/2s}g(y)$, Eq. (8.2) becomes

$$\nabla^{2p}g-g+g^{2s+1}=0. \tag{8.16}$$

It follows that

$$Q(\omega)=\omega^{1/s-d/2p}\int d^dr\ g^2(r) \tag{8.17}$$

The stability condition (8.15) reduces to

$$d<2p/s \tag{8.18}$$

For the usual NLSE ($s=p=1$), this reduces to the condition that $d<2$. For more general forms of dispersion and nonlinear interaction, the behavior of $Q(\omega)$ is more complicated than given by Eq. (8.17), and must be evaluated numerically. The most important generalization is to the case of a saturable nonlinearity of the form $|\Psi|^2/(1+|\Psi|^2)$. Then the stability criterion (8.15) holds for $d=1,2$ for all $\omega>0$, whereas for $d=3$, it holds only for certain frequencies $\omega>\omega_{\rm cr}$. In particular $\omega_{\rm cr}$ is the point where $Q(\omega)$ is a local minimum [52].

B. Solitary wave stability for the nonlinear Dirac equation

For a nonlinear Dirac type of equation, with a linear spectrum which is unbounded from below, the derivation of a stability criterion analogous to Eq. (8.15) is more problematic. Although an eigenvalue condition of form (8.7) can be obtained, a mathematically rigorous reduction of this eigenvalue problem to a stability criterion of form (8.15) requires certain assumptions about the role of the negative continuous

spectrum of the Dirac operators. We delineate these assumptions below and provide numerical evidence for their validity.

Consider the perturbed spinor field

$$\Psi(\vec{r},t)=\Psi_o(\vec{r})+\delta\Psi(\vec{r},t), \tag{8.19}$$

where Ψ_o is a solution to Eq. (2.7) and $\delta\Psi \ll \Psi_o$. Here, we consider the generalization of the 1D soliton solution to d dimensions, which corresponds to including $\partial^2/\partial y^2$ in two dimensions and $\partial^2/\partial y^2+\partial^2/\partial z^2$ in three dimensions. This equation arises from the two fold symmetry point of the Brillouin zone, and is common to all of the crystal symmetry groups. Inserting Eq. (8.19) into Eq. (2.5) (with two transverse dimensions) and keeping only terms up to first order in $\delta\Psi$, we obtain the equations.

$$-i\delta\dot{E}_1=L_1\delta E_1+\lambda' E_o^2\delta E_1^*+L_2\delta E_2+\lambda'|E_o|^2\delta E_2^* \tag{8.20a}$$

and

$$-i\delta\dot{E}_2=L_1^*\delta E_2+\lambda' E_o^{*2}\delta E_2^*+L_2^*\delta E_1+\lambda'|E_o|^2\delta E_1^*. \tag{8.20b}$$

Here

$$L_1\equiv i\partial_x+\partial_{yy}+\partial_{zz}+\delta+4\lambda'|E_o|^2, \tag{8.21a}$$

$$L_2\equiv\beta+\lambda' E_o^2, \tag{8.21b}$$

and $\lambda'=2\alpha/3$. Separating the real and imaginary parts of $E_o=u_o+iv_o$, $\delta E_1=u_1+iv_1$, $\delta E_2=u_2+iv_2$, and defining the four-component spinor field $\delta\psi^\dagger=(v_1,u_1,v_2,u_2)$, Eq. (8.20) can be expressed as

$$\hat{M}\,\delta\psi=\gamma\dot{\delta\psi}, \tag{8.22a}$$

where

$$\gamma=-i\sigma_y\begin{pmatrix} I & 0\\ 0 & I\end{pmatrix} \tag{8.22b}$$

and

$$\hat{M}=\begin{pmatrix}\hat{O} & \beta I\\ \beta I & \hat{O}\end{pmatrix}+\begin{pmatrix}V_1 & V_2\\ V_2^\dagger & -V_1\end{pmatrix} \tag{8.22c}$$

Here $\hat{O}=(I+\sigma_z)\hat{O}_1/2+(I-\sigma_z)\hat{O}_2/2$, $V_1=\lambda'(\phi_o^\dagger\sigma_x\phi_o)\sigma_x$, and $V_2=2\lambda'[\phi_o^\dagger\sigma_z\phi_o-(\phi_o^\dagger\phi_o)\sigma_z+i(\phi_o^\dagger\sigma_x\phi_o)\sigma_y]$. $\phi_o^\dagger=(u_o,v_o)$ and the operators $\hat{O}_1$ and $\hat{O}_2$ are defined as

$$\hat{O}_1=\partial_{yy}+\partial_{zz}+\delta+5\lambda' u_o^2+3\lambda' v_o^2, \tag{8.23a}$$

$$\hat{O}_2=\partial_{yy}+\partial_{zz}+\delta+3\lambda' u_o^2+5\lambda' v_o^2. \tag{8.23b}$$

Introducing the new set of variables $u=u_1+u_2$, $\tilde{u}=u_1-u_2$, $v=v_1+v_2$, and $\tilde{v}=v_1-v_2$, Eq. (8.22) can be written as

$$[\hat{O}_2+(\beta-4\lambda' v_o^2)]v+(\partial_x-2\lambda' u_o v_o)\tilde{u}=-\dot{u}, \tag{8.24a}$$

$$[\hat{O}_1+(\beta+4\lambda' u_o^2)]u+(-\partial_x+6\lambda' u_o v_o)\tilde{v}=\dot{v}, \tag{8.24b}$$

$$[\hat{O}_2-(\beta-4\lambda' v_o^2)]\tilde{v}+(\partial_x+6\lambda' u_o v_o)u=-\tilde{u}, \tag{8.24c}$$

$$[\hat{O}_1-(\beta+4\lambda' u_o^2)]\tilde{u}+(-\partial_x-2\lambda' u_o v_o)v=\tilde{v}. \tag{8.24d}$$

From the conserved quantity $Q=\int d^d\vec{r}(\Psi^\dagger\Psi)=\text{const}$, the condition for an energy conserving perturbation can be written as

$$\int d^d\vec{r}(u_o u+v_o\tilde{v})=0. \tag{8.25}$$

Equations (8.24) can be compactly reexpressed in terms of the two-component spinor fields $\phi_1^\dagger=(u,\tilde{v})$ and $\phi_2^\dagger=(\tilde{u},v)$:

$$\hat{M}_1\phi_1=i\sigma_y\dot{\phi}_2 \tag{8.26a}$$

$$\hat{M}_o\phi_2=-i\sigma_y\dot{\phi}_1. \tag{8.26b}$$

Here

$$\hat{M}_1=\begin{pmatrix}\hat{O}_1+(\beta+4\lambda' u_o^2) & -\partial_x+6\lambda' u_o v_o\\ \partial_x+6\lambda' u_o v_o & \hat{O}_2-(\beta-4\lambda' v_o^2)\end{pmatrix} \tag{8.27a}$$

and

$$\hat{M}_o=\begin{pmatrix}\hat{O}_1-(\beta+4\lambda' u_o^2) & -\partial_x-2\lambda' u_o v_o\\ \partial_x-2\lambda' u_o v_o & \hat{O}_2+(\beta-4\lambda' v_o^2)\end{pmatrix}. \tag{8.27b}$$

If we assume solutions of the form $\phi_1(\vec{r},t)=\phi_1(\vec{r})\sin(\Omega t)$ and $\phi_2(\vec{r},t)=\phi_2(\vec{r})\cos(\Omega t)$, then Eqs. (8.26) become

$$\tilde{M}_1\phi_1=\Omega\tilde{\phi}_2, \tag{8.28a}$$

$$\tilde{M}_o\tilde{\phi}_2=\Omega\phi_1, \tag{8.28b}$$

where we introduced $\tilde{\phi}_2=i\sigma_y\phi_2$, $\tilde{M}_o=\sigma_y\hat{M}_0\sigma_y$, and $\tilde{M}_1=-\hat{M}_1$. The operators $\tilde{M}_1$ and $\tilde{M}_o$ are defined as

$$\tilde{M}_1=-[i\sigma_y\partial_x+\partial_{yy}+\partial_{zz}+\delta+\beta\sigma_z+3\lambda' V(\phi_o^\dagger,\phi_o)], \tag{8.29a}$$

$$\tilde{M}_o=-[i\sigma_y\partial_x+\partial_{yy}+\partial_{zz}+\delta+\beta\sigma_z+\lambda' V(\phi_o^\dagger,\phi_o)]. \tag{8.29b}$$

and $V(\phi_o^\dagger,\phi_o)$ is given as

$$V(\phi_o^\dagger,\phi_o)=(\phi_o^\dagger\sigma_x\phi_o)\sigma_x+(\phi_o^\dagger\sigma_z\phi_o)\sigma_z+2(\phi_o^\dagger\phi_o). \tag{8.30}$$

Here ϕ_o satisfies the nonlinear wave equation

$$[i\sigma_y\partial_x+\partial_{yy}+\partial_{zz}+\delta+\beta\sigma_z+2\alpha(\phi_o^\dagger\phi_o)]\phi_o=0. \tag{8.31}$$

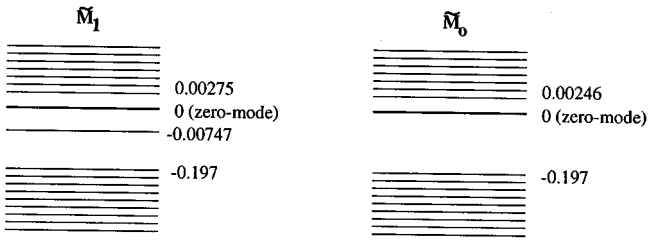

FIG. 21. Illustrated are the spectra of the operators $\tilde{M}_1$ and $\tilde{M}_o$ for the 1D gap soliton case. Both operators exhibit a negative continuum. $\tilde{M}_1$ has a zero eigenvalue corresponding to the usual Goldstone mode and a negative bound state at $-0.007\,47$. The $\tilde{M}_o$ operator has no negative bound states, and the lowest bound solution has an eigenvalue zero, for which the eigenfunction is the gap soliton solution ϕ_o. Here $\alpha=+1$ and $\beta=0.1$.

For concreteness, we consider the case $\lambda'=2\alpha/3>0$. We first examine the spectra of $\tilde{M}_o$ and $\tilde{M}_1$ separately. It can easily be verified that the linear part of the operators $\tilde{M}_o$ and $\tilde{M}_1$, exhibits both positive and negative continua, whereas the potential $V(\phi_o^\dagger,\phi_o)$ is a positive definite operator. $\tilde{M}_1$ has d-fold degenerate eigenfunctions $\nabla_j\phi_o$, $j=x,y,z$ $(d=1,2,3)$ with zero eigenvalue, corresponding to the usual translational (Goldstone) mode of the solitary wave. In the solution $\phi_o^\dagger=(u_o,v_o)$, u_o has one node and v_o is nodeless. It follows that the translational mode $\nabla_j u_o$ has two nodes and $\nabla_j v_o$ has one node. In analogy with the Schrödinger operator, we expect that a bound state $\phi^\dagger=(u,v)$ of the operator $\tilde{M}_1$ with a negative eigenvalue exists, where u has one node and v is nodeless. The operator $\tilde{M}_o$ has a zero eigenvalue corresponding to the solution ϕ_o. In analogy with the Schrödinger operator, we expect that $\tilde{M}_o$ has no negative eigenvalue bound states. We have numerically verified these expected properties of the operators $\tilde{M}_o$ and $\tilde{M}_1$, by expanding their eigenfunctions in terms of the complete orthonormal basis functions used in the finite element analysis. The eigenvalues and eigenvectors of the resulting finite-dimensional matrix are then found by standard methods. To give a numerical example in one dimension, we consider the parameters $\beta=0.1$ and $\delta=0.0975$ (near the upper band edge). It is found that in addition to the negative and positive continua, there is only one negative eigenvalue bound state of the operator $\tilde{M}_o$ at -0.00747, and no negative eigenvalue bound states of the operator $\tilde{M}_o$. In Fig. 21 we illustrate the spectra of the operators for one dimension. Similar results are found for the 2D case.

Equations (8.28) may be combined, as in the GNLSE case, to give

$$\tilde{M}_o\tilde{M}_1\phi_1=\Omega^2\phi_1. \tag{8.32}$$

The solitary wave solution is unstable if there exists an eigenfunction ϕ_1 of Eq. (8.32) with negative eigenvalue Ω^2 in the subspace $\langle\phi_o|\phi_1\rangle=0$. Now it can be easily shown that the linear part (setting $V=0$) of the operator $\tilde{M}_o\tilde{M}_1$ is positive definite, by considering solutions of the form e^{ikr}. The continuous spectrum of $\tilde{M}_o\tilde{M}_1$ is given by

$$\Omega_\pm^2=[\delta-(k_y^2+k_z^2)\pm\sqrt{\beta^2+k_x^2}]^2. \tag{8.33}$$

In the presence of the potential $V(\phi_o^\dagger,\phi_o)$ the operator $\tilde{M}_o\tilde{M}_1$ does not contain a negative continuum, and may have only a finite number of discrete negative eigenvalues corresponding to localized states. In other words, all perturbations corresponding to extended states result in $\Omega^2>0$, and we only have to consider the negative bound states. In what follows, it is convenient to denote negative continuum states of the operators $\tilde{M}_o$ and $\tilde{M}_1$ as the subspace G. We refer to the orthogonal complement of this subspace by the symbol G^c.

In the subspace for which $\langle\phi_o|\phi_1\rangle=0$ we can define the inverse of the operator $\tilde{M}_o$. Accordingly Eq. (8.32) can be reduced to the form obtained for the GNLSE:

$$\Omega^2=\frac{\langle\phi_1|\tilde{M}_1|\phi_1\rangle}{\langle\phi_1|(\tilde{M}_o)^{-1}|\phi_1\rangle}. \tag{8.34}$$

Here we only consider perturbations ϕ_1 that are spatially localized, since we know from Eq. (8.32) that any extended perturbation leads to $\Omega^2>0$. This can also be seen from the fact that $\tilde{M}_1=\tilde{M}_o-2\lambda' V(\phi_o^\dagger,\phi_o)$ and the expectation value becomes $\langle\phi_1|\tilde{M}_1|\phi_1\rangle=\langle\phi_1|\tilde{M}_o|\phi_1\rangle-2\lambda'\langle\phi_1|V(\phi_o^\dagger,\phi_o)|\phi_1\rangle$. The eigenfunctions for the negative continuum correspond to extended states so that for any perturbation ϕ_1 spanned by the negative continuum of the operator $\tilde{M}_o$, the corresponding expectation value $\langle\phi_1|\tilde{M}_1|\phi_1\rangle$ is also negative. This follows from the fact that the expectation value $\langle\phi_1|V(\phi_o^\dagger,\phi_o)|\phi_1\rangle$ is positive. The lowest bound state of the operator $\tilde{M}_o$ corresponds to the eigenfunction ϕ_o, with zero eigenvalue. Consequently $\tilde{M}_o$ has no bound state solutions with negative eigenvalues in the subspace $\langle\phi_o|\phi_1\rangle=0$. On the other hand, the operator $\tilde{M}_1$ has at least one bound state with a negative eigenvalue. Therefore the sign of Ω^2 will be determined by the expectation value of $\langle\phi_1|\tilde{M}_1|\phi_1\rangle$.

In general there are three distinct cases: (i) If the operator $\tilde{M}_1$ has no bound states with negative eigenvalues, then the solitary wave is stable. (ii) If $\tilde{M}_1$ has more than one bound state with a negative eigenvalue, then the solitary wave is unstable. This follows from the fact that it is always possible to construct a perturbation ϕ_1 as a superposition of the negative bound states which also satisfies the constraint $\langle\phi_o|\phi_1\rangle=0$. (iii) If $\tilde{M}_1$ has precisely one negative bound state, then the stability of the solitary wave reduces to a stability criterion similar to that obtained in the NLSE. We consider case (iii) in more detail below.

The minimum value of the numerator in Eq. (8.34) within the subspace $\langle\phi_o|\phi_1\rangle=0$ can be found by solving the spectral problem

$$\tilde{M}_1\phi_1=\lambda\phi_1+\alpha\phi_o, \tag{8.35}$$

where λ and α are Lagrange multipliers, introduced to enforce the constraints $\langle\phi_1|\phi_o\rangle=0$ and $\langle\phi_1|\phi_1\rangle=1$. We now expand ϕ_1 and ϕ_o in terms of the complete set of eigenfunctions $\{\tilde{\phi}_n\}$ of $\tilde{M}_1$. Using the fact that ϕ_o, $\phi_1\ \epsilon G^c$, it is

plausible that the expansion $\phi_o=\Sigma_n\langle\phi_o|\tilde{\phi}_n\rangle\tilde{\phi}_n$ and $\phi_1=\alpha\Sigma_n[\langle\tilde{\phi}_n|\phi_o\rangle\tilde{\phi}_n/(\lambda_n-\lambda)]$ contain only those values of n for which $\tilde{M}_1\tilde{\phi}_n=\lambda_n\tilde{\phi}_n$ and λ_n is not part of the negative continuum of $\tilde{M}_1$. We denote this restriction on the summation over n with a prime. The orthogonality condition of $\langle\phi_1|\phi_o\rangle=0$ then yields

$$f(\lambda)=\sum_n{}' \frac{|\langle\tilde{\phi}_n|\phi_o\rangle|^2}{(\lambda_n-\lambda)}=0. \tag{8.36}$$

As in the GNLSE, the problem is reduced to determining the quantity, $\lambda_{\min}$, defined by the condition $f(\lambda_{\min})=0$. Once again $\lambda_{\min}$ is the minimum value of the quantity $\langle\phi_1|\tilde{M}_1|\phi_1\rangle$ subject to the relevant constraints. We denote the negative discrete eigenvalue of $\tilde{M}_1$ by λ_o. λ_1 is absent in the summation (8.36) since it corresponds to the translational mode which is orthogonal to ϕ_o. Since the function $f(\lambda)$ is monotonic in the interval (λ_0,λ_2), the sign of $f(0)$ is determined by the sign of $\lambda_{\min}$. If $f(0)<0$ then $\lambda_{\min}>0$. If $f(0)>0$ then $\lambda_{\min}<0$. Following the analysis of the GNLSE, we write

$$f(0)=\sum_n{}' \frac{|\langle\tilde{\phi}_n|\phi_o\rangle|^2}{\lambda_n}=\langle\phi_o|(\tilde{M}_1)^{-1}|\phi_o\rangle. \tag{8.37}$$

In the last equality in Eq. (8.37), we have made use of our assumed orthogonality of ϕ_o to each of the eigenfunctions $\tilde{\phi}_n$ in the negative continuum of $\tilde{M}_1$. By virtue of this orthogonality, the summation above can be replaced by an unrestricted sum, yielding the spectral representation of the operator $\tilde{M}_1^{-1}$. Taking the derivative of Eq. (8.31) with respect to δ we obtain

$$\tilde{M}_1\frac{\partial\phi_o}{\partial\delta}-\phi_o=0. \tag{8.38}$$

Substituting Eq. (8.38) into Eq. (8.37) yields

$$f(0)=\left\langle\phi_o\left|\frac{\partial\phi_o}{\partial\delta}\right\rangle\right.=\frac{1}{2}\frac{\partial\langle\phi_o|\phi_o\rangle}{\partial\delta}. \tag{8.39}$$

This leads to the necessary condition for stability that

$$\frac{\partial Q}{\partial\delta}<0, \tag{8.40}$$

where $Q=\langle\phi_o|\phi_o\rangle$. The stability criteria can be summarized as follows: (i) If the $\tilde{M}_1$ operator has more than one negative eigenvalue corresponding to a bound state, then instability takes place irrespective of Eq. (8.40). (ii) If the operator $\tilde{M}_1$ has only one negative bound sate, then the solitary wave is stable provided the conserved quantity Q satisfies condition (8.40). For a negative nonlinear Kerr coefficient, condition (8.40) must be replaced by $\partial Q/\partial\delta>0$, due to the fact that the operators are now defined as $\tilde{M}_1=M_1$ and $\tilde{M}_o=M_o$.

C. Comparison with other models

Before discussing the stability of solitary waves in a PBG material, we illustrate the stability criterion given by Eq. (8.40) with some widely studied nonlinear spinor equations. The first one is the integrable massive Thirring model (MTM), defined by the nonlinear wave equation

$$\left(i\partial_t+i\sigma_z\partial_x+m\sigma_x+\frac{\kappa}{2}[(\psi^\dagger\psi)-(\psi^\dagger\sigma_z\psi)\sigma_z]\right)\psi=0. \tag{8.41}$$

Here it is known that stable localized soliton solutions exist of the form [53]

$$\psi=\sqrt{2(m-\omega)/\kappa}\frac{\operatorname{sech}(ax)}{1+b^2\tanh^2(ax)}\begin{bmatrix}1\\ b\tanh(ax)\end{bmatrix}e^{-i\omega t}, \tag{8.42}$$

where $a=\sqrt{(m^2-\omega^2)}$ and $b=\sqrt{(m-\omega)/(m+\omega)}$. For these solutions,

$$Q=\int dx(\psi^\dagger\psi)=\frac{8}{\kappa}\arctan\sqrt{\left(\frac{m-\omega}{m+\omega}\right)}. \tag{8.43}$$

Here ω takes the place of δ in Eq. (8.40). Clearly, $\partial Q/\partial\omega<0$ for $-m<\omega<m$, indicating stability of solitons throughout the gap.

The Gross-Neveu model is defined by the equation [53]

$$\{i\partial_t+i\sigma_y\partial_x-m\sigma_x+\kappa[(\psi^\dagger\sigma_z\psi)\sigma_z]\}\psi=0 \tag{8.44}$$

Here the soliton solution takes the form [53]

$$\psi=\sqrt{2(m-\omega)/\kappa}\frac{\operatorname{sech}(ax)}{1-b^2\tanh^2(ax)}\begin{bmatrix}1\\ b\ \tanh(ax)\end{bmatrix}e^{-i\omega t}, \tag{8.45}$$

where a and b are the same as in the MTM, and $Q=2(m-\omega^2)^{1/2}/\omega$. This soliton is stable for the region $0<\omega<m$, in agreement with numerical studies [54]. An extension of the Gross-Neveu model to (3+1) dimensions is the Soler model. In this case an analytical expression for Q is not available. Nevertheless, it has been shown numerically that Q exhibits a local minimum as a function of ω at some frequency $\omega_{\rm cr}$. Consequently, $\partial Q/\partial\omega$ changes sign at $\omega_{\rm cr}$ and the soliton is unstable for $\omega>\omega_{\rm cr}$. In both numerical [54] and analytical [55] studies of the Soler model, this result was confirmed.

In the case of a photonic band gap, the 1D gap soliton is believed to be stable [5]. We may generalize the 1D gap soliton to two- and three-dimensional gap solitary waves by estimating the conserved quantity Q from the variational results of Sec. IV. This gives the dependence of Q on the detuning frequency δ. In Fig. 22 we plot the quantity Q versus the detuning parameter δ for $d=1$, 2, and 3. In both $d=1$ and 2, $Q_\delta=(\partial Q/\partial\delta)<0$ for the entire band gap region. However for $d=3$, Q_δ is positive between $\delta_{cr}<\delta<\delta_+$, indicating instability in upper band edge region and stability in the rest of the band gap. This behavior of the total energy is reminiscent the case of the GNLSE with a saturating nonlinear potential. For the symmetric 3D W solitary wave a local minimum also exist for the quantity Q but is now much closer to the band edge, in which stable solutions may be possible for most of the band gap region. In

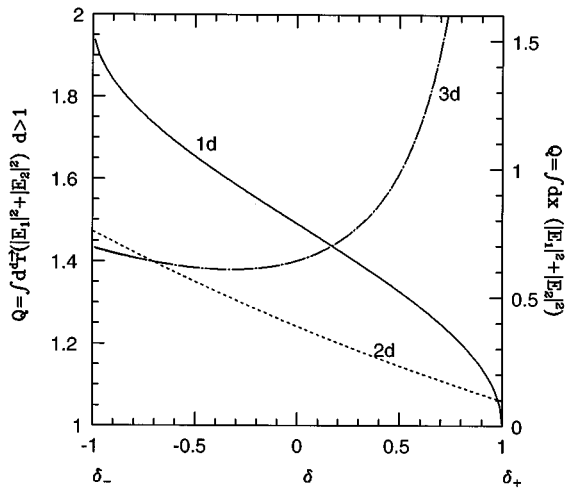

FIG. 22. Plotted is the dependence of the conserved quantity Q, for $d=1$ (solid line, left scale), $d=2$ (dotted line, right scale), and $d=3$ (long-dashed dotted line, right scale) on the detuning parameter δ. The stability condition $\partial Q/\partial\delta<0$ is satisfied for $d=1$ and 2 throughout the band-gap region, whereas, for $d=3$, stable solutions may only exist for $\delta>\delta_{\rm cr}$. Here $\delta_{\rm cr}$ is the detuning for which Q has a local minimum.

Sec. III we showed that an effective nonlinear Schrödinger equation describes gap solitary waves near the band edge. For $d=3$, the NLSE solitary wave solution is unstable. This is consistent with the behavior of Q_δ. For $d=2$, the conserved quantity can be approximated near the upper band edge as, $Q=c_1+c_2(\beta-\delta)$, where c_1 and c_2 are positive numbers. Unlike the case of the NLSE in two dimensions, for which Q is independent of δ, in the 2D PBG system we have $Q_\delta<0$. The apparent stability of the 2D gap solitary wave is a new prediction of our stability criterion (8.40). Finally, our stability criterion suggests the existence of stable three-dimensional solitary waves deep inside the photonic band gap in a Kerr medium, a new result which may not be extrapolated by simple consideration on the nonlinear Schrödinger equation. It is of importance to extend this study to the case of a saturable nonlinearity and to determine the stability of 3D ''light bullets'' throughout the PBG for this, more realistic, situation.

D. Relationship between stability and the minimum property of the action functional

We conclude this section with a discussion of the relationship of linear stability analysis and the scaling and minimization properties of the action functional. A precise connection exists for nonlinear wave equations with a positive definite continuous spectrum such as the nonlinear Schrödinger equation. However, for Dirac-type wave equations exhibiting an unbounded negative spectrum, this equivalence appears to be lost. We start with the GNLSE in d dimensions. The stationary solution to Eq. (8.1) is an extremum of the action functional

$$S=\int d^d\vec{r}\left(|\nabla\Psi|^{2p}+\omega|\Psi|^2-\frac{1}{(2s+2)}|\Psi|^{2s+2}\right), \tag{8.46}$$

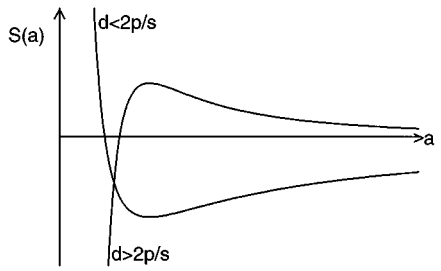

FIG. 23. Plotted is the action functional $S(a)$ of the generalized nonlinear Schrödinger equation (GNLSE) with respect to the scaling parameter a. The functional $S(a)$ has a stable minimum when $d<2p/s$, and an unstable maximum when $d>2p/s$. For the standard nonlinear Schrödinger equation ($s=p=1$), the solitary wave is stable for $d<2$.

with the conserved quantity $Q=\int d^d\vec{r}|\Psi|^2$. Our linear stability analysis indicated that the solitary wave solution is stable when $d<2p/s$. This condition can also be deduced from the action functional by considering a one-parameter scaling form $\Psi=\Psi(x/a)/a^{d/2}$ of the solitary wave, which preserves Q. Substituting this scaling form into Eq. (8.46) yields

$$S(a)=\frac{I_1}{a^{2p}}+\omega I_2-\frac{I_3}{a^{ds}}, \tag{8.47}$$

where I, I_2, and I_3 are positive numerical constants. The linear stability condition is equivalent to the statement that $\partial^2 S/\partial a^2|_{a=1}>0$. This corresponds to the requirement that $ds(2p-ds)I_3>0$. Since $dsI_3>0$, the condition for a local minimum of the functional is that $(2p-ds)>0$. This is exactly the same condition obtained from the linear stability analysis. It can be seen from Fig. 23 that for $d<2p/s$, $S(a)$ has a stable minimum, whereas for $d>2p/s$ the extremum point corresponds to a maximum, in which case the functional S diverges as $a\to 0$. Physically, the instability takes place whenever the nonlinear potential $\int d^d\vec{r}|\Psi|^{2s}$ overcomes the kinetic energy term $\int d^d\vec{r}|\nabla\Psi|^{2p}$. In general solitary waves are stable when the nonlinear potential is bounded, as is the case for a saturable nonlinear susceptibility. Another stabilization mechanism is the inclusion of higher order derivative terms in the kinetic energy term. For example in the NLSE ($s=p=1$), if the nonlinear refractive index is replaced by an expression of the form $\alpha_1|\Psi|^2-\alpha_2|\Psi|^4$ ($\alpha_{1,2}>0$), then the action functional scales as

$$S(a)=\frac{I_1}{a^2}+\omega I_2-\frac{I_3}{a^d}+\frac{I_4}{a^{2d}}. \tag{8.48}$$

Here all the $I_1\cdots I_4$ are positive numbers. The extremum condition now becomes

$$\left.\frac{\partial^2 S}{\partial a^2}\right|_{a=1}=(2d-d^2)I_3+4(d^2-d)I_4. \tag{8.49}$$

It is easy to verify that 3D solitary waves are stable in this medium provided that $I_4>I_3/8$. Moreover, in a saturable medium with a nonlinear refractive index of the form

$f(|\Psi|^2)=|\Psi|^2/(1+|\Psi|^2)$, stable solutions exists in general for $d=1$ and 2. For $d=3$, stable solutions are possible only above some critical frequency $\omega>\omega_{\rm cr}$ [52].

Clearly, there is a direct connection between the minimum property of the action functional and stability of the solitary wave solutions in the nonlinear Schrödinger type equations. This connection can be made more precise by considering a perturbation of the form $\Psi-\Psi_o=(u+iv)$ in the functional S. Collecting up to quadratic terms in u and v, we obtain the second variation of S

$$\delta^2 S=\int d^d r(vL_o v+uL_1 u). \tag{8.50}$$

Here, the operators $L_{o,1}$ are defined as in Sec. VIII A. In order to have $\delta^2 S>0$, both terms in Eq. (8.50) must be positive definite in the subspace $\langle u|\Psi_o\rangle=0$. Since we already know that in this subspace L_o is positive definite, a sufficient condition for stability is that $\langle u|L_1|u\rangle$ is positive definite. This condition leads to the same spectral eigenvalue problem defined by Eq. (8.8) which in turn leads to the stability criterion (8.15).

In the case of spinor fields satisfying a nonlinear Dirac type of equation, we show below that the linear stability criterion and the minimum of the action functional are not equivalent. Consider the second variation of the functional S_L defined in Eq. (7.9). Expanding $\Psi=\Psi_o+\delta\Psi$ and keeping quadratic terms in $\delta\Psi$, we obtain

$$\delta^2 S_L=\int d^d r(\phi_1^\dagger \widetilde{M}_1 \phi_1+\widetilde{\phi}_2^\dagger \widetilde{M}_o \widetilde{\phi}_2). \tag{8.51}$$

Here the operators $\widetilde{M}_1$ and $\widetilde{M}_o$ are precisely those in Eqs. (8.29a) and (8.29b). In order to make $\delta^2 S_L$ positive definite, the operator

$$M_s=\begin{pmatrix} \widetilde{M}_1 & 0 \\ 0 & \widetilde{M}_o \end{pmatrix} \tag{8.52}$$

must be positive definite. Clearly this is impossible, since the operator M_s exhibits a negative continuum. The eigenvalue problem arising here differs significantly from the one obtained in linear stability analysis. Our earlier time-dependent stability analysis led to a spectral problem for the operator $\widetilde{M}_s=\sigma_x M_s$ which does not exhibit a negative continuum. In general, the action functional, S_L, exhibits a saddle point instead of a minimum. As an illustration, consider the scaling of the form $\Psi=\Psi_s(x/a,y/b)/\sqrt{ab}$ for 2D gap solitary wave. For the X solitary wave the action functional can be written as ($\alpha=+1$)

$$S_X(a,b)=\frac{I_{yy}}{b^2}-\frac{I_x}{a}-\frac{I_{\rm NL}}{ab}, \tag{8.53}$$

where, I_{yy}, I_x, and $I_{\rm NL}$ are positive numbers. In order to have $\delta^2 S_X>0$, the following conditions must be satisfied:

$$\left.\frac{\partial^2 S_X}{\partial \tau_i^2}\right|_{a,b=1}>0, \quad \tau_i=a,b, \tag{8.54a}$$

$$\Delta=\left|\begin{array}{cc} \dfrac{\partial^2 S_X}{\partial a^2} & \dfrac{\partial^2 S_X}{\partial a\,\partial b} \\ \dfrac{\partial^2 S_X}{\partial b\,\partial a} & \dfrac{\partial^2 S_X}{\partial b^2} \end{array}\right|_{a,b=1}>0. \tag{8.54b}$$

In actual fact, $\partial^2 S_X/\partial a^2|_{a,b=1}=0$, $\partial^2 S_X/\partial b^2|_{a,b=1}=I_{\rm NL}>0$, and $\Delta=-I_{\rm NL}^2<0$ indicating that the solitary wave is a saddle point in the parameter space (a,b). On the other hand our linear stability analysis suggested that the solitary wave is stable in two dimensions. Clearly, the two methods are not equivalent. A similar conclusion applies the M solitary wave.

In summary, for solitary waves where the linear differential operator which enters the nonlinear wave equation is not positive definite, scaling arguments are not a reliable indicator of stability and careful consideration of the time-dependent linear stability is essential.

IX. DISCUSSION AND CONCLUSIONS

In this paper, we have demonstrated the existence of stable solitary waves in 2D and 3D nonlinear photonic band-gap materials exhibiting a nonresonant $\chi^{(3)}$ Kerr type of nonlinearity. Unlike the 1D Bragg gratings studied by others, the higher-dimensional periodic structures exhibit multiple symmetry points in the Brillouin zone, resulting in at least two distinct types of solitary wave solutions. Solutions of the first type, which are associated with a twofold symmetry point, break the full symmetry of the crystal under rotation and exist only for a positive Kerr coefficient for $d>1$. Solutions of the second type, which are associated with a higher order symmetry point, exist for both positive and negative Kerr coefficients. Solitary waves of the first type can travel at any velocity from zero up to the average speed of light in the medium. This can be seen by applying a Lorentz boost to the corresponding stationary solution. For a purely 1D system, the moving soliton experiences a Lorentz contraction. In $d>1$, the moving solitary wave experiences additional transverse expansion due to the decay of the wave amplitude in the transverse direction. In general, as the soliton velocity increases, the average frequency of the soliton moves away from the center of the PBG and the total soliton energy decreases. If the average frequency is outside of the PBG, such solitons are degenerate in frequency with propagating linear electromagnetic modes. This leads to couplings not included in our model, and may in turn lead to instability of the solitary wave.

Near a photonic band edge, our solitary wave solutions are well described by a simple nonlinear Schrödinger equation. Deeper inside the PBG, these solitary waves probe the full structure of the nonlinear Dirac equation obtained in the context of the SVEA. It is well known that for $d=3$, solitons of the NLSE are unstable. This is consistent with our near band edge results. However, deeper inside the PBG, we obtain the entirely new prediction that 3D solitary waves are stable with respect to small perturbations. In addition we find stable solitary wave solutions throughout the PBG for $d=1$ and 2.

The solitary wave solutions we have obtained correspond

to ultrashort, high intensity light pulses. Near the center of a PBG with a gap to center frequency ratio $\Delta\omega/\omega_o \simeq 0.10$, these nonlinear pulses have a spatial extent of only several optical wavelengths. For 3D light bullets in a fcc photonic crystal, the total energy of the pulse is on the scale of picojoules. If such a pulse were to move in vacuum, the corresponding peak intensity is on the scale of GW/cm^2. In this sense, our gap center solitary wave corresponds to a compressed version of the pJ solitons envisaged in fiber optic telecommunication networks [12]. As the average frequency of the solitary wave is chosen closer to the photonic band edge, the compression of the pulse is relaxed, and it can have an arbitrarily large spatial extent.

In practice, the speed of propagation of the light bullet through the PBG material will be limited by the speed of the nonlinear optical response in the material. For a pulse which extends over only a few optical wavelengths, in a material with picosecond nonlinear response time, the maximum soliton velocity may be considerably less than the average speed of light in the medium. A proper description of this effect would require the inclusion of retardation effects in the nonlinear response of the material. Nevertheless, our analysis indicates that while PBG materials are ''emptier than physical vacuum'' with respect to classical, linear, wave propagation, they are quite rich in nonlinear electromagnetic wave effects.

Our results indicate a number of avenues for further research. In our model, we have described the electromagnetic field by a scalar wave field. It is important to extend this analysis to include electromagnetic polarization effects. It is well known that the band structure of the realistic vector electromagnetic fields differs quantitatively from the corresponding scalar wave band structure. Nevertheless, we believe that our scalar solitary wave solutions provide a valuable, qualitative starting point for more detailed studies. Our studies have been limited to materials with a $\chi^{(3)}$ nonlinear response. It would be of interest to extend these studies to PBG materials with a large $\chi^{(2)}$ response [56], as well as to include the nonlinear saturation effects which are inevitable at high light intensities.

In optical fibers, soliton propagation is well described by the classical nonlinear Schrödinger equation. The quantum version of the NLSE can be solved [57] by the Bethe ansatz method [58]. It would be of interest to determine the quantum correlations of photons comprising the gap solitary wave, and the possibility of quantum noise reduction. Studies of this nature have already been performed for optical fiber solitons [59].

Finally, it is of considerable importance to study the coupling of an external laser pulse to the predicted soliton modes of the PBG material. Studies of how to launch a gap soliton have been restricted so far to 1D Bragg gratings [60]. It would be of considerable interest to understand the behavior of a general time-dependent laser pulse incident on PBG material in regard to pulse reshaping effects, bistability effects, and possible chaotic behavior [61]. In view of the large variety of solitary wave solutions predicted in higher-dimensional PBG materials, such studies may be particularly fruitful.

ACKNOWLEDGMENTS

We are grateful to Dr. Kurt Busch for helpful discussions on photonic band structure. This work was supported in part by the National Sciences and Engineering Research Council of Canada and Photonics Research, Ontario.

[1] H. G. Winful, J. H. Marburger, and E. Garmire, Appl. Phys. Lett. **35**, 379 (1979).
[2] W. Chen and D. L. Mills, Phys. Rev. Lett. **58**, 160 (1987).
[3] A. Hasegawa and F. Tappert, Appl. Phys. Lett. **23**, 142 (1973).
[4] D. L. Mills and S. E. Trullinger, Phys. Rev. B **36**, 947 (1987).
[5] A. B. Aceves and S. Wabnitz, Phys. Lett. A **141**, 37 (1989).
[6] W. Thirring, Ann. Phys. (Leipzig) **3**, 91 (1958).
[7] C. M. de Sterke and J. E. Sipe, in *Progress in Optics XXXIII*, edited by E. Wolf (Elsevier, Amsterdam, 1994), Chap. III.
[8] N. D. Sankey, D. F. Prelewsitz, and T. G. Brown, Appl. Phys. Lett. **60**, 1427 (1992).
[9] C. J. Herbert and M. S. Malcuit, Opt. Lett. **18**, 1783 (1993).
[10] B. J. Eggleton *et al.*, Phys. Rev. Lett. **76**, 1627 (1996).
[11] G. V. Agrawal, *Nonlinear Fiber Optics* (Academic, New York, 1995).
[12] M. N. Islam, Phys. Today **47** (5), 34 (1994).
[13] Y. R. Shen, *The Principles of Nonlinear Optics* (Wiley, New York, 1984) p. 303.
[14] *Photonic Band Gap Materials*, Vol. 15 of *NATO Advanced Study Institute, Series E: Applied Sciences*, edited by C. M. Soukoulis (Kluwer, Dordrecht, 1996).
[15] S. John and N. Aközbek, Phys. Rev. Lett. **71**, 1168 (1993).
[16] K. Ohtaka, Phys. Rev. B **19**, 5057 (1979).
[17] S. John, Phys. Rev. Lett. **58**, 2486 (1987).
[18] E. Yablonovitch, Phys. Rev. Lett. **58**, 2059 (1987).
[19] H. G. Winful, Appl. Phys. Lett. **46**, 527 (1985).
[20] E. Yablonovitch, T. J. Gmitter, and K. M. Leung, Phys. Rev. Lett. **67**, 2295 (1991).
[21] S. John and T. Quang, Phys. Rev. Lett. **78**, 1888 (1997).
[22] JV. Mizrahi *et al.*, Electron. Lett. **30**, 780 (1994).
[23] G. P. Agrawal and S. Radic, IEEE Photonics Technol. Lett. **6**, 995 (1994).
[24] E. Özbay, E. Michel, G. Tuttle, R. Biswas, M. Sigalas, and K. M. Ho, Appl. Phys. Lett. **64**, 2059 (1994).
[25] M. Philal, A. Shambrook, and A. A. Maradudin, Opt. Commun. **80**, 199 (1991); M. Plihal and A. A. Maradudin, Phys. Rev. B **44**, 8565 (1991).
[26] P. R. Villeneuve and M. Piché, Phys. Rev. B **46**, 4969 (1992); **46**, 4973 (1992); Prog. Quantum Electron. **18**, 153 (1994).
[27] R. D. Meade, K. D. Brommer, A. M. Rappe, and J. D. Joannopoulos, Appl. Phys. Lett. **61**, 495 (1992).
[28] S. L. McCall and P. M. Platzman, Phys. Rev. Lett. **67**, 2017 (1991).
[29] W. M. Robertson, G. Arjavalingam, R. D. Meade, K. D. Brommer, A. M. Rappe, and J. D. Joannopoulos, Phys. Rev. Lett. **68**, 2023 (1992).

[30] P. L. Gorley *et al.*, Appl. Phys. Lett. **64**, 687 (1994); **60**, 2714 (1992).
[31] A. Rosenberg, R. J. Tonucci, H. B. Lin, and A. J. Campillo, Opt. Lett. **21**, 830 (1996).
[32] U. Grüning, V. Lehman, s. Ottow, and K. Busch, Appl. Phys. Lett. **68**, 747 (1996); U. Grüning, V. Lehmann, and C. M. Engelhardt, *ibid.* **66**, (1995).
[33] V. N. Astratov *et al.*, Nuovo Cimento D **17**, 1349 (1995); Phys. Lett. A **222**, 349 (1996); Y. A. Vlasov *et al.*, Phys. Rev. B **55**, R13 357 (1997); Appl. Phys. Lett. **71**, 1 (1997).
[34] R. Baughman and A. Zakhidov (unpublished).
[35] H. S. Sözüer, J. W. Haus, and R. Inguva, Phys. Rev. B **45**, 13 962 (1992).
[36] V. I. Karpman, Phys. Rev. E **53**, R1336 (1996).
[37] S. K. Turitsyn, Pis'ma Zh. Eksp. Teor. Fiz. **61**, 458 (1995) [JETP Lett. **61**, 469 (1995)].
[38] D. G. Salinas, C. M. de Sterke, and J. E. Sipe, Opt. Commun. **111**, 105 (1994); C. M. de Sterke, D. G. Salinas, and J. Sipe, Phys. Rev. E **54**, 1969 (1996).
[39] D. K. Campbell, M. Peynard, and P. Sodano, Physica (Amsterdam) **190**, 165 (1986).
[40] D. Anderson, Phys. Rev. A **27**, 3135 (1983).
[41] R. L. Sutherland, *Handbook of Nonlinear Optics* (Dekker, New York, 1996).
[42] T. D. Krauss and F. W. Wise, Appl. Phys. Lett. **65**, 1739 (1994).
[43] M. J. LaGasse, K. K. Anderson, C. A. Wang, H. A. Haus, and J. F. Fujimoto, Appl. Phys. Lett. **56**, 417 (1990).
[44] G. Stegeman and P. Likamwa, in *Nonlinear Optical Materials and Devices for Applications in Information Technology*, edited by A. Miller, K. R. Welford, and B. Daino (Kluwer, Dordrecht, 1995), p. 285.
[45] B. L. Larence, M. Cha, W. E. Torruellas, and G. I Stegeman, Appl. Phys. Lett. **64**, 2773 (19994).
[46] JS. Molyneux, A. K. Kar, B. S. Wherrett, T. L. Axon, and D. Bloor, Opt. Lett. **18**, 2093 (1993).
[47] Estimated from J. D. Joannopoulos, R. B. Meade, and J. N. Winn, *Photonic Crystal* (Princeton University Press, Princeton, 1995), p. 123.
[48] M. J. D. Powell, in *Numerical Methods for Nonlinear Algebraic Equations*, edited by P. Rabinowitz (Gordon and Breach, London, 1970).
[49] R. K. Jain and M. B. Klein, Appl. Phys. Lett. **35**, 454 (1979).
[50] R. McLeod, K. Wagner, and S. Blair, Phys. Rev. A **52**, 3254 (1995).
[51] G. H. Derrick, J. Math. Phys. **5**, 1252 (1964).
[52] N. G. Vakhitov and A. A. Kolokolov, Radiophys. Quantum Electron. **16**, 783 (1975).
[53] Ph. Blanchard, J. Stubbe, and L. Vazquez, Phys. Rev. D **36**, 2422 (1987).
[54] A. Alvarez and M. Soler, Phys. Rev. Lett. **50**, 1230 (1986).
[55] W. A. Strauss and Luis Vazquez, Phys. Rev. D **34**, 641 (1986).
[56] T. Preschel, V. Peschel, F. Leferer, and B. A. Malomed, Phys. Rev. E **55**, 4730 (1997).
[57] Y. Lai and H. A. Haus, Phys. Rev. A **40**, 844 (1985); S. J. Carter, P. D. Drummond, M. D. Reid, and R. M. Shelby, Phys. Rev. Lett. **58**, 1841 (1987).
[58] H. A. Bethe, Z. Phys. **71**, 205 (1931).
[59] P. D. Drummond, R. M. Shelby, S. R. Friberg, and Y. Yamamoto, Nature (London) **365**, 307 (1993).
[60] C. M. de Sterke and J. E. Sipe, Opt. Lett. **14**, 871 (1989); J. Opt. Soc. Am. B **6**, 1722 (1989).
[61] C. M. de Sterke and J. E. Sipe, Phys. Rev. A **42**, 2858 (1990).